ABSTRACT

Title of Document: CHARACTERIZATION OF LUMINESCENT MATERIALS FOR APPLICATION IN THE SPACE ENVIRONMENT

Michael H. Sanders, PhD, 2014

Directed By: Associate Professor, Raymond Sedwick, Aerospace Engineering Department

The medium Earth orbital (MEO) altitudes are greatly underutilized due to the harsh radiation environment. In thinking of alternative ways to work in this environment, luminescent materials are proposed as a replacement or augmentation

for power. An investigation into the radiation resilience of some luminescent materials for use in space was undertaken. The results have been integrated into a baseline design for utilizing such materials for power generation via luminescent solar concentrators (LSC) in the space environment. The performance of such a system is compared to that of existing solar cell based power generation.

Rhodamine 6G, Fluorescein and Cytodiagnostics Large Stokes Shift 500 dye was used in the radiation experiments. Rhodamine 6G and Fluorescein were chosen due to their well-documented history, while Cytodiagnostics dye was selected to further characterize a non-traditional, potential luminophore. Concentrations of the luminescent materials were mixed with polymer host materials and dissolved in a solvent, then spin coated onto quartz substrates to produce thin film test samples. Absorption and emission measurements were taken and analyzed to determine the materials radiation tolerance. The results showed a good tolerance for Rhodamine 6G while the other materials did not perform as well.

To enhance the understanding of the environmental constraints, a thermal simulation was performed to investigate the extreme operating temperatures, and how heating may affect the materials in the power generation system. An interesting trade caused by temperature effects was shown. The solar cell in the LSC system operates at a lower, more efficient temperature, but the luminophores become less efficient from solar heating. The end result is that the overall LSC system efficiency remains fairly constant as the system is heated.

CHARACTERIZATION OF LUMINESCENT MATERIALS FOR APPLICATION IN THE SPACE ENVIRONMENT

By

Michael H. Sanders

Dissertation submitted to the Faculty of the Graduate School of the
University of Maryland, College Park, in partial fulfillment
of the requirements for the degree of
Doctor of Philosophy
2014

Advisory Committee:
Professor Raymond Sedwick, Chair
Professor David Akin
Professor Jeremy Munday
Professor Martin Peckerar
Professor Robert Sanner

Dedication

To all my sailors that I have, are, and will serve with. Even an Airdale can accomplish great things when backed by the finest. Fly safe, work safe, play safe and come home safe.

Acknowledgements

This work is personally supported by friends and co-workers at the Naval Research Lab. Without their time, resources and encouragement, this dissertation could not have been completed. In particular, Gary Kushto, Bill Scharpf, Cory Cress, Gary Chen, Raymond Hoheisel, Rob Walters, Adam Yingling and, finally, Hap and Pat. I would like to thank Scott Messenger, even though he has moved from NRL. Also, I would like to thank the NCST for all their support and encouragement throughout the past 6 years. Thanks GP and Pete. Your endorsements got me here.

Thank you to everyone at the University of Maryland who made this project possible. My advisor, Ray Sedwick, for his guidance and support over the last 4 years. Thanks to Jeremy Munday who started me on this path and for Marty Peckerar who helped me finish. Thanks to Dave Akin for being my first inspiration at UMD and showing the passion for all things space. Thanks to Rob Sanner for showing the passion in teaching. Thank you to Dave Burke for your advice and critiques. To my lab mates, I thank you for all the study sessions. I am here because of your willingness to help the old and infirmed. Good luck.

Thanks to those that were ahead of me, showing me the ideas and potential. Raul Bose, Dan Ferrell, and Martyn Fisher for sharing your experiences and knowledge.

Finally, the huge thank you to my family, for putting up with late nights, for missing events, and for general grouchiness. God bless you, Jen, Libby, Debra, Liam Courtney, Keegan, Ella, and little Nathan. And Grandma Pat.

Table of Contents

List of Tables

List of Figures

List of Abbreviations and Symbols

AM0	Air Mass Zero
ANOVA	Analysis of Variation
ATJ	Advances Triple Junction
BOL	Beginning of Life
ddf	denominator degrees of freedom
EOL	End of Life
EQE	External Quantum Efficiency
FF	Fill Factor
GCR	Galactic Cosmic Rays
GEO	Geostationary Earth Orbit
GPS	Global Positioning System
Gy	Greys
HEO	Highly Elliptical Orbit
LSC	Luminescent Solar Concentrator
LSS	Large Stokes Shift
MEO	Medium Earth Orbit
MJ	Multi-junction
MPV	Multi-junction Photovoltaic
ndf	numerator degrees of freedom
PCE	Photon Cascade Emission
PMMA	Poly(methyl methacrylate)
PV	Photovoltaic
PVP	Polyvinylpyrrolidone
Q	absorbed heat
QE	Quantum Efficiency
rads	unit of absorbed radiation dose
Re	Earth Radius
RTG	Radioisotope Thermoelectric Generators
TACSAT4	Navy sponsored communication satellite
UV	Ultraviolet

α	absorbance
ε	emissivity
η	efficiency
λ	Wavelength
σ	Stefan-Boltzmann constant or cross-section

Chapter 1 Introduction and Motivation

1.1 Background

With the discovery of a third radiation belt[1] and from personal experience with an experimental communication satellite, there is strong motivation for a radiation resistant power generation system. The Medium Earth Orbit (MEO) has long been underutilized for spacecraft operations due to its harsh radiation environment. The Global Positioning System (GPS) is an example of a system that traverses the MEO altitudes in order to fulfill its operational requirements. The recent launch of an experimental communication satellite, named TACSAT4, showed the potential of this neglected orbit for other uses besides GPS. By using a lower altitude as compared to a Geostationary Earth Orbit (GEO) communications satellite, the power requirement for proper transmission and receiving of radio signals is much less. The power required falls off by the square of the distance, based on the transmission equation:

$$\frac{P_r}{P_t} = G_t G_r \left(\frac{\lambda}{4\pi R}\right)^2 \tag{1.1}$$

where P_r is power received, P_t is power transmitted, G_t and G_r are the respective antenna gains, λ is the transmitted wavelength and R is the distance between source and receiver. The shortening of the transmission distance from a GEO satellite of 36,000 km to the TACSAT4 distance of 12,050 km greatly reduces the required power ratio to only 10% of the original power required. This reduced requirement permits other communication system tradeoffs, such as accepting a loss in antenna

gain by using an omnidirectional receiver. An omnidirectional antenna has less gain but is better suited for operating with deployed users. In order to use such an orbital regime, a highly radiation resistant power generation system is needed.

Based on experience while working on TACSAT4, the engineers had to confront many challenges when designing for this particular space environment. As depicted in Figure 1.1, the TACSAT4 concept of operations drives the orbital regime needed to properly perform its communication mission.[2] TACSAT4 operates in a Highly Elliptical Orbit (HEO) to perform its high latitude communications mission, thus passing through a high radiation altitude in space. The design of the satellite had to take into account the non-typical space radiation environment.

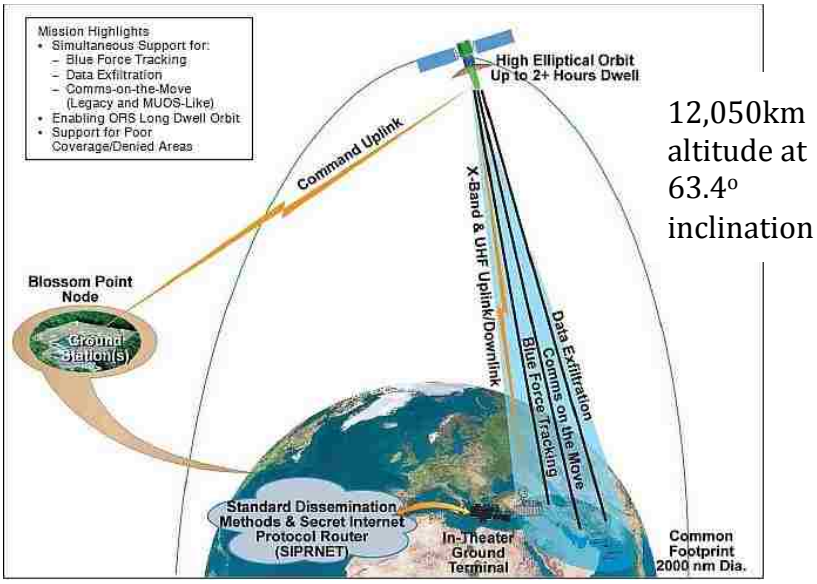

Figure 1.1: TACSAT4 Concept of Operations[2]

To better understand the radiation environment, Figure 1.2 shows the inner and outer van Allen belts at distances in units of Earth radii (R_e).[3] The scale starts with blue and extends to red, which represents the most intense radiation exposure at 0.05 rads per second. These radiation levels were duly noted at the conception of the

TACSAT4 program. From the TACSAT Solar Cell Experiment, "The HEO orbit of TacSat-4 is providing a high radiation environment with an anticipated photovoltaic (PV) array degradation of 25% in one year for triple-junction III-V cells."[2]

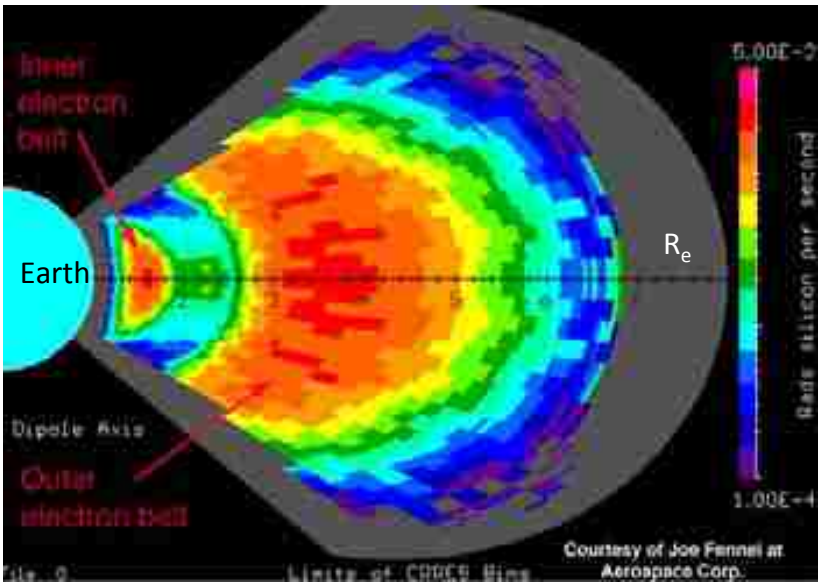

Figure 1.2: van Allen or radiation belts at distance measured in Earth radii (Re).[3]

To use such an orbital regime, a highly radiation resistant energy generation system is needed. This prompted an initial investigation into alternative means of power generation while being able to withstand the harsh radiation effects.

1.2 Current Photovoltaic Technology

Since the first use of solar cells on the Vanguard satellite system[4], photovoltaic (PV) cells have been used to power a large variety of space systems. The first satellites operated on batteries alone[5], which severely limited the operation of these systems. Other power generation sources have been utilized, such as the Radioisotope Thermoelectric Generator (RTG). RTG's have been limited to deep space missions due to the environmental and political concerns of launching

radioactive materials into space. Here, PV cells would be too inefficient to service the satellite at the lower solar illumination intensities of the outer planets. For near Earth applications, PV cells have been the main power generation system for satellites due to their fairly high specific power and their compact size.

The first PV cells used were silicon solar cells. As the technology advanced, more exotic materials, such as Gallium Arsenide (GaAs), were used to boost both power conversion efficiency and radiation tolerance. The most efficient, modern solar cells are the multiple junction photovoltaic (MPV) cells.[6] MPV cells are, in a simplistic view, three separate solar cells stacked in series. The overall cell efficiency is determined by the amount of current produced by the cell supplying the least amount of current. Figure 1.3 shows the monolithic stacking of the series of cells, and how different wavelengths of light are absorbed.

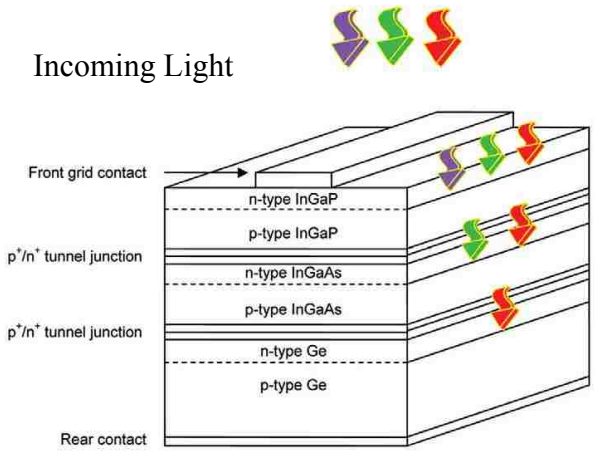

Figure 1.3: A simplified schematic of a three-band gap tandem multi-junction photovoltaic cell.[7]

Using different spectral responses from multiple materials, a multi-junction solar cell is able to better utilize the entire solar spectrum. Figure 1.4 illustrates the discrete,

semiconducting materials, which convert different regions of the solar spectrum to extract more current from the incoming light.

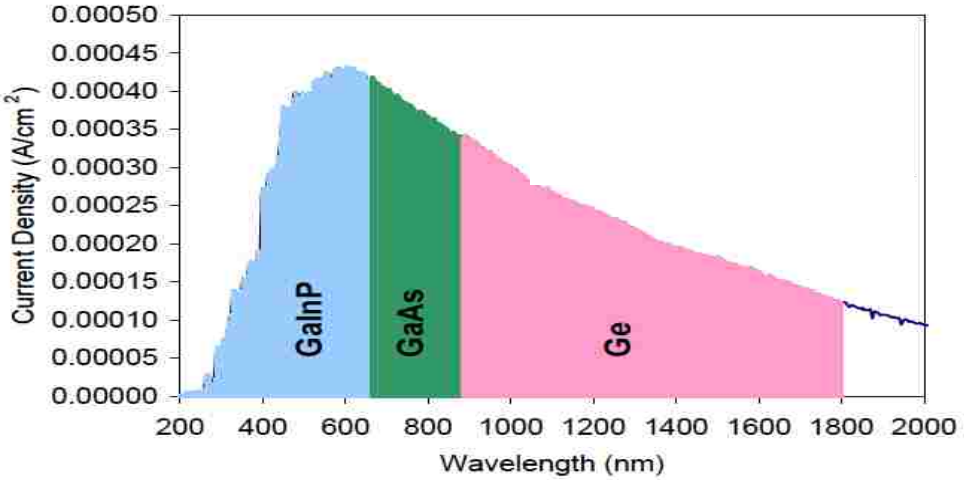

Figure 1.4: Extra-terrestrial or Air Mass Zero (AM0) spectrum with approximate partitions for a typical triple junction GaInP/GaAs/Ge solar cell[8]

The state-of-the-art test MPV cell has just surpassed 40% efficiency[9], while top-rated, production solar cells for space applications are currently capped at 30% efficiency[10]. Under concentration, MPV cells have achieved over 44% efficiency.[11] While MPV cells are more efficient at converting the solar spectrum, the restriction on current means that the MPV cells are reaching their limits. These high efficiencies still produce the most power generation for the least amount of system mass. While these are great performance systems, they suffer two major space environmental problems – radiation damage and thermalization.

1.3 Degradation due to radiation and thermalization

All PV cells are susceptible to radiation damage. High-energy particles damage the lattice structures of the semiconductor materials, which are referred to as

displacement damage. This damage degrades the electrical transport properties of the material, in particular, the minority carrier lifetime. Another source of radiation damage is from ionizing radiation. Ionizing radiation creates trapping centers between the valence and conduction band, thus reducing the output.[12] MPV cells are fairly radiation resistant, but they still degrade from exposure. Table 1.1 shows the degradation of voltage, current, power and efficiency in a modern MPV produced by Emcore.

Table 1.1: Radiation Degradation for Emcore's 27.5% Advanced Triple Junction (ATJ) Solar Cells[13]

Radiation Performance at 1 MeV Electron Irradiation, EOL/BOL Ratios

Fluence (e/cm^2)	V_{mp}	I_{mp}	P_{mp}	Efficiency
5.00E+13	0.97	1.00	0.97	0.97
1.00E+14	0.96	1.00	0.96	0.96
5.00E+14	0.92	0.96	0.89	0.89
1.00E+15	0.90	0.94	0.85	0.85
3.00E+15	0.85	0.87	0.74	0.74

For the power engineer, this loss of efficiency over the lifetime of the spacecraft must be taken into account. Therefore, the satellite system must be designed for the End of Life (EOL) of the satellite, knowing that the MPV cell will lose part of its power generation capacity due to radiation damage. This degradation has diminished the utilization of the middle space altitudes.

Another decrease to solar cell efficiency is the reduction due to elevated operating temperatures of the solar cells. This decrease is experienced immediately after launch and must be accounted for in the power system design. At the Beginning of Life (BOL) of the solar cell system, a standard temperature, usually 25 or 27

degrees Celsius, is used when rating the efficiency of the solar cells. Most solar panels on satellites do not operate at that standard temperature, so the solar cell is not operating at the rated efficiency. With full sun exposure, the normal operating temperature is much higher at GEO, about 116 ^{o}C.[14] The only way for a spacecraft to shed excess heat to the outside environment is through radiative heat transfer. Since solar cell efficiency decreases as temperature increases, these higher operating temperatures reduce the solar cell's power generation.

Though not directly related to the design of a power system for use in the middle altitudes, a system like TACSAT4 would have a fair amount of sun exposure with limited eclipse times. Its solar cells will operate at higher temperature than the standard reference temperature and suffer an overall reduction in efficiency.

1.4 A Possible Solution: Luminescent Solar Concentrator

A Luminescent Solar Concentrator (LSC) was proposed in the 1970's as an alternative power source to a solar cell.[15] It uses a cheaper material to generate a concentration effect onto a solar cell, thereby lowering the amount of expensive material and the overall cost. An LSC consists of a luminescent material and a waveguide that is connected to a solar cell. See Figure 1.5 for a typical thin film example. Another benefit is that the luminescence of the material can better match the optimal light conversion wavelength of the attached solar cell. With optimal optical input and concentration, a smaller solar cell area can be utilized.

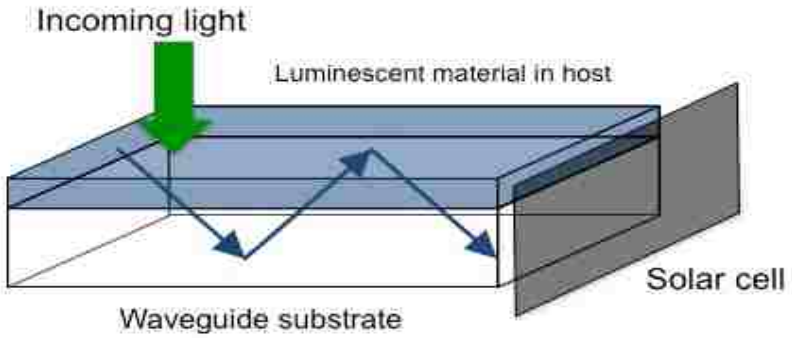

Figure 1.5: Sample thin film LSC

From a space perspective, the arrangement of the solar cell in an LSC affords more benefits. The solar cells are along the edges, so they are not as exposed to the environment as compared to a typical solar array. The solar cell can be better shielded in many directions from the harmful effects of radiation. See a cross sectional view of an LSC in Figure 1.6, with a green line showing the shielding effect on the solar cells.

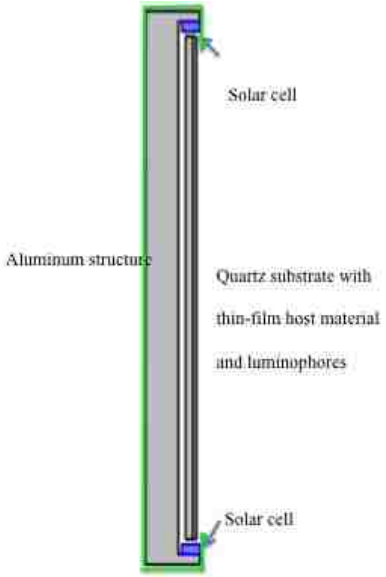

Figure 1.6: Cross-sectional view of an LSC showing protective features in green.

The traditional shielding method of solar cells is to add a thin layer of cover glass over the entire solar cell. This shielding comes at a price: radiation causes some

minor losses in the transmission of the light through the shielding and the shielding adds an appreciable amount of weight to the system. As shown in Figure 1.6, the solar cells in an LSC would not need this extra shielding, since the housing structure would be a suitable covering for the solar cells. The mass would not necessarily decrease appreciably, since an LSC uses a quartz substrate as a waveguide to direct light to the solar cells. As shown in Figure 1.7, an LSC cell is in the approximate mass range of a solar cell, assuming the wiring and connection masses are the same for both systems.

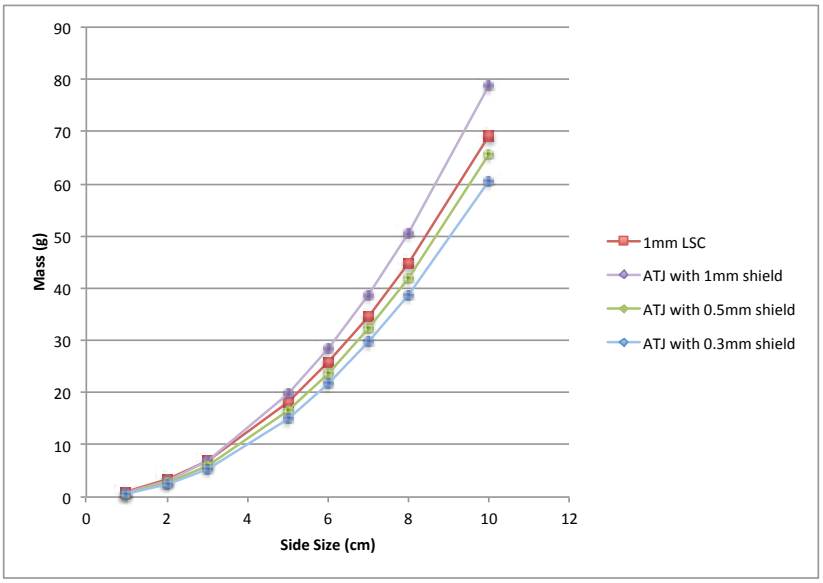

Figure 1.7: Calculated weight comparison for Emcore's ATJ solar cell and a proposed LSC design

An LSC cell with dimensions of 5cm x 5cm x 1mm has slightly more mass than a typical ATJ cell with cover glass. The LSC cell has 20% more mass as compared with an ATJ with 0.3mm cover glass and 10% more mass as compared with an ATJ with 0.5mm cover glass. The LSC cell is 9% less massive than an ATJ with 1mm cover glass. This led to the first research question: while mass is similar, will the LSC withstand the radiation environment better than the standard solar cells?

Another potential benefit for a LSC is that the backing of the LSC plate is usually a diffuse, reflective material. Thus, the energy not used by the system is reflected back into space, resulting in less heating of the system. The back housing structure will act as a large radiator for the dissipation of thermal energy. The small area of solar cells will have a large radiator to remove the unused energy, thereby permitting them to operate within a much more efficient temperature range.

An analysis was conducted using the AP8/AE8 space radiation models from the SPENVIS website[16] -- along with the thermal data from the simulations -- to determine whether an LSC system can ever be competitive with a high efficiency triple junction solar cell. In Figure 1.8, an LSC system using a GaAs solar cell is compared to Emcore's Advanced Triple Junction solar cell with cover glass. It depicts the potential of an improved LSC cell to surpass a traditional solar cell after several years on orbit. As seen in the Figure 1.8, a 21.5% efficient LSC system becomes competitive with a 27.5% Advanced Triple Junction solar cell after 10 years of operation.

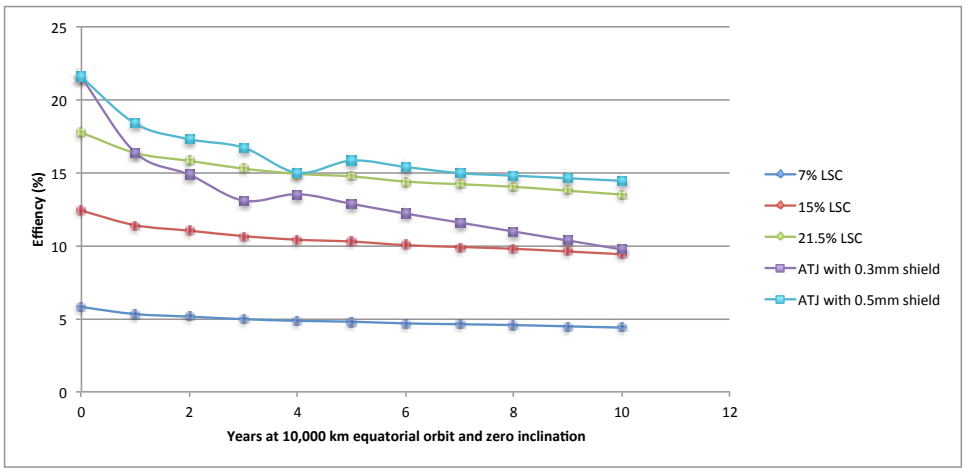

Figure 1.8: Efficiency changes to an LSC cell and a triple junction cell due to temperature and radiation degradation over simulated years of orbit.

Finally, from out of the traditional acquisition trade space -- performance, schedule and cost -- the performance of the space power generation system is usually the most important driver. In particular, as a result of the high launch costs and limited shroud volume, the size and mass of a space power system typically override the cost of procuring such systems. Even though multi-junction photovoltaic (MPV) cells may cost hundreds of dollars more per cell than a single junction photovoltaic (PV) cell, the weight per watt makes MPV cells more attractive for space applications. In terrestrial applications, the potential of a cheaper LSC system replacing solar cells would be important. For space systems, due to the emphasis on performance over cost, a monetary savings probably would not channel space companies to switch to an LSC at the current state-of-the-art.

1.5 Purpose and contributions of this work

While the current state-of-the-art LSC does not provide a competitive alternate to the state-of-the-art MPV cells under benign environmental conditions, the goal of

this research is to show that, in the extreme radiation environment of the van Allen belts, an LSC system may offer long-term advantages through their radiation tolerance. In particular, it will motivate how improvements in LSC performance might translate into greater mission sustainability. Specifically, this research makes the following contributions:

- Extension of LSC knowledge, by characterizing the absorption and emission data of a non-traditional luminescent material (Cytodiagnostics Large Stokes Shift 500 Dye)
- Characterization of the degradation of luminescent materials exposed to various levels of radiation
- Development of a thermal model to evaluate the temperature effects on system efficiency
- Design of an LSC system for a sample orbit, based on the changes induced by radiation and thermal exposure

Even though LSC comes with a list of technical challenges, which will be discussed in Chapter 2, luminescent materials have a viable place in space as a power source or as power augmentation.

Chapter 2 Background

2.1 Chapter Introduction

The space environment presents many different challenges for engineers in the design of spacecraft. A review of the major space environmental effects is presented, specifically the radiation and thermal effects, along with the background and rationale for investigating luminescent materials for use on spacecraft. This section will also present the literature review into the 30 years of investigative work in Luminescent Solar Concentrators and spectral down-conversion used to augment solar cells.

2.2 Space Environment

The presence of high-energy particles and the lack of a protective atmosphere create a very harsh environment for spacecraft. Engineers have to design for the degradation of materials due to radiation and out-gassing, while taking into account the inability to perform maintenance on spacecraft. The Hubble Telescope was one example of an exception to this general rule. It was launched in 1990 with a faulty primary mirror. In 1993, a repair mission was launched to replace the defective part and four other repair missions were done to upgrade and replace old parts. With the retirement of the space shuttle, no more repair missions are planned.[17] Eventually the space environment will degrade every spacecraft; currently, repairs to the vast majority are not feasible.

Degradation causes from the space environment can be broken into five categories: neutrals, plasma, radiation, micrometeoroid/orbital debris damage, and vacuum. The neutral effects include aerodynamic drag and atomic oxygen. Aerodynamic drag slows the spacecraft. Atomic oxygen attacks various components, causing corrosion and degradation. While drag and atomic oxygen are mainly low Earth orbit effects, a small portion of the neutral environment becomes ionized, thus creating plasma in space. Plasma causes spacecraft charging. This charging results in dielectric breakdown, and creates unexpected electrical discharges that can damage the spacecraft's components and power generation. Micrometeoroids/orbit debris impinges on satellite surfaces causing structural and material damage. The environmental radiation degrades solar cells through ionization and displacement damage and causes single event upsets to computer and electrical systems. The vacuum effects include out-gassing of materials and difficulty maintaining thermal balance. This out-gassing can change the properties of the materials and damage or degrade other sensitive parts of the spacecraft, such as optical lenses. Also, the manufacturing of the satellite must account for this absence of environmental pressure, which often manifests as a change in the adhesive, cohesive and frictional forces leveraged by various fasteners. Without a repair facility near, a fastener failure can be catastrophic to a satellite. A final effect from the vacuum environment is that thermal stability in space creates another uniquely different problem, due to only radiative heat transfer.

2.3 Thermal

There are three main modes to transfer heat in order to maintain thermal stability: conduction, convection, and radiation. Conduction is the transfer of thermal energy due to the presence of temperature gradients in contacting materials. Convection transfers thermal energy through the use of the flow of a fluid over a material. Lastly, thermal radiation is the emission of electromagnetic energy generated due to the thermal motion of particles. All materials with a temperature above absolute zero generate some thermal radiation, which is important for thermal control in spacecraft.

Maintaining the proper thermal parameters for satellite operations presents its own issues. Even though the spacecraft is moving at thousands of miles per hour, due to the vacuum and micro-gravity environment, both forced and free convective heating or cooling are non-existent. While conduction of heat through the spacecraft is used to maintain internal temperatures, radiation is the only way for excess heat generated in the spacecraft to be shed to the outside environment.[18] The craft will absorb heat, Q, from the sun according to:

$$Q_{in} = \alpha_S A_n S \tag{2.1}$$

where α_S is the material's solar absorbance, A_n is the surface area normal to the solar flux, and S is the solar flux per unit area. A craft will radiate heat according to:

$$Q_{out} = \varepsilon A_{tot} \sigma T^4 \tag{2.2}$$

where ε is the material emissivity, $A_{tot}$is the total surface area, T is the temperature and σ is the Stefan-Boltzmann constant. The material property of emissivity greatly

determines heat transfer characteristics due to radiation. Every material has an associated emissivity value and is measured against the ideal blackbody value of unity. The closer the value is to unity, the more radiation the material will emit.

A more specific problem with thermal generation and the rationale for this research will be presented in Chapter 3.

2.4 Radiation

For spacecraft, external radiation comes from three major sources: galactic cosmic rays (GCR), solar particle events, and trapped radiation from the van Allen belts around the Earth. The GCR consist of approximately 85% protons, 14% alpha particles, and 1% heavy ions, together with x-ray and gamma ray radiation. Most effects are caused by particles with energies between 1E8 and 2E10 eV. While the atmosphere protects terrestrial objects, the high energy of these particles makes them almost unstoppable and very little can be done to protect the sensitive parts of a satellite. Fortunately, the low flux of the particles means that the probability of damage is small and the overall damaging effects are minimal due to such a small number of particles that strike the spacecraft. The effects of the solar winds, solar flares, and coronal mass ejections are greatly shielded by the magnetosphere of the Earth. See Figure 2.1 for a depiction of the interaction of the sun and the Earth's magnetosphere.

Figure 2.1: Solar interaction with Earth's magnetosphere[19]

While the sun's effects can cause disturbances in the high altitude orbits, like GEO, most of the solar effects cause a change in the radiation belts around the Earth. Solar effects influence the particles trapped in the van Allen belts and cause the radiation belts to change in size and shape depending on the solar flux. For the middle altitudes, the van Allen belts are the most influential of the radiation sources. The van Allen belts contain electrons (up to 10 MeV) and protons (up to 100 MeV) trapped by the magnetic field of the Earth. See Figure 2.2 for NASA's latest diagram. The particle flux can vary depending on the conditions of the sun and the Earth's magnetosphere. These trapped particles pose a problem to the electronics and power generation systems for near Earth orbiting satellites.

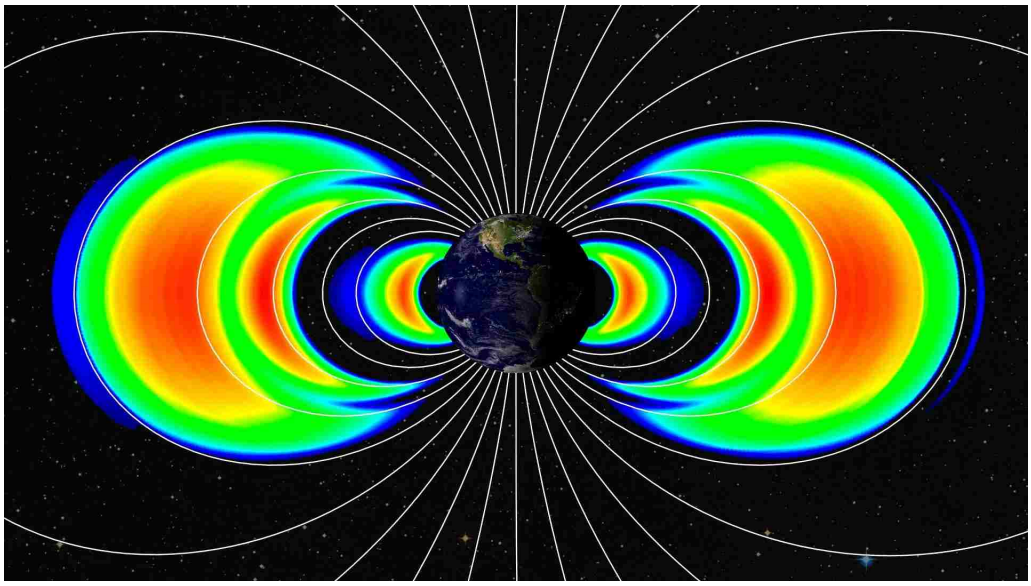

Figure 2.2: Depiction of the inner and outer van Allen radiation belts[20]

There are two major forms of radiation damage for spacecraft: displacement damage and ionization. Displacement damage is the introduction of a high-energy particle that displaces atoms from lattice sites, thereby creating point defects in the irradiated material. Ionizing radiation is radiation with sufficient energy to remove electrons from the orbits of atoms resulting in charged particles. One of the ionization effects is the activation of color centers: a consequence of the changes in the valence electrons and their effects on absorption and transmission. As an electron is stripped from an atom, thus ionizing it, the ion enters a meta-stable excited state. These created, discrete states are capable of absorbing a different wavelength, thus changing the optical properties of the material. For clear glass, the change is from being non-interactive to being absorptive.[21] Color center formation can be reversed through annealing by heating the material. Heating will weaken the inter-atomic bonds, allowing the formation of new, lower energy bonds. Thus, the material reverts toward its original state.

In this study, gamma irradiation is used to determine total dose radiation effects and characterize how the luminescent materials would survive the radiation environment over the life span of the spacecraft. Gamma ray interaction with matter creates ionizing effects based on the energy of the incoming photon. These are broken into three major events: photoelectric effect, Compton effect, and pair production.

In the photoelectric effect, an atom electron absorbs a gamma ray photon, thereby freeing the electron of its bond. By losing energy through ionization and radiation, the free electron is brought to rest. This effect is very dependent on the atomic number of the material and the gamma photon energy. To a first approximation, the cross section varies as[22]:

$$\sigma_{photo} \sim \frac{Z^4}{(h\nu)^3} \tag{2.3}$$

where $h\nu$ is the gamma ray energy and Z is the atomic number. The exponents for Z and gamma ray energy vary depending on the energy of the photon. For low energy photons, the photoelectric effect dominates, and Equation 2.3 represents the low energy behavior.[23]

The Compton effect (also called *Compton scattering*) is the result of a high-energy photon colliding with a target, which releases loosely bound electrons from the outer shell of the atom or molecule. The cross section for Compton scattering is given by the Klein-Nishina formula.[24] For unpolarized radiation the formula is written:

$$\sigma_{Compton} = \frac{r_0^2}{2}\left(\frac{\nu'}{\nu_0}\right)\left[\frac{\nu_0}{\nu'} + \frac{\nu'}{\nu_0} - 2cos^2\theta\right] d\Omega \tag{2.4}$$

where $r_0 = e^2/m_0c^2 = 2.8 \times 10^{-13}$ cm is the classical electron radius, $v_0 = E_0/h$ is the initial frequency, $v' = E'/h$ is the scattered frequency, and $d\Omega$ is the solid angle element into which the photon scatters.

Pair production is when a gamma photon creates an electron-positron pair near the nucleus of an atom. The energy of each particle is essentially one-half of the difference between the initial photon energy and the resting energy of the pair (1.02 MeV). Thus, pair production requires higher photon energies, greater than 1.02 MeV. The electron and positron annihilate each other, releasing two photons. These photons scatter until finally absorbed by the photoelectric effect.[23]

The cross section for pair production as a function of energy (E^+) can be written[25]:

$$\sigma_{pair} = \frac{Z^2 P \sigma_0}{hv - 2m_0c^2} dE^+ \tag{2.5}$$

where $\sigma_0 = 5.8 \times 10^{-28}\ cm^2/nucleus$, and P is a dimensionless quantity which varies from:

$$0(hv \leq 2m_0c^2) \text{ to } \sim 20(hv = \infty).$$

All three processes affect the behavior of gamma photons in matter. The cross sectional behavior versus photon energy is illustrated in Figure 2.3.[23]

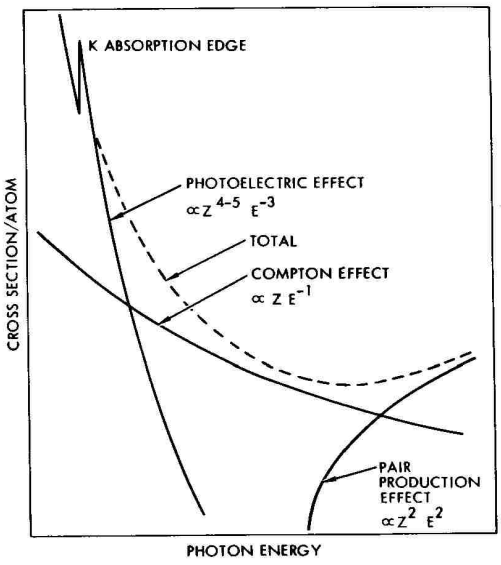

Figure 2.3: Combined cross sectional behavior[28]

The energy regions of dominance are based on the photon energy, and the *Z* of the atom. The boundaries spread apart for lower *Z*. See Figure 2.4 as a comparison of energy regions in carbon, aluminum, iron, and lead.[23]

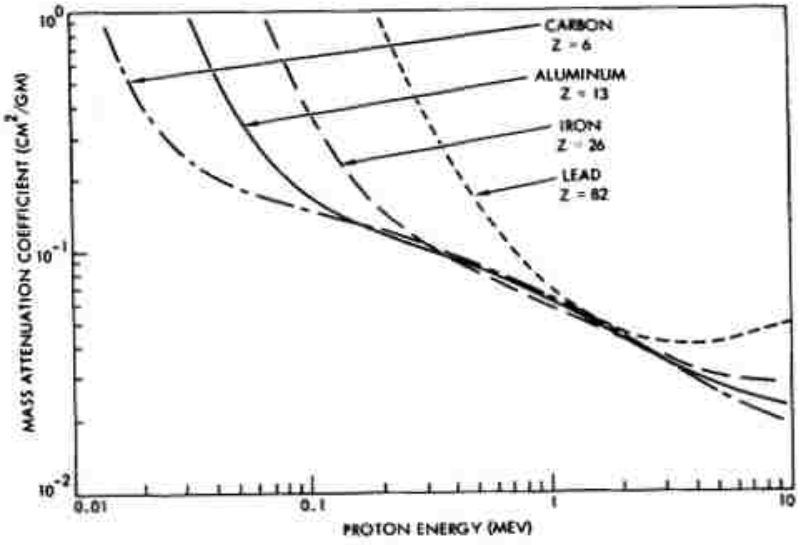

Figure 2.4: Mass attenuation coefficients for photons[29]

Typically, the photoelectric effect occurs with photons having energies from a few electron volts to over 1 MeV. At the high photon energies comparable to the electron

rest energy of 511 keV, Compton scattering may occur. Pair production may take place at energies over 1.02 MeV.[26]

The three processes control a gamma ray photon life expectancy. Assuming the photon starts at the higher end of energy and takes part in a pair production event, it will re-emit lower energy photons as the electron and positron annihilate each other. Through energy loss via Compton scattering, the photon will continue to lose energy until it is finally captured by the photoelectric effect.

2.5 Optical Properties

A small number of general phenomena describe the optical properties of solid-state materials. The simplest groups are reflection, propagation, and transmission. Propagation is further separated into refraction, absorption, luminescence, and scattering. Refraction is essentially a change in light wave direction due to a velocity change at a medium interface. The light intensity does not usually change as a function of refraction. Absorption occurs if the frequency of the light is resonant with the transition frequencies of the atoms. Thus, the light energy is transformed to internal energy in the absorbing material. Absorption causes attenuation of the incoming light as it progresses through the material. Luminescence, along with similar optical properties, is defined in the next section. The luminescent light is emitted in all directions and usually has a different frequency than the incoming light. Scattering is when the light changes direction and possibly its frequency, due to interaction with the material. Scattering has a similar attenuation effect as absorption. See Figure 2.5 for different properties of the propagation of light through a medium.

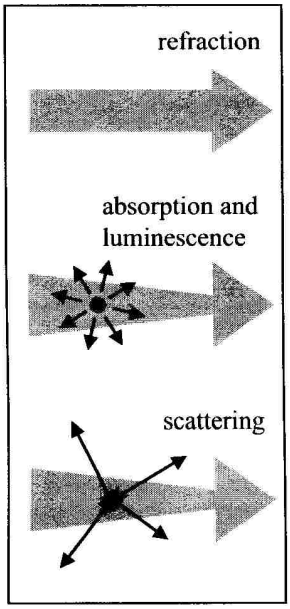

Figure 2.5: Light propagation in materials[27]

The optical properties can be quantified using a number of coefficients. One set is defined in terms of reflectance (R), transmittance (T), and absorptance (A), as depicted in Figure 2.6.

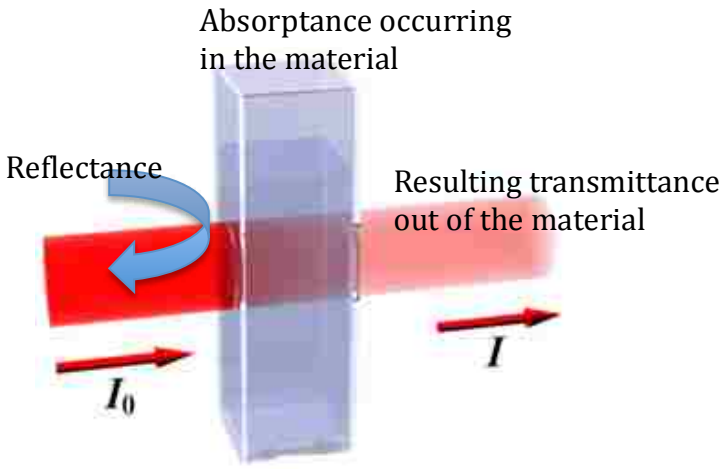

Figure 2.6: Example showing the properties of reflectance, transmittance, and absorbance.[28]

Assuming negligible reflectance, the transmittance is just:

$$T = \frac{I}{I_0} \tag{2.6}$$

where I_0 and I are the intensity of the incident light and transmitted light.

The intensity of the light changes as the light moves through the medium and depends on the material's absorption characteristics as quantified by its absorption coefficient (α).

$$dI = -\alpha dl \times I(l) \tag{2.7}$$

Integrating the above,

$$I(l) = I_0 e^{-\alpha l} \tag{2.8}$$

The result is the Beer-Lambert law, showing the exponential relationship between the intensity (or transmission) of the light through a substance, the material's absorption coefficient, and the distance the light travels (l). The absorption coefficient is strongly dependent on the light frequency, so a material may absorb one color but not another.

The absorptance relationship for non-gaseous materials is related to the absorption coefficient as[28]:

$$A = -\log_{10}\left(\frac{I(l)}{I_0}\right) = \frac{\alpha l}{\log_e 10} = 0.434\alpha l \tag{2.9}$$

After the application of conservation of energy, the summation of the reflectance, transmittance, and absorptance of the incident flux must equal unity:[29]

$$R + T + A = 1 \tag{2.10}$$

In most measurements, R is negligible due to the relative measurement technique that negates the reflectance. Along with the Beers-Lambert Law, this equation develops the relationship between the transmission and absorption of testing of materials.

2.6 Luminescence

2.6.1 Defining the luminescence terms

Luminescence is the general term given to the process of spontaneous emission of light by excited atoms in a solid-state material. Energy is normally absorbed, causing an excited state to exist. As the atom relaxes to a ground state, light is emitted. See Figure 2.7 below showing the electron energy states.

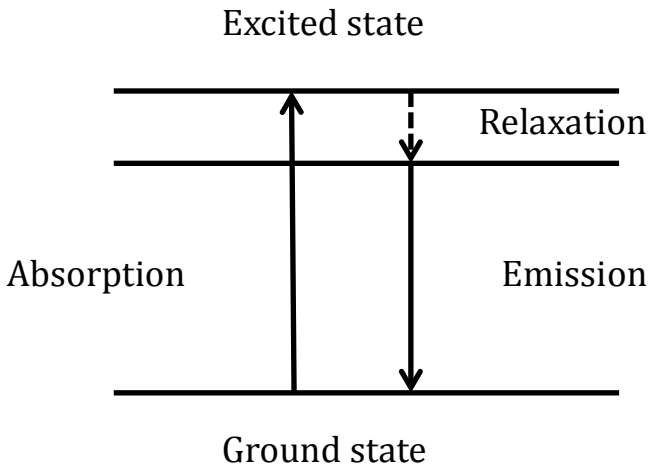

Figure 2.7: Electron energy states in an atom showing the luminescent process.

Photoluminescence describes the phenomenon of light emission from any form of matter after the absorption of photons.

Luminophore is an atom or atomic grouping in a chemical compound that manifests luminescence. There exist both organic and inorganic luminophores.

Fluorescence is the emission of radiation, especially of visible light, by a substance during exposure to external radiation, as light or x-rays.

Phosphorescence is the emission of light by a substance as a result of having absorbed energy from a form of electromagnetic radiation, such as visible light or x-rays. Unlike fluorescence, phosphorescence continues for a short while after the source of radiation is removed.

Emit is to give off radiation or particles.

Emission is the act of emitting.

Emittance is the total flux emitted per unit area.

Scintillation is a flash of light produced by certain materials when they absorb ionizing radiation.

2.6.2 Luminescent Solar Concentrator (LSC)

A typical LSC is shown in Figure 2.8, consisting of luminophores embedded in a transparent plate.

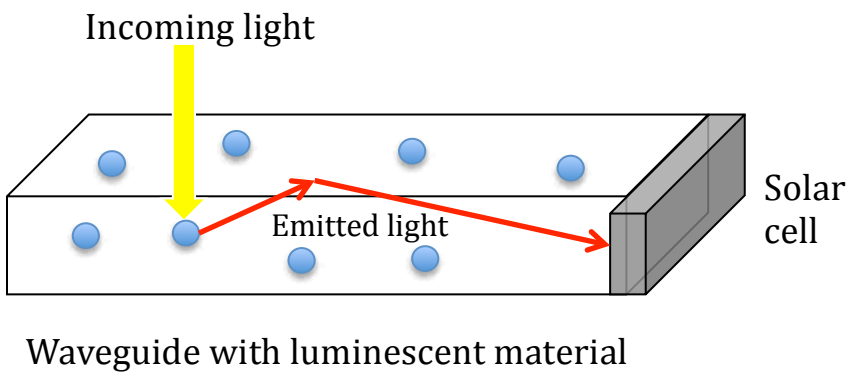

Figure 2.8: Typical LSC example incorporating luminophores in bulk material showing absorption, emission, and wave guiding of light to the solar cell.

The luminophores absorb incoming light and re-emit light that is then trapped within the plate by total internal reflection (TIR) due to the differences in the refractive

indices between the plate and its surroundings. The re-emitted light is guided to the edges of the plate where solar cells convert the light to electrical energy. Current designs for luminescent solar concentrators may be composed of multiple thin, flat layers of alternating luminescent and transparent materials, placed in order to gather incoming light on their broad flat surfaces and emit concentrated luminescent light around their edges for solar cell utilization.[30] Other designs have been proposed, including cylindrical materials with a Fresnel lens for more concentration. See Figure 2.9.

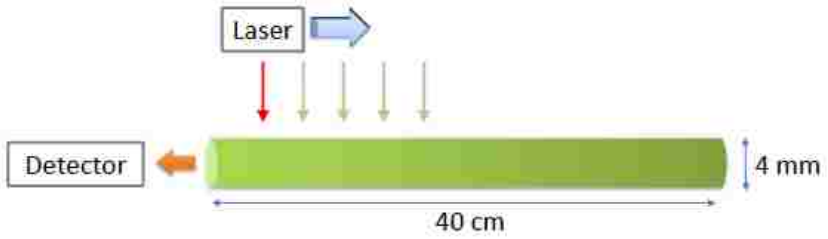

Figure 2.9: Cylinder luminescent bar experiment[31]

Based on the TIR, the capture and guidance of emitted light to the edges are the main principles that make an LSC possible.

2.6.3 LSC Principles

2.6.3.1 Light Capture

Light capturing is based on the well-known Snell's law:

$$\frac{sin\theta_i}{sin\theta_t} = \frac{n_2}{n_1} \tag{2.11}$$

where θ is the angle with the normal for the incident and transmitted rays and n is the refractive index for the materials when light refracts as it encounters differences in materials. See Figure 2.10 for the relationship between materials.

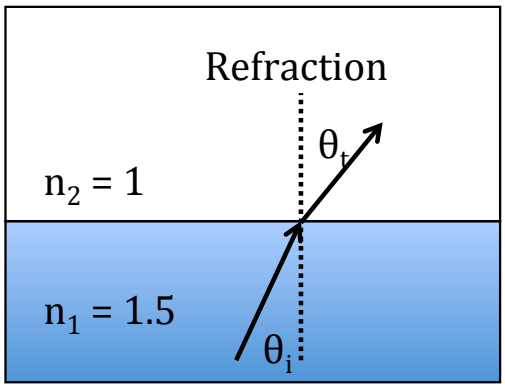

Figure 2.10: Snell's Law showing the refraction of light at an interface of different materials

This refraction leads to a capturing of the light if the angle is sufficient to reflect the light back toward the origin. This angle is called the critical angle (θ_c), when the transmission angle $\theta_t = 90°$ and thus $\sin\theta_t = 1$. From Snell's law, the critical angle is:

$$\theta_c = arcsin\left(\frac{n_2}{n_1}\right) \tag{2.12}$$

At precisely the critical angle, the refracted light is tangential to the boundary. See Figure 2.11 for the different refraction cases as an interface example.

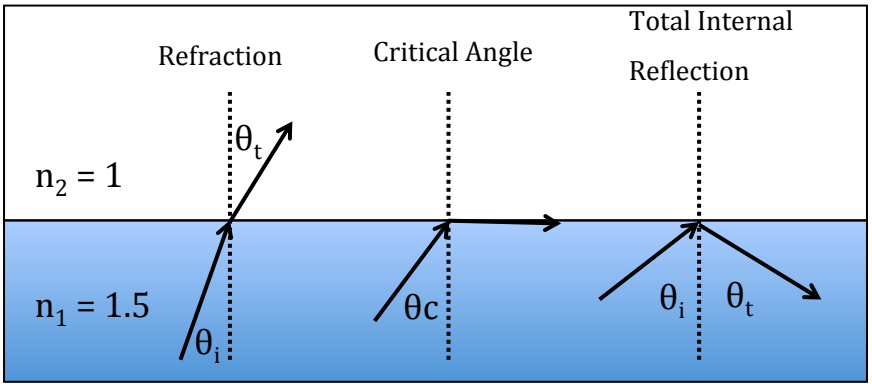

Figure 2.11: Three different refractive cases based on angle of incident

As can be seen from Figure 2.11, anything at or greater than the critical angle will result in the light being captured in the material. Beyond the critical angle, the light

reflects toward the edges of the material, functioning as a waveguide for the luminescent emission of the LSC.

2.6.3.2 Wave guiding

As shown in the above section, light incident at or above the critical angle will be directed through total internal reflection to the edge of the material. For a piece of polymer with an index of refraction of 1.5 and vacuum with an index of refraction of 1, the critical angle is computed to be $41.8°$. The intensity of this reflection as light moves from one medium to another, with differing indices of refraction, is described by the Fresnel equations. The intensity of reflection is dependent upon the polarization of the light, whether perpendicular or parallel. The reflectance for perpendicular or s-polarized light (R_s) is:

$$R_s = \left|\frac{n_1 \cos\theta_i - n_2 \cos\theta_t}{n_1 \cos\theta_i + n_2 \cos\theta_t}\right|^2 \tag{2.13}$$

and for parallel or p-polarized light (R_p) is:

$$R_p = \left|\frac{n_1 \cos\theta_t - n_2 \cos\theta_i}{n_1 \cos\theta_t + n_2 \cos\theta_i}\right|^2 \tag{2.14}$$

where, as before, θ is the incident and transmitted angle to the normal, and *n* is the index of refraction for the different materials.[32] Figure 2.12 shows this relationship of reflection.

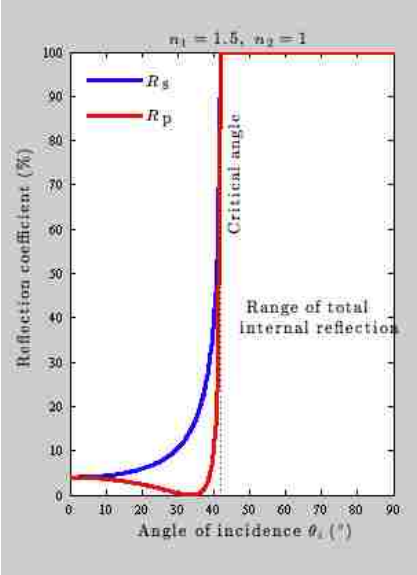

Figure 2.12: Fresnel equation relationship showing range of TIR for a higher index of refraction to lower index of refraction.[37]

With the critical angle and the effects of TIR, an escape cone for light not captured and guided to the edges can be determined by integrating in spherical coordinates from the luminophore to the top and bottom of the plate.

$$escape\ cone = \int_0^{2\pi} d\varphi \int_0^{\theta_c} \sin\theta\ d\theta \tag{2.15}$$

where θ is the angle from the normal and φ is the azimuthal angle. See Figure 2.13 as an illustration of the escape cones.

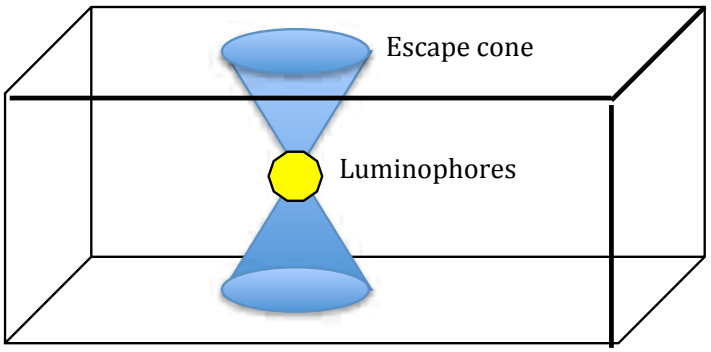

Figure 2.13: Escape cones in LSC

Goldschmidt et al. were able to determine the fraction of lost emitted light due to the escape cone.[33] See Figure 2.14 for an example of their escape cone losses.

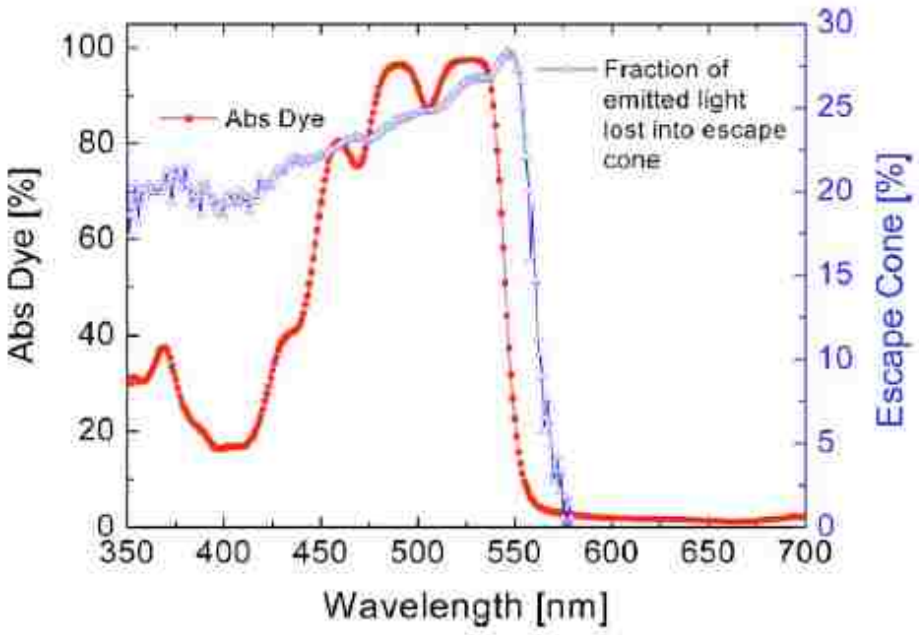

Figure 2.14: Fraction of emitted light lost due to the escape cone.[38]

The theoretical value for escape cone losses under ideal conditions is 26% loss. Among other factors, the escape cone losses are a major contributor to the efficiency losses for the entire LSC system.

2.6.3.3 Efficiency

The efficiency losses of the LSC system are well documented. Figure 2.15 illustrates the major deficiencies that cause inefficiencies in LSCs, which are summarized as follows:

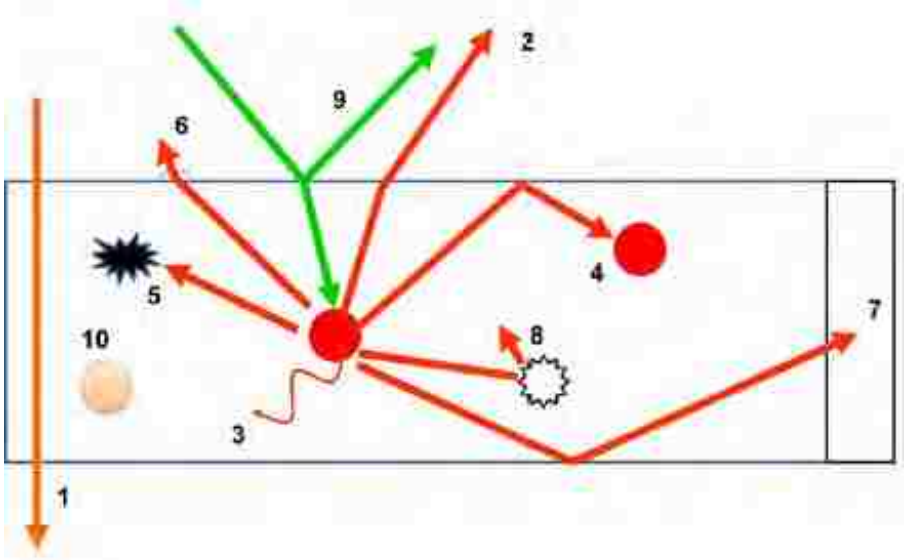

Figure 2.15: Loss mechanisms in an LSC[34,35]

1. Incoming light not absorbed by luminophore

2. Luminescent light exits via the escape cone

3. Light is not emitted because quantum efficiency is less than one

4. Reabsorption of luminescent light by other luminophore

5. Absorption of light by waveguide material

6. Surface scattering

7. Solar cell losses

8. Internal waveguide scattering

9. Reflection of incident light on the surface

10. Limited dye stability.

The performance of an LSC is given by the effective concentration ratio, which is the product of the geometrical gain and the optical conversion efficiency of the collector. The geometrical gain is given as the ratio of surface area to plate edge area:

$$G = \frac{A_{LSC\ plate}}{A_{LSC\ edge}} \tag{2.16}$$

The optical conversion efficiency $\eta_{optical}$ is the ratio of light delivered on the edges to the light incident on the plate:

$$\eta_{optical} = \frac{P_{edges}}{P_{plate}} \tag{2.17}$$

where *P* is the power delivered accordingly. Based on the LSC loss mechanism described in Figure 2.15,the optical (conversion) efficiency of the plate can be written as:[36]

$$\eta_{optical} = (1 - R)\eta_{abs}\eta_F\eta_S\eta_t\eta_{tr}\eta_{self} \tag{2.18}$$

where *R* is the Fresnel reflection, η_{abs} is the ratio of photons absorbed by the plate to photons incident on the plate, η_F is the ratio of photons emitted to the photons absorbed, η_S is the Stokes efficiency, which is the ratio of the average energy of emitted photons to the average energy of the absorbed photons as given by $\eta_S = v_{emit}/v_{absorb}$, η_t is the fraction of light trapped in the collector as given by $\eta_t = (1 - 1/n^2)^{1/2}$, η_{tr} is the transport efficiency which takes into account losses due to material absorption and scattering, and η_{self} is the efficiency loss due to self-absorption. The overall output energy of the LSC is based on the input energy, solar cell conversion efficiency, and optical conversion efficiency, which are given by:[36]

$$E_{out} = E_{in}\eta_{optical}\eta_{solar\ cell}(\lambda) \tag{2.19}$$

Finally, in order to compare the LSC efficiency to the solar cell as exposed to the entire solar spectrum, the ratio of power from a solar cell attached to an LSC to the power from the same solar cell exposed to the solar spectrum is:[36]

$$F = \eta_{optical}\left(A_{surface}/A_{edge}\right)\left(\eta_{solar\ cell}(\lambda)/\eta_{sun}\right) \quad (2.20)$$

where η_{sun} is the efficiency of the solar cell with respect to the entire solar spectrum. As the equation states, the efficiency of the LSC system depends on the optical efficiency, the geometric gain, and the solar cell efficiency. Improving any of these three areas will result in an improved system.

2.6.4 State-of-the-Art LSC

One of the greatest challenges in the beginning of LSC was the photo-stability of organic dyes. Since the start of research into LSC, photo-stability has improved significantly. Though it is dependent on the processing and polymeric environment, photo-stability is still being understood.[37] There is much promise in encapsulating organic molecules such as those found in the Organic LEDs with expected lifetimes of up to 30 years.[38] Quantum dots and other nano structures are being investigated due to the long life expectancy[39] and tunable absorption spectrum[40], but the lower quantum yield of the dots presents another problem.[41] New, second generation devices are characterized by either directional luminophores or photonic filters which enhance the wave guiding mechanism.[42, 43]

Other materials being researched for LSC consideration are the rare Earth element ions such as neodymium (Nd^{3+}) or ytterbium (Yb^{3+}).[35,44,45] The rare Earth elements are considered for use as LSC's due to their large Stokes shift. The Stokes shift is the difference in wavelength between positions of the band maxima of the absorption and emission spectra. The advantage of a large Stokes shift is a low re-

absorption of emitted photons by the luminescent material. This low re-absorption is expected to improve the optical efficiency.

Mirrors and reflectors can improve the overall efficiency. It has been shown that mirrors on the edges and on the back can improve the LSC efficiency.[46,47,48] It is further shown that using a diffuse mirror on the back can recapture some of the light that may have reflected through the plate of the LSC. Other demonstrations have used selective coatings that permit the absorption wavelengths to enter the plate of the LSC while the coating reflects the luminescent wavelengths. This traps more emission light in the waveguide,[44, 42] a improving the light trapping efficiency of the LSC.

Though not a true LSC, the idea of using luminophores to alter the incoming light spectrum through up or down conversion to augment a solar array has been demonstrated. In order to improve the efficiency of solar cells, the spectrum more closely matches the photon energy and the band gap of the semiconductor material. Luminescent materials can convert the broad incident spectrum into a particular wavelength, thereby minimizing the losses in the solar cell energy conversion process.[49] The literature has been mixed on the promise of improved efficiency from these methods.[49] Luminescent down-conversion has been demonstrated to improve overall efficiency, but only for solar cells starting with very low efficiency.[50,51] While the conversion methods have shown some improvements in efficiency, more research must be done for the conversion methods to be implemented in solar cell design.

2.7 Chapter Conclusions and rationale for testing methods and materials

While the focus of previous LSC research has been to lower the cost per watt, in a space environment, cost is usually not the primary driver. The space environment, similar to the marine environment, is much more harsh on materials and has limited or no reparability. This environment causes stringent design parameters with higher reliability, which costs more. With the elevated cost in mind, this research started with a look into alternative power generation sources for space.

From Reisfeld's work, the LSC offers some advantages over other solar concentrators and arrays. LSC's collect both direct and diffuse light. There is good heat dissipation of non-utilized energy by the large area of the collector, thus only light from the luminescent emission reaches the solar cells. Since an LSC can use both diffuse and direct light, solar tracking is not necessary. The matching of the luminescence with the maximum conversion of the solar cells permits greater efficiency. Additionally, the expensive and sensitive solar cells are reduced to the smaller area of the LSC edges.[36]

Many of Reisfeld's advantages can be advantages in space. One of the most important inefficiencies in space is the heating of the solar arrays, whether via concentrators or direct solar flux. The heat dissipation advantage of an LSC is therefore a great advantage in space. This topic will be discussed in-depth in Chapter 3, but the large, radiated area of the LSC as compared to the small size of the heat generating solar cell make this advantage worth investigating. Thermal analysis was

simulated using COMSOL Multiphysics software to determine the effects and advantages of the large thermally radiating plate of the LSC, and how the solar cells on the edges could benefit from the more benign thermal environment.

A major consideration for luminophores to be used in space is whether these materials could survive the radiation exposure. Bower's et al. stated, "Organic luminophores, as a rule, exhibit high radiation resistance."[52] Luminescent materials can, in principle, survive in space. Due to limited resources, only certain, available materials were tested for total dose radiation. All of these materials were built in the lab from available supplies. The purpose was not to demonstrate the absolute best material for space, but to show whether some luminophores could be used in a radiation environment.

Based on the literature[53,54,55,56], easy-to-build, thin-film slides were constructed for the radiation exposure tests. The samples were constructed by dissolving the luminophores in a host material, usually Poly(methyl methacrylate) (PMMA), and then spin coating the mixture onto a clear substrate, usually glass or fused quartz. See Figure 2.16 for a picture of the thin-film slides with spin coated luminophores.

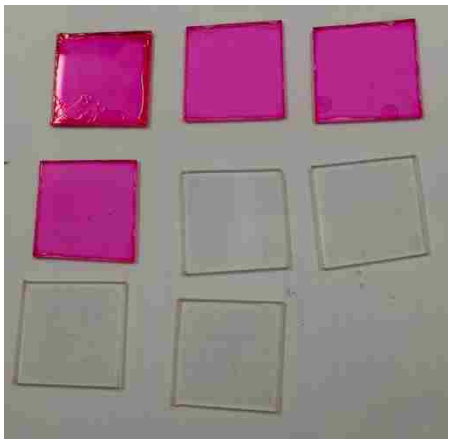

Figure 2.16: Experimental examples of samples with Rhodamine 6G and Large Stokes shift dye

Rhodamine 6G was selected as the primary organic luminophore due to its ease of use and well documented characteristics. Rubrene, Fluorescein, and Cytodiagnostics Large Stokes Shift 500 Dye were also used to explore some other fluorescent materials for comparison. Various in-laboratory-made, inorganic Quantum Dots (QD) were used to explore this emerging area of luminescent material.

Again, the use of luminophores in space products is the primary focus of this research. This area has not been explored due to the current lower efficiencies of the LSC, and the previously mentioned emphasis on performance over cost. The advantage of radiation resistant luminophores coupled with possible thermal benefits could mean a better way to augment or perform power generation for some high radiation space applications.

Chapter 3 Design characteristics of an LSC in space

3.1 Size and shape

LSC systems are influenced by the shape and size of the LSC plate to a greater extent than for solar cells. As presented in Chapter 2, the geometric gain determines the concentration of the LSC system and contributes to the overall efficiency.

Since a circle is the shape that yields the most area while constraining the perimeter, a circle provides the maximum geometric gain of a luminescent plate. The relationship between different shapes and their geometric gains was presented in the work of Bose.[56] Table 3.1 is from his dissertation.

Table 3.1: Geometric gain calculated from geometric principles for four shapes with a thickness of *d*.[56]

Shape	Perimeter	Area	G	G/G_{square}
Square	$4l$	l^2	$\frac{l}{4d}$	1
Equilateral Triangle	$3s$	$\frac{\sqrt{3}}{4}s^2$	$\frac{s}{4\sqrt{3}d}$	$\frac{2}{27^{1/4}} \approx 0.88$
Hexagon	$6s$	$\frac{3\sqrt{3}}{2}s^2$	$\frac{\sqrt{3}s}{4d}$	$\sqrt{\frac{2}{\sqrt{3}}} \approx 1.07$
Circle	$2\pi r$	πr^2	$\frac{r}{2d}$	$\frac{2}{\sqrt{\pi}} \approx 1.13$

As was computed, the circle has the greatest geometric gain for a given area, but due to the difficulty in constructing such an LSC system, other shapes are better suited. A hexagon better approximates a circle, but, similar to the circle, the added gains are not sufficient to justify the difficulties in forming the solar cell edging and

manufacturing as compared to a simple square LSC plate. For the purposes of this study, the square LSC plate was assumed.

After the shape is selected, the size of the LSC plate will greatly influence the efficiency of the system. A study was done by Goldschmidt et al.[57] that altered the area incrementally to illustrate how the changes in size affect the output electrical characteristics of an LSC system. The illuminated area of an LSC with a white bottom reflector was stepwise changed with the use of black blinds. See Figure 3.1 for their sketch of the area changing LSC.

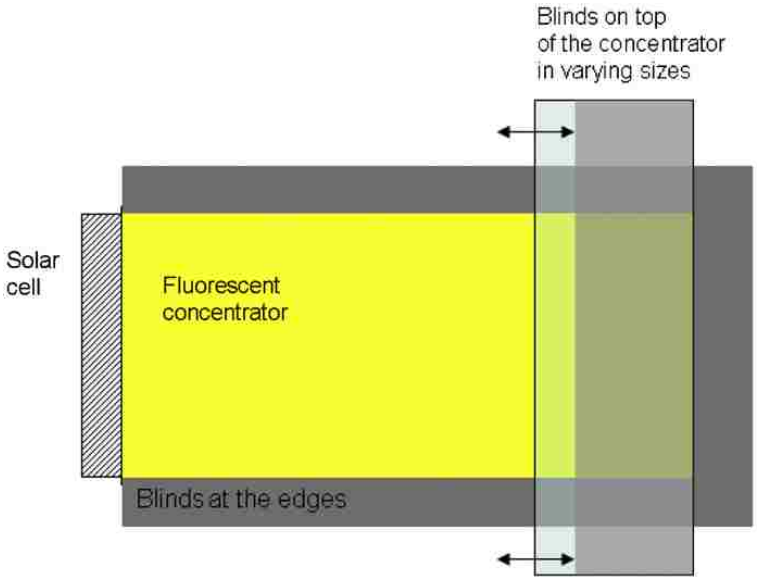

Figure 3.1: Goldschmidt et al. LSC with stepwise alterable area of LSC plate to characterize the changes due to size[57]

At each step, I-V measurements were taken on each side. The short circuit current was calculated with respect to the illuminated area. Figure 3.2 shows the open circuit voltage (V_{oc}) and short circuit current (I_{sc}) for each area.

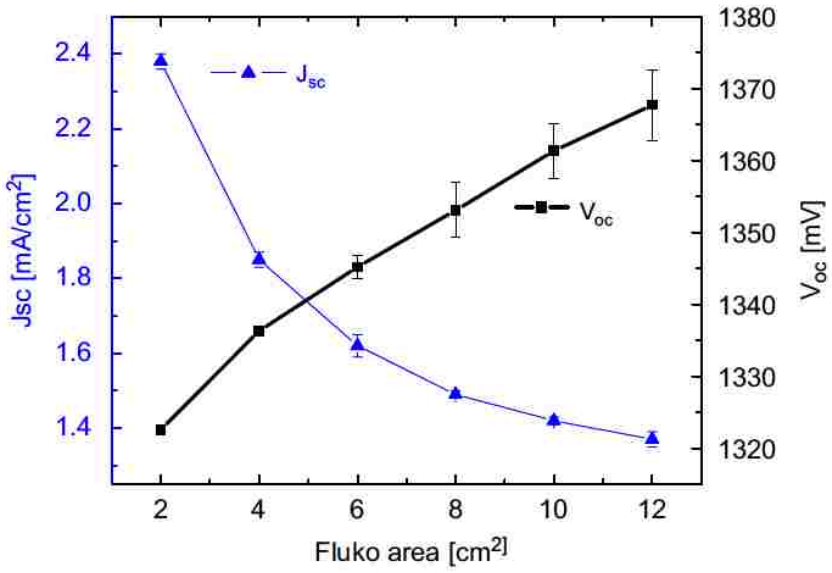

Figure 3.2: Open circuit voltage *Voc* and short-circuit current *Isc* of an LSC system dependence on illuminated area with 3mm thick plate[57]

As seen in Figure 3.2, the V_{oc} increases with increased area. Short circuit current decreases with increasing area due to the increased chances of photon reabsorption in the material and escape cone losses. These results were used as the basis for the sizing of the conceptual design in the current research, and it has been assumed that a more efficient LSC system will have similar I-V characteristics. The LSC system power was computed for each area of the tested LSC system. A power law curve was fit to the data for use on points outside of the original test range, as shown in Figure 3.3. As can be seen, the power generated approaches zero as the area increases, consistent with the increased probability of reabsorption in a larger plate.

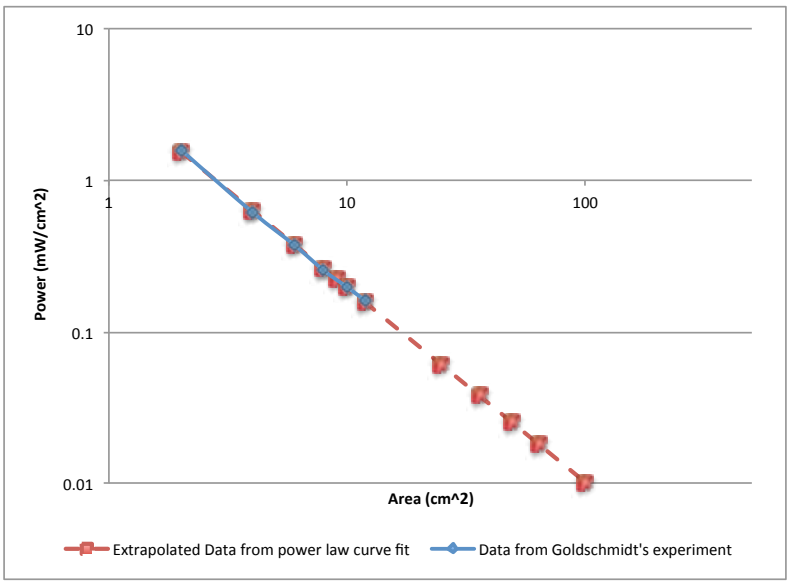

Figure 3.3: Computed power based on area of LSC (blue line) and extrapolated power law curve (red line) used for sizing analysis

Initially, the *pvtrace* ray-tracing program written by Ferrell was used to determine the optical efficiency (as defined in Eq. 2.18) for various sized LSC plates.[58] The *pvtrace* program is a Monte-Carlo ray-tracing modeling written in Python for ease of use versus speed of calculation. A large number of rays are traced through the LSC until the ray is lost from the system or escapes from a surface. Absorption and emission events are governed by material properties, Beer-Lambert law, and randomly generated numbers tested against calculated probabilities. Reflection, transmission, and absorption/reabsorption are taken into account. From Figure 3.4, a thicker, smaller area LSC plate generates a more optically efficient LSC system.

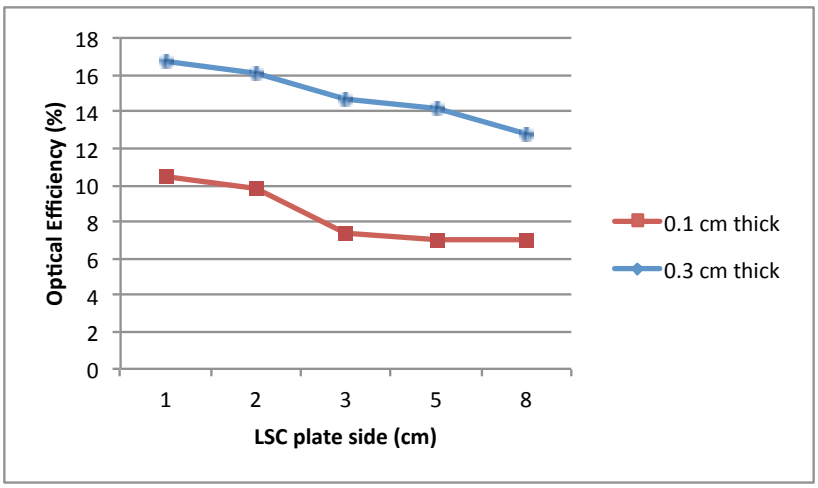

Figure 3.4: Optical efficiency for various sizes and thickness of the LSC plate

The optical concentration (C) was calculated to combine the effects of the optical efficiency and geometric gain.

$$C = G * \eta_{optical} \tag{3.1}$$

where G is the geometric gain and $\eta_{optical}$ is the optical efficiency. Several variations in plate thicknesses as well as size were simulated.

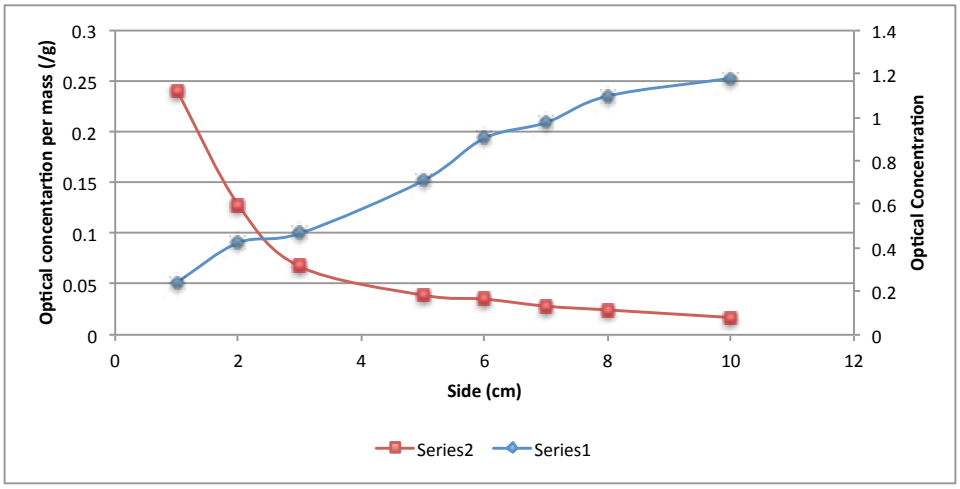

Figure 3.5: Optical concentration and optical concentration per mass for various sized, 1mm thick LSC plates to include thermal effects.

As the size of the LSC plate increases, the geometric gain increases more rapidly than the decrease in optical efficiency. The conclusion is that a larger plate

will increase the performance of the LSC system, but other constraints show that this may not be the final word. From Figure 3.5, the mass to include a 1 cm border on two sides was calculated. Then, the optical concentration per mass was plotted (shown as the red line) along with just the optical concentration (shown as the blue line). In this case, the better LSC system is a smaller, less optically efficient LSC system that maximizes the optical concentration per mass.

A comparison using the extrapolated data from Figure 3.3 determined the power per area and specific power for various sizes of the LSC plate. Figure 3.6 shows the calculated results. As with optical concentration per mass, more specific power is generated for smaller and thinner LSC systems. The conclusion from both analyses is that a small, thin LSC plate is the best to optimize optical concentration and power per area. A thinner LSC plate greatly reduces the optical efficiency (as seen in Figure 3.4) and too small of an area causes a decrease in the power per area (as seen in Figure 3.6). Based on these results, a 2cm x 2cm x 1mm would be the best LSC plate for this application. In Section 3.3.2, thermal simulations were conducted on various sizes to determine if the smaller samples still performed the best.

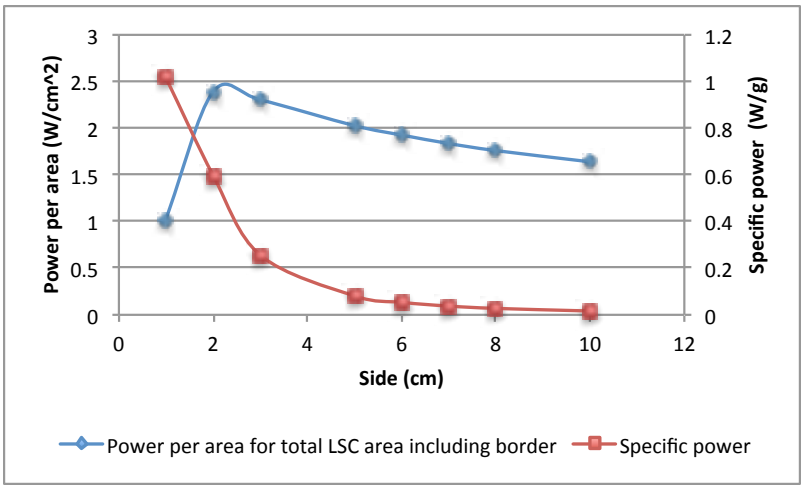

Figure 3.6: Comparison of power per area (blue line) and power per area per mass (red line) for various LSC plate sizes at 1mm thick.

A comparison of LSC sizes under radiation and thermal conditions was then computed for three single junction solar cells. The results are presented in Section 3.5.

3.2 Improvements to LSC efficiency

3.2.1 Selective reflection

One major improvement of the advanced fluorescent concentrator concept is the use of a selective mirror to reduce the losses due to the escape cone of the total internal reflection.[57] The application of a photonic structure on the surface permits the incoming shorter wavelengths to enter the LSC plate, but reflects the longer emitted light within the waveguide material. An example LSC system with a photonic structure from Goldschmidt's work is illustrated in Figure 3.7.

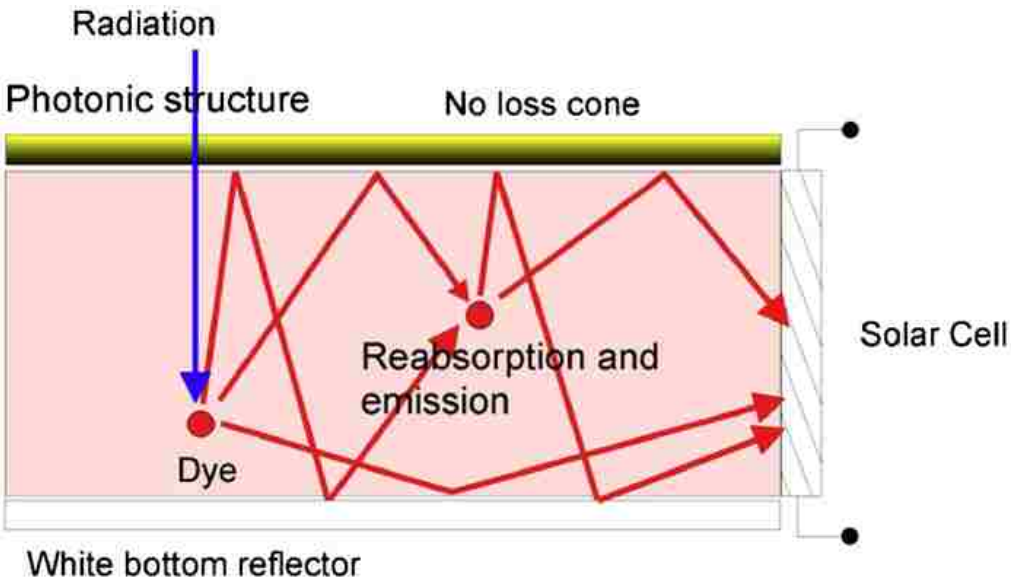

Figure 3.7: Photonic structure that reduce escape cone losses[57]

Cholesteric liquid crystals, Bragg reflectors, and Rugate filters have been used as this selective mirror.[59,48,35,60] Cholesteric liquid crystals create a twist of the light between adjacent layers, resulting in a reflection of a narrow band of light. A Bragg reflector is a structure formed from multiple layers of alternating materials with a varying refractive index, in essence bending the longer wavelength back toward the waveguide. Though similar to a Bragg reflector, a Rugate filter is an optical structure that has a continuous variation of refractive index perpendicular to the plate, thus capturing longer wavelengths within the waveguide and lowering escape cone losses. Simulations have suggested that an ideal selective surface mirror could improve luminescent emission along the LSC plate edges by 50%.[35]

In practical photonic structures, the emission of the luminophores is well matched, but not all photons are reflected within the structure. The first experiment from previous works was to compare the emission band to a possible photonic structure to see the feasibility of such a structure. As seen in Figure 3.8, from the

work of Goldschmidt et al, a properly designed photonic structure that matches the emission and filter is quite realistic.

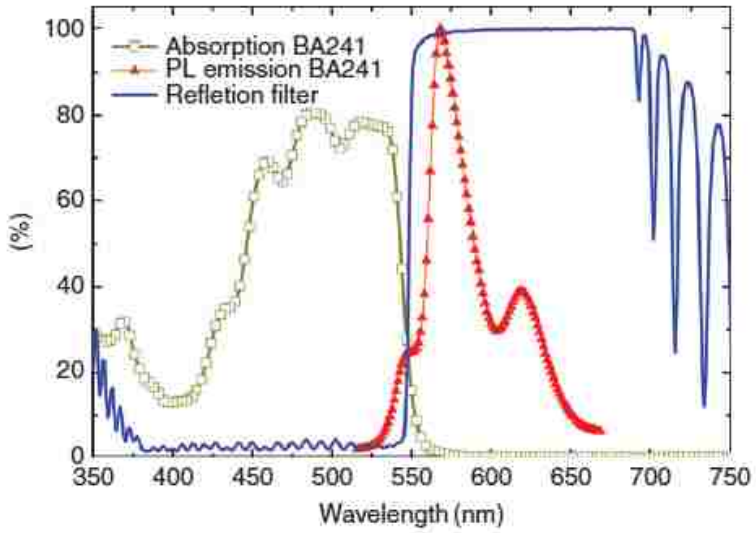

Figure 3.8: Photonic structure and emission matching for a BA241 luminescent dye[61]

Experiments with cholesteric coatings have shown an increase in edge emission of ~12%.[59] As depicted in Figure 3.9, a signal strength experiment showed a relative increase of 20% after adding a Rugate filter to the surface of the LSC plate. These previous works indicate one way in which an LSC system can improve its capability.

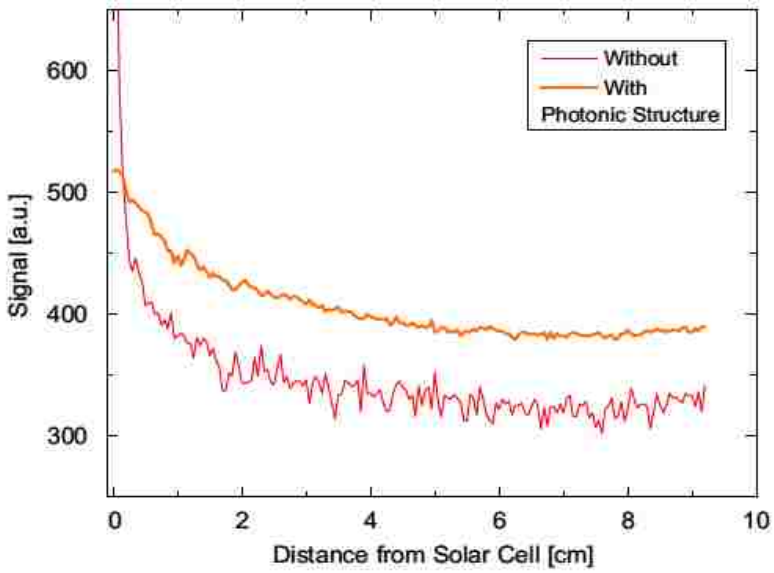

Figure 3.9: Averaged line scans of 2cm x 2cm x 3mm LSC using four InGaP solar cells with and without a surface photonic structure. [57]

3.2.2 Back Mirrors

The use of a reflective surface on the back of the LSC plate was one of the first experiments to improve its external quantum efficiency (EQE). EQE is the ratio of the number of carriers collected by the solar cell to the number of incident photons of a given energy. "The reflecting back layer effectively doubles the path length of the incident light through the dye layer for enhanced absorption."[57] Again, from work of Goldschmidt et al., improvements in an LSC's light utilization and efficiency have been demonstrated by the use of reflective surfaces on the back side of the waveguide. Figure 3.10 compares the effect of a white, reflective bottom to a black, non-reflective bottom.

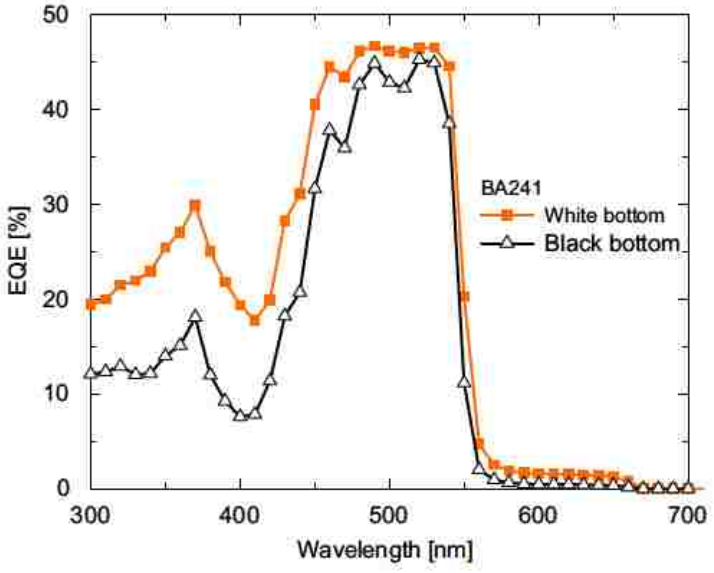

Figure 3.10: Comparison of EQE for white bottom reflector and a black bottom.[57]

Positioning of the reflector is also important to get the best use from the LSC. Goldschmidt et al. performed an experiment that varied the distance from the back reflector to the solar cell. As can be seen in Figure 3.11, the distance from the back reflector to the solar cell significantly increases EQE. Another improvement in EQE was shown to be from the back reflector reflecting light directly onto the solar cell.[57] These two experiments show a strong case for the use of a reflective back surface to improve LSC performance.

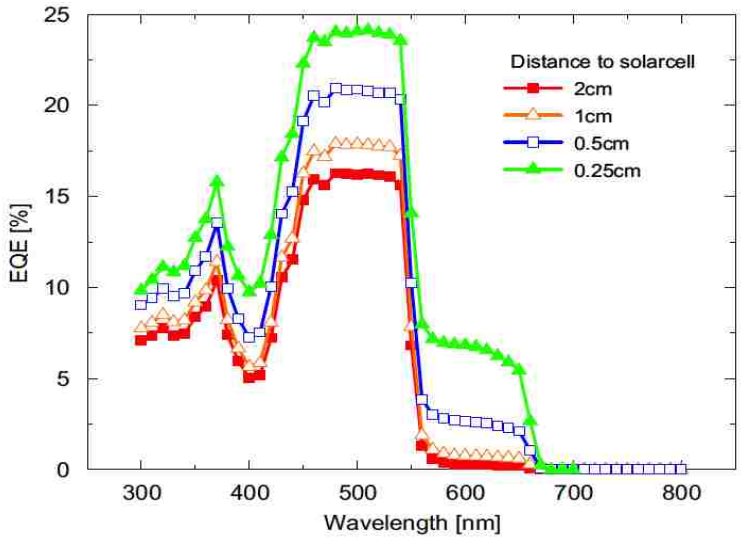

Figure 3.11: External Quantum Efficiency measurements of an LSC with white bottom reflector at different distances to the solar cell.[57]

3.3 Thermal Effects

As noted in the previous Chapter 2, the thermal environment creates many issues for spacecraft. Thermal regulation using radiation is the only method for shedding unwanted energy to outer space. In current solar cell arrays, the operating temperatures of the solar panels are higher than the optimal conditions. This means that the solar cell operates at a lower efficiency, in effect degrading the solar cell function due to heating of the material. In a solar cell, only a fraction of the incoming photon energy is needed to liberate an electron-hole pair. The remaining energy is wasted, and mostly converted to heat energy.

In a simple explanation of the temperature dependence of solar cells, an increase in temperature causes a reduction in the band gap of the material. The decrease in the band gap means that less energy is needed to form an electron-hole

pair. The result is an increase in the short circuit current, but a decrease in the open circuit voltage. Figure 3.12 is the generic I-V curve changes due to increasing the temperature on solar cells.

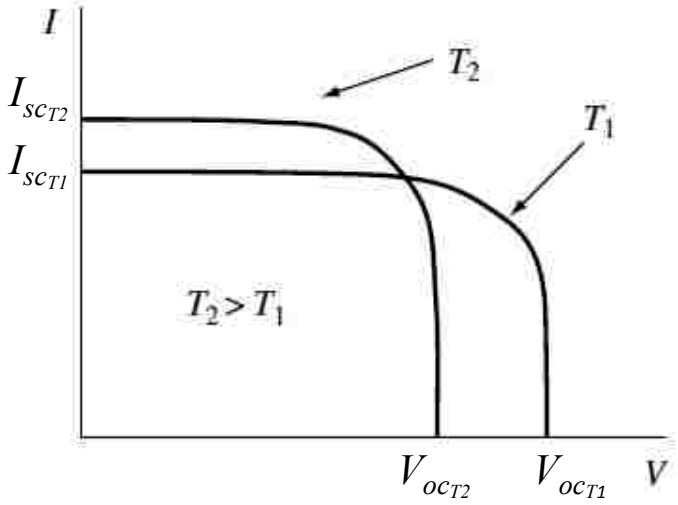

Figure 3.12: Effects of increasing temperature on solar cell I-V response[62]

An analysis for Si solar cells was conducted to see how the temperature decreases associated with an LSC could affect the system. Reviewing the "Effects of Temperature" on the PV education website,[63] the changes in open circuit voltage (V_{OC}), short circuit current (I_{SC}), and fill factor (*FF*) due to temperature (*T*) increases can be calculated from the following equations:

$$\frac{dV_{OC}}{dT} = -\frac{V_{BG_0} - V_{OC} - \gamma\frac{kT}{q}}{T} \approx -2.2mV\ /\ ^\circ C \qquad (3.2)$$

for Si, where V_{BG_0} is the band gap voltage, γ is a constant that incorporates other thermal dependencies, *k* is the Stefan–Boltzmann constant, and *q* is the electronic charge.

$$\frac{1}{I_{SC}}\frac{dI_{SC}}{dT} \approx 0.0006\ /\ ^\circ C \qquad (3.3)$$

for Si for normalized current.

$$\frac{1}{FF}\frac{dFF}{dT} \approx \frac{1}{V_{OC}}\frac{dV_{OC}}{dT} - \frac{1}{T} \approx -0.0015/\,^{\circ}C \tag{3.4}$$

for Si for normalized Fill Factor. The Fill Factor is the ratio of the maximum power from the solar cell to the product of V_{OC} and I_{SC}. Fill Factor, along with the V_{OC} and I_{SC}, determine the maximum power. Therefore, the effect on maximum power (P_m) is:

$$\frac{1}{P_m}\frac{dP_m}{dT} \approx \frac{1}{V_{OC}}\frac{dV_{OC}}{dT} + \frac{1}{FF}\frac{dFF}{dT} + \frac{1}{I_{SC}}\frac{dI_{SC}}{dT} \approx -0.004/\,^{\circ}C \tag{3.5}$$

for Si. Thus, the net result is that max power decreases as temperature increases. In other words, as temperature decreases, the solar cell maximum power and efficiency increases.

For an understanding of the temperature benefit on solar cell efficiency, a quick calculation of a Si solar cell was done. A change of -50 ^{o}C results in a power increase of ~20%. Assuming the incident power flux does not change, a Si solar cell with a 14.7% efficiency at standard temperature will improve its efficiency to over 17% by decreasing its temperature by 50 degrees. Increasing the efficiency of the solar cell will, in turn, improve the efficiency of an LSC system. This benefit will be examined in more detail in Section 3.3.3.

The solar cell temperature effects were explored extensively in the work of Guenette.[64] He calculated the effects of temperature on solar cells, and then used experiments to show the real effects. Figure 3.13 shows this relationship between temperature and solar cell efficiency, as drawn from his thesis.[64] The theoretical and experimental values match to within experimental error down to 150 K, which is well within the range of the simulated LSC's solar cell temperatures.

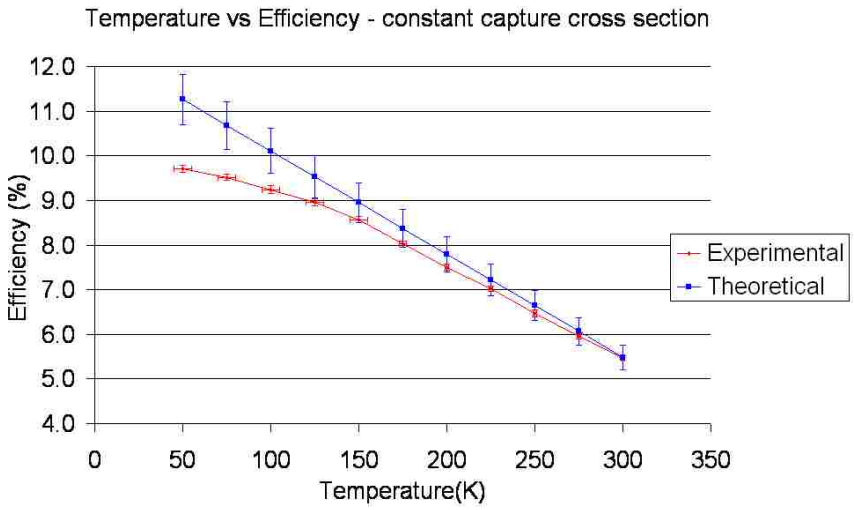

Figure 3.13: Theoretical and experimental temperature effects on solar cell efficiency[64]

Guenette also calculated the Shockley-Queisser efficiency limits at different temperatures based on band gap energy.[64] The Shockley-Queisser limit refers to the maximum theoretical efficiency of a solar cell using a p-n junction.[65] Figure 3.14 illustrates the theoretical potential for different band gap energies to improve their performance as temperature decreases.

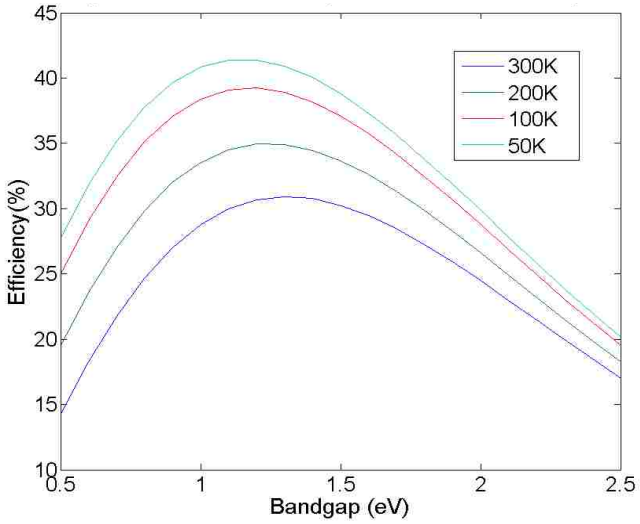

Figure 3.14: Calculated solar cell Shockley-Queisser efficiency limit for different temperatures.[64]

In order to reduce the effect of higher temperatures on the solar cell efficiency, two methods used in an LSC can improve the solar cell efficiency -- reducing the size of the heat generating parts and reducing the ratio of heat generation area to thermal radiating area. The current proposed LSC approach accomplishes both. As previously stated in Section 3.2, a diffuse bottom mirror is used to improve the chances of a photon striking a luminophore and creating an emission of proper wavelength for the material. Thus, the incident light is mainly used in the optical down conversion or is reflected through the material, versus being absorbed by the material as heat. Also, due to the nature of the luminescent process of down conversion, the energy loss due to conversion is minimal. The conclusion is that the LSC does not have as much wasted energy being converted into heat by the material, and the down-conversion processes are inherently thermally efficient.

In a typical solar array design, the front of the array faces the sun and the back side is used to radiate excess heat to space. In essence, the heat-removing radiator has the same area as the heat generating solar cells in the array. For solar panels in near continuous sun exposure, thermal equilibrium is in excess of 100°C. This high operating temperature reduces the efficiency of the solar cells, as shown in Table 3.2, which lists the measured temperature coefficients for various solar cells.

Table 3.2: Measured temperature coefficients for various solar cells[66]

Cell type	Temp [°C]	η (28°C)	$(1/\eta)(d\eta/dT)$ [$\times 10^{-3}$/°C]
Si	28–60	0.148	−4.60
Ge	20–80	0.090	−10.1
GaAs/Ge	20–120	0.174	−1.60
2-j GaAs/Ge	35–100	0.194	−2.85
InP	0–150	0.195	−1.59
a-Si	0–40	0.066	−1.11 (nonlinear)
$CuInSe_2$	−40–80	0.087	−6.52

In an LSC, the ability to shield the solar cells from the direct sunlight exposure, match the solar cell spectral response to the light emitted by the LSC's luminophores, and reduce the area of the solar cell could greatly reduce the operating temperature for the solar cells. A simple thermal resistive model, followed by further analysis using COMSOL's Multi-physics software, was used to illustrate these advantages in Sections 3.3.1 and 3.3.2.

3.3.1 Simple Thermal Resistive Model

A simple one-dimensional (1D) resistive model was used to understand if such thermal improvements would be effective at improving LSC performance and solar cell efficiency. See Figure 3.15 for the model representation.

Due to conservation of heat energy, in steady-state the heat transfer in must equal the heat transfer out ($\dot{q}_{in} = \dot{q}_{out}$). The resistive heat flux equation is:[67]

$$\frac{\dot{q}}{A} = \frac{\sigma\left(T_{in}^4 - T_{out}^4\right)}{\frac{1}{F} + \frac{1-\varepsilon_1}{\varepsilon_1} + \frac{L}{k} + \frac{1-\varepsilon_2}{\varepsilon_2} + \frac{1}{F} + \frac{1-\varepsilon_3}{\varepsilon_3} + \frac{1}{F}} \qquad (3.6)$$

where σ is the Stefan-Boltzmann constant, F is the view factor (1 in this case), ε_1 is the high emissivity from a heat shedding paint, ε_2 is the emissivity of a highly reflective surface, ε_3 is the emissivity of the quartz plate, L is the thickness of the aluminum plate, and k is the thermal conductivity of the aluminum plate.

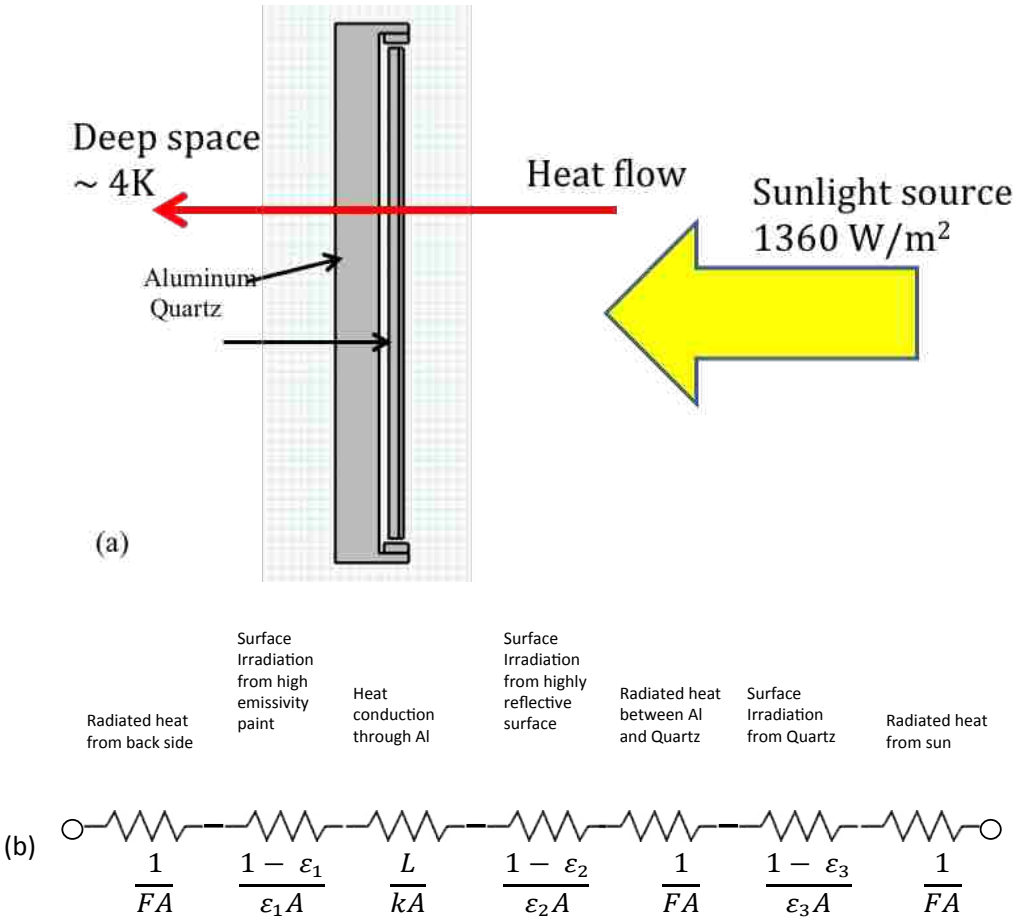

Figure 3.15: (a) Cross section of 1D thermal calculation. (b) Thermal resistive representation of 1D LSC

An analysis was done with the results showing that there can be a great thermal advantage to an LSC system versus a typical solar array. Assuming a deep space temperature of 4 K, the resulting surface temperature is 408 K from the 1360 $\mathrm{W/m^2}$ incident sunlight, and the aluminum plate temperature was calculated to be 171 K. With proper thermal shielding to the incoming light source and good thermal

conductivity between the solar cell and aluminum plate, a much more efficient operating temperature for the solar cell is possible, improving the overall efficiency of the LSC system. Due to the simplistic nature of the 1D model, simulations were conducted to better understand the thermal environment.

3.3.2 Thermal Simulations

Based on the simple model, a more complete 2D model was built in COMSOL's Multiphysics 4.4 simulation software. The software has the capability to take into account the coupled thermal radiation effects between the various plates of the LSC, and it provides a first order analysis of orbital variations. Simulations were initially conducted to thermal equilibrium. The equilibrium test was used to emulate a continuous sun exposure such as would be found at GEO. Using the time dependent modeling in the software and running multiple simulations using the output of a previous simulation as the input parameters, the results provide a thermal analysis based on a sample orbit. This orbital analysis characterized the highest and lowest temperatures expected on an orbit similar to TACSAT4, a 4-hour orbit with an approximate half-hour eclipse.

The first simulations were conducted on the simple plate with full sun exposure at equilibrium to see how the luminophore plate, the aluminum plate, and the thin solar cell plate interacted. See Figure 3.16 and Figure 3.17 for the progression of modeling used. The surface radiation application in COMSOL's heat transfer module was used with an incoming power flux of $1360\ W/m^2$, an ambient temperature set for deep

space (4 K), and emitted radiation in the positive normal direction. The heat gap conduction was set to zero due to the vacuum environment.

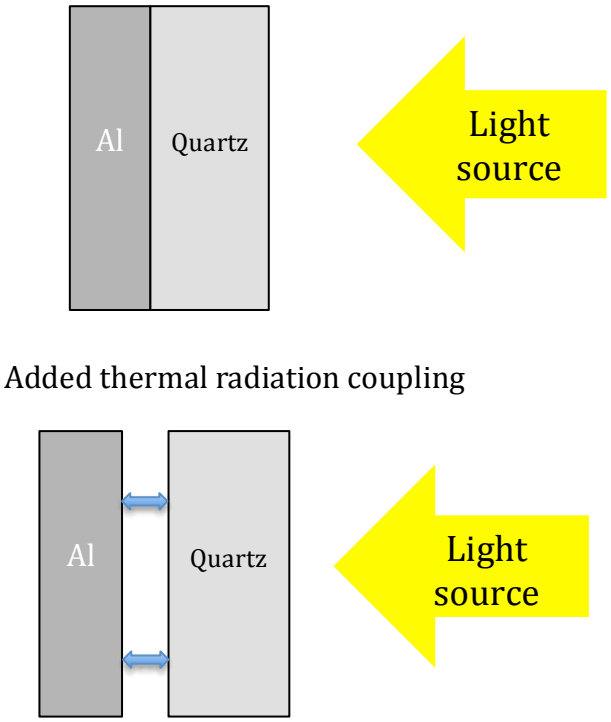

Figure 3.16: Thermal coupling of Aluminum and Quartz plates, with contact and without contact (not to scale)

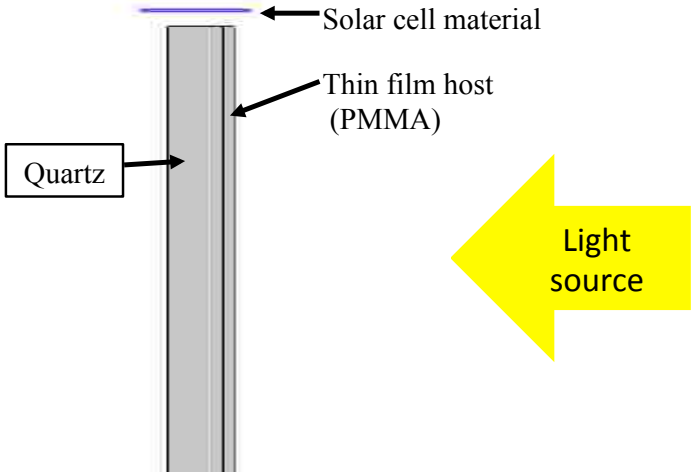

Figure 3.17: First simulation showing thermal coupling of solar cell, quartz substrate, and host material

By narrowing the solar cell exposure to the incident light, the temperature of the solar cell was markedly less than the overall temperature of the system. This initial model demonstrated the changes for the solar cell but was not very accurate in its structure.

To improve on the fidelity of the results, new models were built to better represent the physical structure as depicted in Figure 3.18(a).

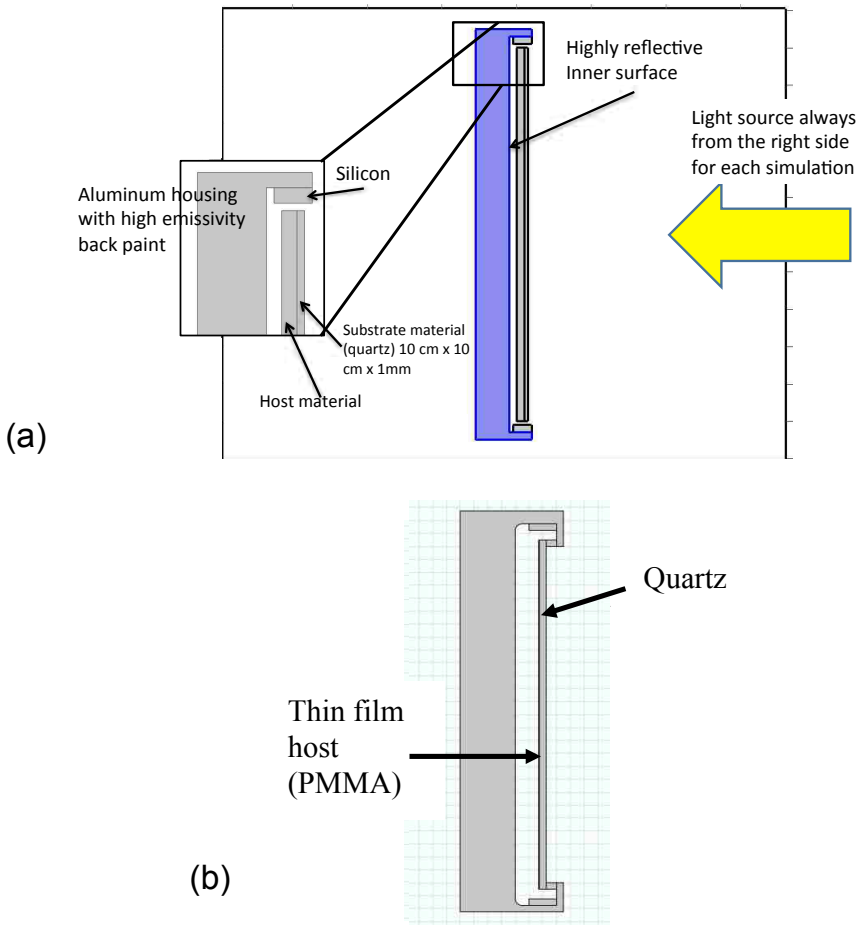

Figure 3.18: Progression of improvements to updated model incorporating thin film, quartz substrate, solar cell material, and aluminum housing, (a) Incorporated highly emissive back surface and highly reflective front surfaces. (b) Moved quartz substrate in front of host material and added connection elements to the LSC plate.

This new model incorporated an aluminum structure for housing, high emissivity paint on the back side of the aluminum structure, a mirrored surface behind the

luminophore plate, and a semi-conductive material (silicon) on the edges to represent solar cells. The final model version placed the luminophores on the interior of the substrate, and added connecting pieces from the substrate to the aluminum frame, as shown in Figure 3.18(b).

A software-defined "finer" mesh was selected to capture any small changes in the structure. See Figure 3.19 for mesh and stacking representation.

Figure 3.19: Simulation mesh defining solution points for simulation. The figure shows two adjacent LSC's.

A set of LSC systems was stacked on each other to represent the mutual coupling between individual systems. The stacking of two did have an appreciable effect, but a third did not vary the individual systems much – about 2 degrees, depending on the size of the LSC. See Figure 3.20 and Figure 3.21 for the progression of thermal changes as stacking was increased on a 2cm x 2cm x 1mm and 5cm x 5cm x 1mm LSC system, respectively. Due to the minor temperature change

and a substantial increase in computational complexity, an LSC system stack of two was used as the baseline for the thermal analysis.

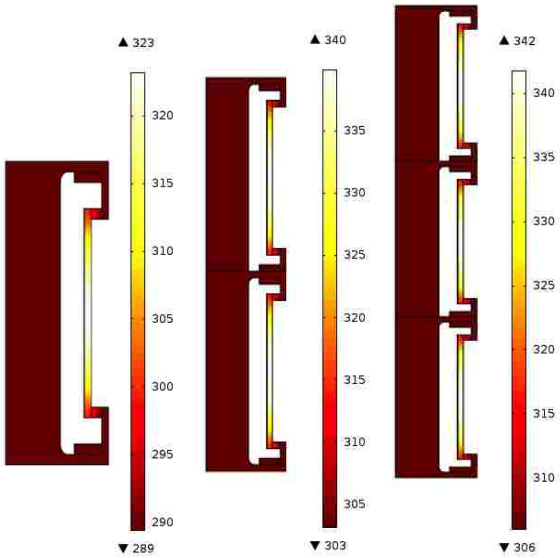

Figure 3.20: Thermal changes caused by stacking of an LSC system for a 2cm x 2cm x 1mm LSC plate (not to same size scale)

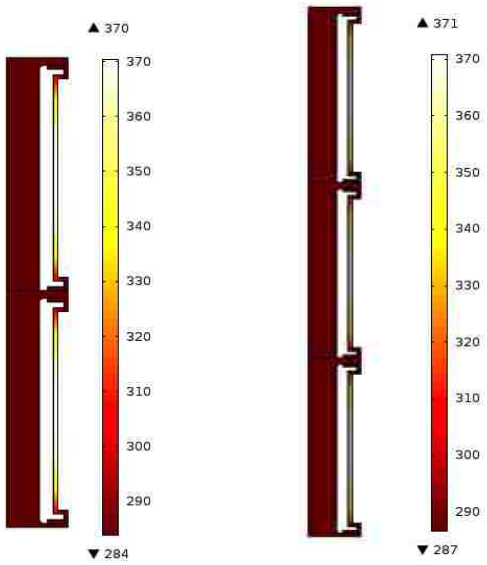

Figure 3.21: Thermal changes caused by stacking of an LSC system for a 5cm x 5cm x 1mm LSC plate (not to same size scale)

Temperature simulations showed a shift toward a cooling effect from the standard temperature for the solar cell material. The increased radiation area and

small incident cross section demonstrate that any solar cell would operate at a much more favorable temperature regime, thus improving its efficiency, and therefore the overall efficiency of the LSC.

One of the first simulations was to compare different sizes of LSC's, based on the assertion of Section 3.1 that size does matter. Since this model is two-dimensional, only the size of a double stack model, not shape, was simulated. Each simulation was conducted to thermal equilibrium. See Figure 3.22 for the results.

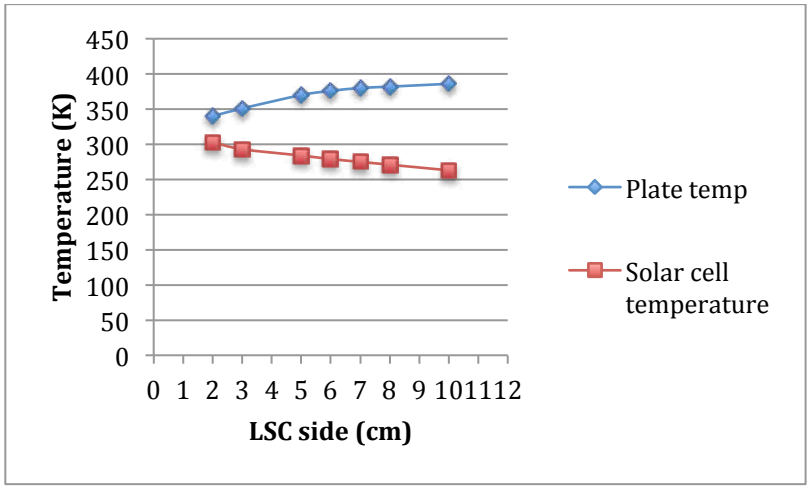

Figure 3.22: Equilibrium Temperature simulation based on LSC size

As may be seen, the peak system temperature approaches a maximum equilibrium point based on LSC size, while the low temperature continues to decrease with size. Intuitively, with the same amount of incoming energy and an increasing amount of radiating surface, the equilibrium temperature will continue to decrease with increasing area.

Based on these results and previous discussions about sizing, a 2cm x 2cm x 1mm LSC plate should develop the most power per area, while keeping the mass near a solar cell with cover glass. To further that thermal analysis, a 5cm x 5cm x 1mm

plate is also represented in the following sections for a comparison in overall LSC performance.

After the preferred size to be used for analysis was determined, a series of simulations were conducted to determine the changes in temperature based on orbital heating and cooling. A medium altitude orbital regime was selected for simulation, offering a more diverse temperature dynamic than a GEO spacecraft and keeping with the orbit of TACSAT4. The simulations were completed iteratively using the previous output of the thermal cycle as the input for the next thermal cycle. The sun-exposed simulation was run for 210 minutes, followed by a 30-minute eclipse period, until maximum and minimum points were established. It took a single orbit to establish the high and low values for this orbit. It was observed that the high temperature was reached approximately one hour after direct sun exposure. The value of the LSC plate varied greatly, from 264 K to 370 K. See Figure 3.23 and Figure 3.24, respectively. Table 3.3 summarizes the temperature changes for a 2cm x 2cm x 1mm and for a 5cm x 5cm x 1mm plate size. This temperature simulation shows that the solar cell in the LSC will be operating at a much more favorable condition than if it is exposed to direct sunlight. As previously stated in Chapter 1, the operating temperature of the solar cells for most GEO satellites is around 116 ^{o}C or 389 K

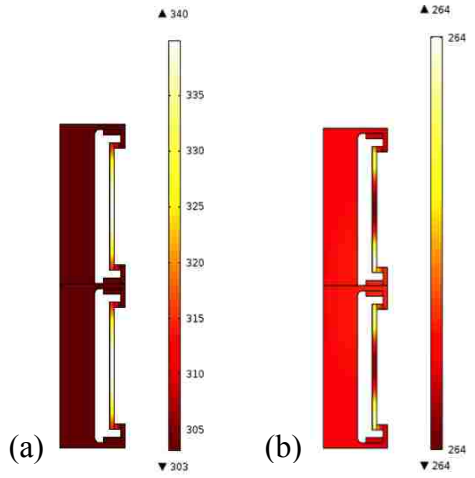

Figure 3.23: Orbital temperature changes for 2x2x0.1 cm^3 LSC system for (a) 210 minute full sun exposure (b) 30-minute eclipse.

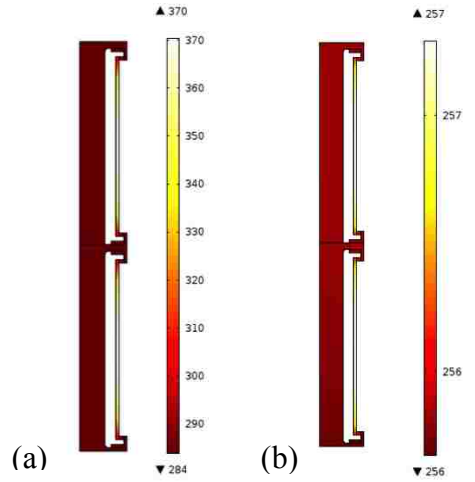

Figure 3.24: Orbital temperature changes for 5x5x0.1 cm^3 LSC system for (a) 210 minute full sun exposure (b) 30 minute eclipse.

Table 3.3: Simulated temperature changes in a two-stacked LSC system for 210 minute solar exposure followed by 30-minute eclipse.

	LSC plate		Aluminum plate and solar cell	
	Low Temperature (*K*)	High Tempertaure (*K*)	Low Temperature (*K*)	High Tempertaure (*K*)
LSC plate size				
2cmx2cmx1mm	264	340	264	303
5cmx5cmx1mm	257	370	256	284

3.3.3 Thermal Effects on Efficiency

As shown in the previous two subsections, the thermal characteristics are very different for an LSC versus a standard solar panel. The temperature trade space is that the luminophores are exposed to a different temperature range while the solar cells operate in a colder regime. The light absorption and emission could not be simulated in the thermal model. A literature search showed that most luminophores degrade with temperature due to the intramolecular conversion of the excitation energy into vibrational energy.[62] This degradation in the luminescent conversion could mean loss of the solar cell improvements. Figure 3.25 was an experiment conducted by Meseguer et al. on the changes to optical density of Rhodamine B due to temperature changes.[68] Figure 3.25(a) is the absorption and emission loss of the material with increasing temperatures. Figure 3.25(b) is the optical density characteristics of the material at different temperatures. The initial losses recover over an extended time. The process is thought to be caused by the rise in aggregation of the dye molecules.[68] In Meseguer et al.'s work, Rhodamine 6G was also tested. Meseguer et al. stated that at no time did it decrease by more than 14% up to 94 ^{o}C. So, the thermal characteristics of the luminescent material must be considered, but previous work shows that temperature tolerant material is available. This topic is further addressed in Section 3.5.2. A luminescent material with a low thermal coefficient would make for the best selection in a space LSC.

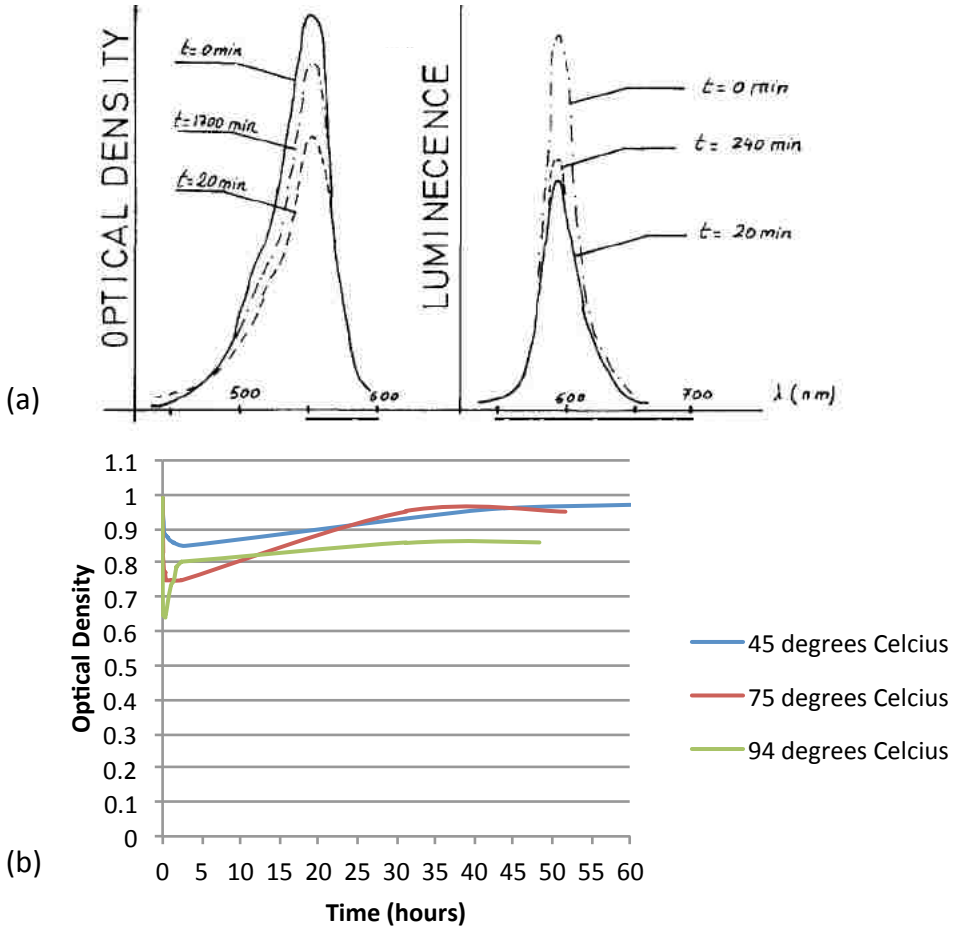

Figure 3.25: Optical Density changes as temperature increases for Rhodamine B. (a) From the original paper, showing the absorption and emission losses over time for Rhodamine B at 94 °C. (b) Derived from the original paper, showing the optical density recovery at three temperatures over time. The initial heating process is caused by the rise in aggregation of the dye molecules.[68]

LSC systems have the potential to be thermally effective for another reason -- solar cell spectral response matching. Even though the enhanced performance generated from matching the spectral response to the output of the waveguide of the LSC plate may be limited due to the generally broad response of many solar cells, the matching reduces the heat loads to the solar cell.[35] This matching of LSC emission output and solar cell spectral response is shown in Figure 3.26. Since the blue line represents the emission of the luminophores in this example, the solar cell would

convert nearly all incoming spectrum into output, thus not wasting energy that would become unwanted heat.

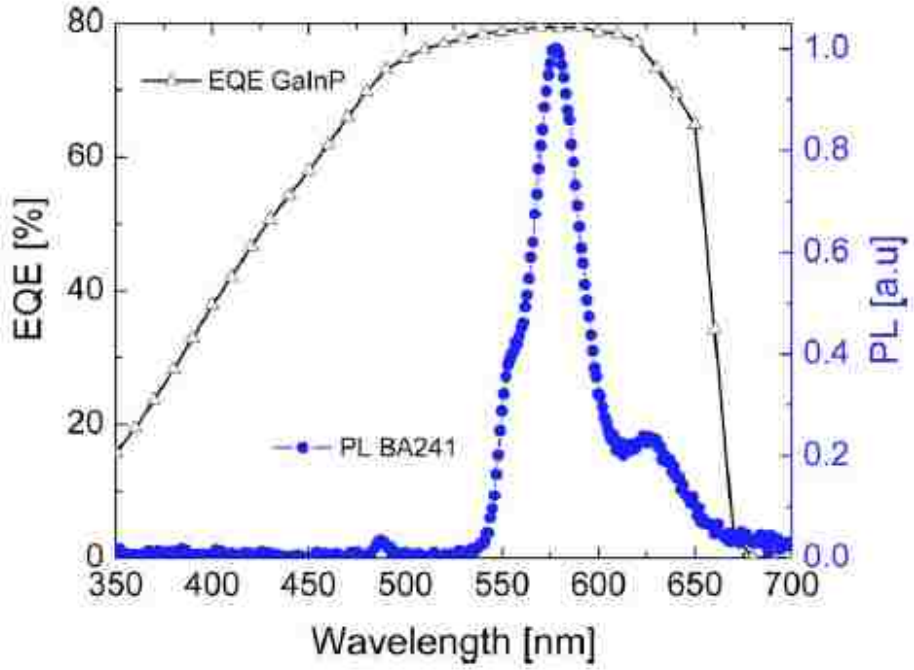

Figure 3.26: The EQE of one InGaP solar cell and photoluminescence spectrum of dye BA241.[33]

Other luminophores can be developed that would better match the spectral response of various solar cells. The effect is a more efficient LSC system with a solar cell operating at more conducive temperatures.

For the thermal effects on this luminophore, *Polymers, Phosphors, and Voltaics for Radioisotope Microbatteries*[52] was consulted to ascertain the temperature effects on many luminophores. Based on its many examples, luminophores have a temperature coefficient range from -0.05 to -1.49 %/^{o}C for temperatures between + 30 ^{o}C to -70 ^{o}C. As stated in the book, there are many different reportings on the various temperature coefficients, but, while this range does not cover the simulated ranges, these linear coefficients can provide a rough extrapolation of the changes in light

output corresponding to the temperature.[52] A representative assumption was reached to consider a luminophore with a -0.2 %/°C temperature coefficient. With this assumption, the optical efficiency will degrade due to the higher temperature range.

The differences in the thermal properties of the luminophores and solar cells produce a design that is temperature independent of size, as shown as the blue line in Figure 3.27. The factor of change in Figure 3.27 is multiplied by the original efficiency of the material in question to determine how it changes from the original efficiency. The temperature used for these calculations is the temperature determined from the various simulations previously discussed in Section 3.3.3.

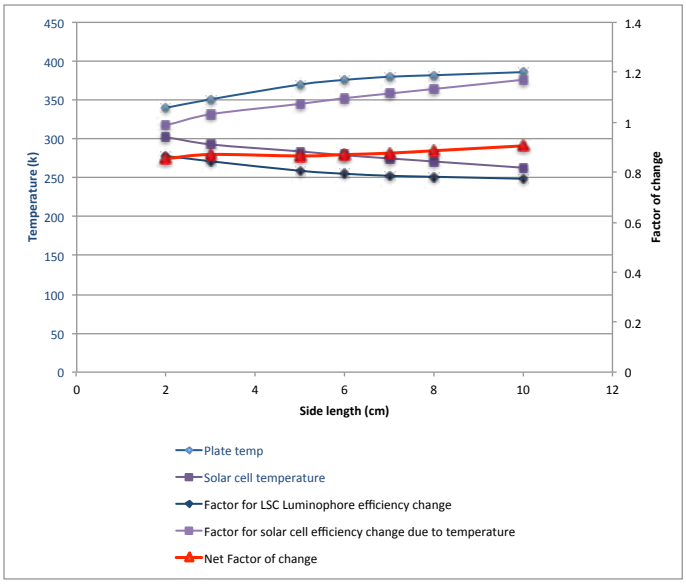

Figure 3.27: Calculated temperature effects on various sizes of a 1mm thick LSC plate. The blue line represents the changes to the luminophores in the LSC plate. The purple line represents the changes to the solar cell. The red line is the net result of luminophore and solar cell factors, showing that temperature effects have minimal changes with LSC plate sizes.

3.4 Radiation Degradation

One of the advantages of the LSC system is that the radiation sensitive solar cells can be better shielded from most forms of irradiation. As discussed in Chapter 2, the extreme high-energy particles will penetrate most materials, but their low fluxes make them negligible. For lower energy radiation particles, the design of the LSC system naturally shields the solar cells, exposing them to only a fraction of the radiation environment. The assumptions for determining the amount of radiation exposed are:

1. The radiation source is omnidirectional.
2. The aluminum case is relatively thick (mm versus mils) so it will block most low and medium energy particles.
3. The only exposed part of the solar cell is covered by the LSC plate, acting as a shield.

This reduced exposure and shielding of the solar cell represents a great system level radiation tolerance and an improved end of life (EOL) performance for the LSC system.

While the experimental effects on the luminescent materials are presented in the next chapter, the efficiency changes of thermal and radiation effects are presented in the next section.

3.5 Efficiency Changes

In order to compare an LSC system to a solar cell system, efficiencies of the different systems are used. The emphasis is on the thermal and radiation effects, knowing that micrometeoroid/orbital debris, atomic oxygen, and other space environmental effects would also alter the overall efficiency of both systems. Using the simulated thermal results and well-known radiation effects, a comparison of the LSC system and high-end space solar cells is presented.

3.5.1 Solar Cell Efficiency Changes

To emphasize the high orbital radiation levels, Bailey and Raffaelle's chart from *Space Solar Cells and Arrays*[62] shows the reduction in power density at various altitudes for a ten year mission. See Figure 3.28. In the strongest radiation regions around the 5000 km altitude, the EOL power is greatly degraded as compared to other operating regimes.

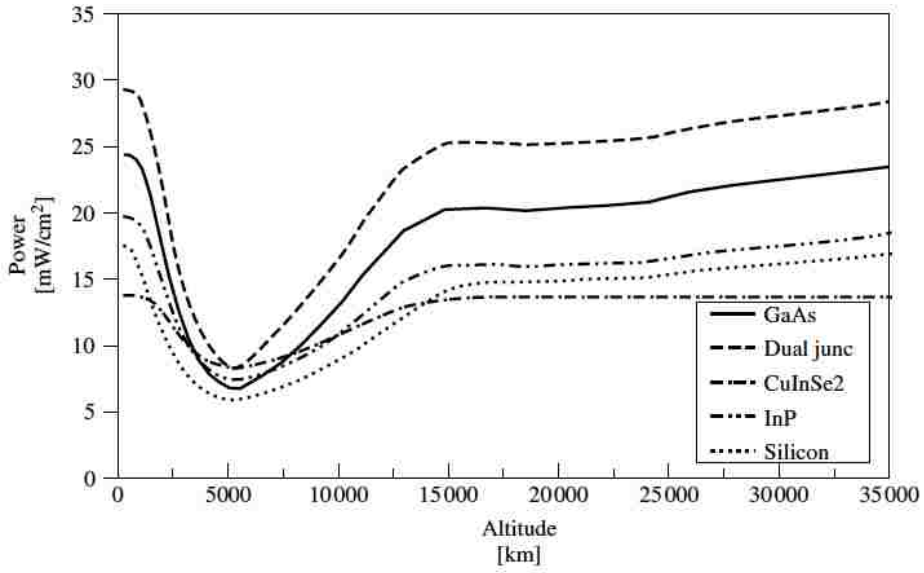

Figure 3.28: Solar cell power density as a function of altitude after 10 years in a 60° orbit with a cover glass thickness of 300 µm.[62]

Using the SPENVIS website,[16] GEO and MEO examples were examined for their radiation exposure to what would be encountered. The SPENVIS website† uses the AP8/AE8 models and the SHIELDDOSE 2 program to estimate the equivalent 1 MeV electron fluence, based on orbital parameters and the mission's life. Table 3.4 summarizes this information from the available solar cells with various cover glass protections and calculated total ionizing doses for a sample 1-year mission life at a GEO and a MEO equatorial orbit.

† SPENVIS is European Space Agency's Space Environment Information System, an internet interface to models of the space environment and its effects. It is accessible through https://www.spenvis.oma.be.

Table 3.4: Equivalent radiation exposure for different shielding for a GEO and MEO circular orbits for a 1 year mission life generated from the SPENVIS website.[16]

Orbit (zero inclination at altitude)	Solar cell Material	Shielding (μm)	Equivalent 1 MeV electron fluence (e/cm^2)	Calculated Effective Total Mission Dose based on Si conversion (Mrad(Si))
GEO (32,000 km)	Emcore ATJ[1]	25	4.781E13	3.82E+00
		76	3.888E13	3.11E+00
		152	3.082E13	2.47E+00
		304	2.104E13	1.68E+00
		1000[2]	5.47E12	4.38E-01
	GaAs	25	6.083E13	4.87E+00
		76	4.777E13	3.82E+00
		152	3.768E13	3.01E+00
		304	2.589E13	2.07E+00
		1000[2]	7.589E12	6.07E-01
	Si	25	5.966E13	4.77E+00
		76	4.810E13	3.85E+00
		152	3.807E13	3.05E+00
		304	2.628E13	2.10E+00
		1000[2]	7.785E12	6.23E-01
MEO (10,000 km)	Emcore ATJ[1]	25.4	6.900E17	5.52E+04
		76	7.319E16	5.86E+03
		152	1.220E16	9.76E+02
		304	1.682E15	1.35E+02
		508	4.424E14	3.54E+01
		1000[2]	6.744E13	5.40E+00
	GaAs	25	1.106E18	8.85E+04
		76	1.089E17	8.71E+03
		152	1.732E16	1.39E+03
		304	2.481E15	1.98E+02
		508	6.674E14	5.34E+01
		1000[2]	8.377E13	6.70E+00
	Si	25	1.561E18	1.25E+05
		76	2.524E17	2.02E+04
		152	5.319E16	4.26E+03
		304	8.900E15	7.12E+02
		508	2.054E15	1.64E+02
		1000[2]	7.785E12	6.23E-01

[1] Selected due to only Emcore multi junction solar available in SPENVIS
[2] Presented for use in the LSC system with 1mm of Fused Silicon acting as a shield of solar cell
[3] Though not completely equitable, the conversion from 1 MeV electron fluence to total dose is based on the 1.25e13 e/cm^3 for 1 Mrad(Si)[69]

From Table 3.4, the high levels of 1 MeV electron fluence cause the displacement damage characteristic of the degradation of solar cells at MEO altitudes.

The exposed solar cells degrade from the displacement damage caused by the particle fluence. The LSC luminophores are expected to degrade from the formation of color centers, due to the ionizing radiation. To illustrate how a solar cell degrades, Table 3.5 shows the change in solar cell efficiency calculated from the Emcore ATJ datasheet.[13] The Emcore ATJ solar cell will lose over 10% of its efficiency even with a thick shield of 0.5 mm.

Table 3.5: Calculated Emcore ATJ solar cell efficiencies after radiation exposure.

1 MeV electron fluence (e/cm^2)	Emcore ATJ solar cell efficiency (%)	Percent change
0	27.5	0.0
5E+13	26.7	-3.0
1E+14	26.4	-4.0
5E+14	24.3	-11.7
1E+15	23.3	-15.4
3E+15	20.6	-25.2

The radiation advantage of the LSC system is the shielding effect of the aluminum encasement and luminescent plate protecting the solar cell.

For this comparison a 1-year mission at a circular, equatorial orbit at 10,000 km altitude was selected. To have a more realistic comparison of current space technology, a high-efficient triple junction solar cell was selected -- Emcore's ATJ solar cell. The ATJ cell is one of the commercially available, high-efficiency solar cells currently used in current space missions; it is also well documented in the SPENVIS model. It was selected for comparison due to its extensive testing and on-orbit performance. The solar cell is one of the highest performing cells with a BOL at standard temperature (27 ^{o}C) of 27.5%. It is designed to withstand typical space radiation and has good temperature coefficients. Even with these good

characteristics, these solar cells will degrade appreciably. The cell will drop to only 20% efficiency at 3E15 e/cm^2. Coupled with the temperature changes, this high-end solar cell does not provide the promised efficiency. See Figure 3.29 for efficiency changes. The dotted line represents data that was extrapolated due to the limits of Emcore's reported data by continuing with the last known temperature effect.

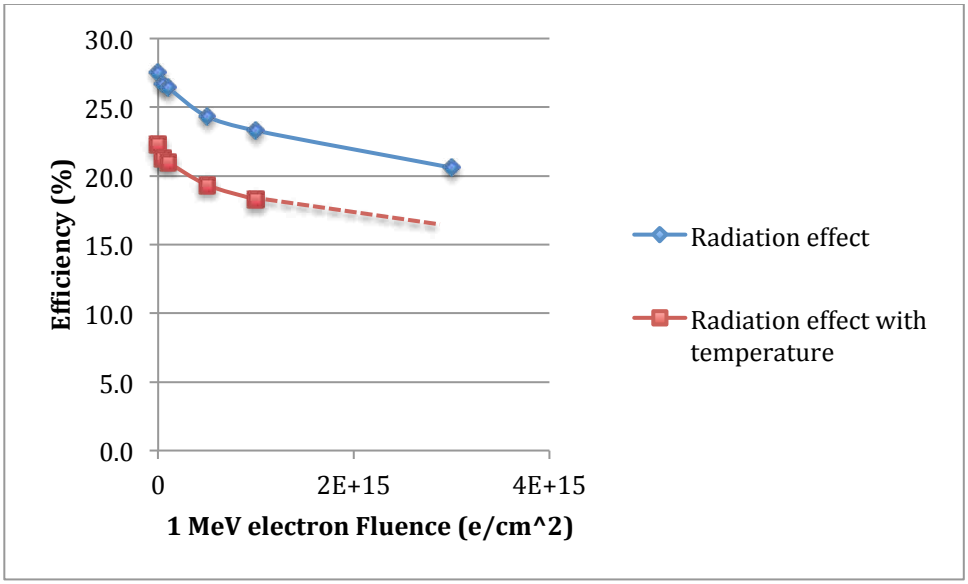

Figure 3.29: Emcore ATJ solar cell calculated efficiency changes due to radiation and thermal effects. (derived from [13])

Even though the temperature coefficient from Emcore's datasheet is not for irradiation at a non-standard temperature, the efficiency of a solar cell also decreases with temperature increases, as previously discussed. With an assumed operating temperature of 393 K and exposure to 1E15 e/cm^2, the EOL efficiency for these solar cells is about 18.3%. In order to compare solar cells to LSC systems, each system is measured in overall system efficiencies. A new efficiency is based on a portion of the BOL efficiency, as calculated from the Emcore radiation performance and temperature coefficients:[13]

$$\eta_{PV-ATJ_{new}} = 0.665 * \eta_{PV-ATJ_{BOL}} \quad (3.7)$$

Obviously, the mission of the spacecraft and shielding will determine the exact radiation exposure. As observed in Table 3.4, traversing the van Allen belts can cause crippling damage, resulting in severe EOL power degradation.

3.5.2 LSC Efficiency Changes

From Chapter 2, the various efficiencies that make the over all efficiency of the LSC system were presented in Equation (2.18) and Equation (2.19). Even though these equations provide a good description of the effects on LSC efficiency, some of the efficiencies are neither easy to calculate, nor directly accessible by standard measurement methods.[61] Based on this situation, the overall optical and solar cell efficiencies were examined for comparison of thermal effects and radiation effects.

A generic, unspecified luminophore is used for analysis. The luminescent material will be based on the state-of-the-art LSC materials but not all parameters will be characterized for a specific material. Radiation and thermal properties affect the LSC system, similar to a solar cell. As previously stated, many organic luminophores exhibit radiation resistance.[52] A main thrust of this dissertation was to show the radiation tolerance of selected luminescent materials and is presented in Chapter 4. As will be shown, some luminescent materials did demonstrate good radiation resistance, while showing minimal changes to the baseline emission out to 10 Mrad of total dose. While other materials did show degradation, for comparison, the LSC selected luminophore is assumed to be radiation tolerant.

As explained in Section 3.3.3, a luminescent material with a temperature coefficient of -0.2 %/^{o}C was assumed to be representative. This value was used for further analysis.

Assuming that the LSC system is originally baselined to the same temperature as the solar cell standard temperature, and that the simulated high temperatures for the LSC systems are 340 K and 370 K for a 2cm x 2cm x 1mm and 5cm x 5cm x 1mm respectively, the luminescent plate will be operating at 67 ^{o}C and 97 ^{o}C above its baseline efficiency. With a temperature coefficient of -0.2 %/^{o}C, the luminescent material will lose 13.4% and 19.4% efficiency respectively for each plate size. The new optical efficiencies are:

$$\eta_{optical_{new}} = 0.866 * \eta_{optical_{old}} \text{ (for 2x2x0.1 cm}^3\text{)} \quad (3.8)$$

$$\eta_{optical_{new}} = 0.806 * \eta_{optical_{old}} \text{ (for 5x5x0.1 cm}^3\text{)} \quad (3.9)$$

While the temperature negatively affects the luminescent plate, the system still has solar cell thermal and radiation changes that can improve the overall efficiency.

As previously stated, the overall LSC system efficiency is affected by the solar cell efficiency. Along with the decrease in radiation exposure, the solar cell can improve the overall LSC system based on Equation (2.20).

Three single junction solar cells for use in an LSC system were examined for thermal and radiation degradation. Their baseline efficiencies and temperature parameters were taken from *Space Solar Cells and Arrays*[62] for consistency. Table 3.6 summarizes the solar cell values used in the analysis.

Table 3.6: Baseline solar cell values used in LSC analysis.[62]

Solar cell	BOL Efficiency (%)	Normalized Temperature Coefficient (/°C)
Si	14.7	-4.60E-03
GaAs	17.4	-1.60E-03
InP	19.5	-1.59E-03

The radiation exposure is based on the shielding effects of 1mm of cover glass for the LSC plate and was taken from Table 3.4.

For the Si radiation damage, the *Solar Cell Radiation Handbook*[70] was used to determine the changes in power, and therefore changes in efficiency. From the normalized power chart at the expected 1 MeV electron fluence of 7.785E12 e/cm^2, a loss of 2% due to radiation damage is expected. Thus, the EOL efficiency of the Si solar cell is 14.4% compared to the baseline of 14.7%. Next, the benefit of the reduced operating temperature was applied. Based on the standard solar cell temperature baseline of 300 K and a simulated operating temperature of 303 K and 284 K for the two sample plate sizes, the differences in temperature are +3 and -16 degrees from the baseline temperature. Using the temperature coefficient, overall cell efficiencies of 14.2% and 15.4% are achieved. The result is a minimal change in the smaller LSC system, with a marked increase of ~5% in the larger LSC system even after a year of exposure. The resulting new LSC efficiency of:

$$\eta_{PV-Si_{new}} = 0.9862 * \eta_{PV-Si_{old}} \text{ (for 2x2x0.1 cm}^3\text{)} \quad (3.10)$$

$$\eta_{PV-Si_{new}} = 1.0736 * \eta_{PV-Si_{old}} \text{ (for 5x5x0.1 cm}^3\text{)} \quad (3.11)$$

For the GaAs solar cell, *GaAs Solar Cell Radiation Handbook*[71] was used for the data to determine the loss of efficiency due to radiation damage. The handbook uses Spectrolabs GaAs/Ge solar cells. From the normalized power chart at the expected 1 MeV electron fluence of 8.377E13 e/cm^2, a loss of 7% due to radiation damage is expected. Thus, the EOL efficiency of the GaAs solar cell is 16.2% from the baseline of 17.4%. As with the previous solar cell, the benefit of the reduced operating temperature was applied. The GaAs solar cell maintains its original efficiency with a small decrease to an overall efficiency of 16.84% and 17.35% for the 2x2x0.1 cm^3 and 5x5x0.1 cm^3 LSC plates. The result is a new LSC efficiency of:

$$\eta_{PV-GaAs_{new}} = 0.9952 * \eta_{PV-GaAs_{old}} \text{ (for 2x2x0.1 cm}^3\text{)} \quad (3.12)$$

$$\eta_{PV-GaAs_{new}} = 1.0256 * \eta_{PV-GaAs_{old}} \text{ (for 5x5x0.1 cm}^3\text{)} \quad (3.13)$$

While neither above example takes into account the solar cell energy conversion through band gap matching, the analysis shows that the solar cells remain near unity relative to BOL after exposure to some of the highest radiation areas in the van Allen belts, offsetting radiation degradation with an improved operating temperature. Based on the promise of the above analysis, another solar cell was investigated for its use in an LSC system.

The InP solar cell has been demonstrated as a radiation hard material. Since the solar cell in the LSC system is still influenced by radiation, it was a logical choice for a more radiation tolerant system. Using Yamaguchi's investigation into InP radiation properties,[72] the above analysis was performed. From this normalized maximum power figure and using the highest 1mm shielded fluence value from Table 3.4 of 8.377E13 e/cm^2, only a 2% loss due to radiation would be experienced by the

InP solar cells. The irradiated solar cell would operate at 19.11%. After applying the temperature effects, a similar result to the Si cell is calculated, resulting in a steady InP solar cell efficiency. The new efficiency is:

$$\eta_{PV-InP_{new}} = 0.9952 * \eta_{PV-InP_{old}} \text{ (for 2x2x0.1 cm}^3\text{)} \quad (3.14)$$

$$\eta_{PV-InP_{new}} = 1.0254 * \eta_{PV-InP_{old}} \text{ (for 5x5x0.1 cm}^3\text{)} \quad (3.15)$$

The LSC system shows promise in combating the detrimental effects of radiation and thermal degradation.

Finally, the overall LSC system efficiency is computed. Table 3.7 summarizes the changes in these efficiencies. The table was constructed by determining the BOL LSC system efficiency that would be required to match the EOL performance of the ATJ solar cell after a year of exposure.

Table 3.7: Effects of radiation and temperature variation on a triple junction solar cell and three LSC systems utilizing different solar cells with 2 different sized plates.

	Plate size (cm^3)	BOL system efficiency (%)[1]	Efficiency change to solar cell due to thermal and radiation effects	Efficiency change to luminophores after radiation and thermal degradation	Overall efficiency changes	New EOL efficiency after 1E15 1 MeV electron fluence and system operating temperature based on thermal simulations (%)
Emcore ATJ solar cell		27.5	0.665	N/A	0.665	18.29
LSC using Si solar cell	2x2x0.1	21.42	0.9862	0.866	0.8540	18.29
	5x5x0.1	21.14	1.0736	0.806	0.8653	18.29
LSC using GaAs solar cell	2x2x0.1	21.22	0.9952	0.866	0.8618	18.29
	5x5x0.1	22.13	1.0256	0.806	0.8266	18.29
LSC using InP solar cell	2x2x0.1	21.22	0.9952	0.866	0.8618	18.29
	5x5x0.1	22.13	1.0254	0.806	0.8265	18.29

[1] Overall LSC system efficiency calculated to achieve EOL ATJ solar cell efficiency of 18.29%

Table 3.7 demonstrates that the LSC system does not need to match the BOL performance of a traditional solar cell system. While the current LSC systems are still far from the efficiencies needed to be competitive with current solar cell systems, an LSC system's component shielding and cooler operating temperature are advantageous.

3.6 Conclusion

The LSC system brings certain advantages to the space environment. The analysis showed that the thermal degradation of the luminophores is offset by the improved operational conditions of the solar cell. The structure of the LSC system serves as a shield for the more sensitive luminophores and solar cells. Thus the result is a power generation system that does not degrade much over the mission life. Based on Debijie and Verbunt's work, a luminophore needs to have the following characteristics for superior efficiency:

• Broad spectral absorption

• High absorption efficiency over the whole absorption spectrum

• Large Stokes shift

• High luminescent efficiency

• Emitted photons matched to the spectral response of the PV-cell

• Solubility in the host matrix material[35]

For the space environment, the thermal coefficient of the luminescent material and radiation effects need to be minimal. As shown by previous work,[52] there are

currently luminescent materials that meet the necessary thermal requirements. Chapter 4 examines the radiation effects of a small sample of possible luminophores.

The LSC system will need many improvements to be competitive, such as selective mirrors, plasmons, band gap matching, high Stokes shift, and optimal sizing and shaping. This list is not all-inclusive, as new methods and technology are sure to be developed. The current assumptions will need to be revisited for continued validity as the LSC systems change in order to achieve improved efficiency.

Finally, other space effects would need to be addressed and evaluated. The small pitting caused by micrometeoroids would degrade the wave guiding properties of the LSC plate. This effect is similar to the textured, antireflective coatings that have been examined and shown not to be viable option.[35] The vacuum environment and out-gassing may also create unforeseen problems with LSC systems. These issues may, to some extent, offset the advantages presented in this chapter and would have to be investigated.

Chapter 4 Radiation Experiments

4.1 Introduction

In order for any system to survive in space, it must survive the degradation of radiation exposure. Extensive testing of the radiation effects on various solar cells has been previously conducted. Further testing of solar cells was not deemed necessary, so the current research concentrated on the effects to luminescent materials. If the luminophores withstand the radiation, then they may be suitable in the space environment.

For luminophore degradation, based on the book *Polymers, Phosphors, and Voltaics for Radioisotope Microbatteries*,[52] an assumption was made that the emission from luminophores was of great enough wavelength that the small displacement damage created by high-energy particles that normally degrade semiconductors is not a factor in the LSC process. This assumption is based on the very small nanometer scale of displacement damage, as compared to the hundreds of nanometer wavelengths of photon emission. The degrading radiation effect that an LSC would encounter is the ionizing of luminophores and the creating of color centers in the waveguide. The formation of color centers cause reabsorption, resulting in less emission from the waveguide material. Based on these assumptions, a more cost effective, ionizing radiation source was used to determine if ionizing radiation degrades the performance of the luminophores.

4.2 Method of testing

4.2.1 Test sample manufacturing method

After reviewing the literature and considering different manufacturing methods, a thin film layer of luminescent material was spin coated onto a substrate. This manufacturing method was shown to be an equally viable method as compared to embedding the luminophores in the material.[56] Due to its inherent radiation tolerance, a quartz substrate was selected. PMMA and Polyvinylpyrrolidone (PVP) were selected for host materials due to their solubility. The luminescent material was selected based on previous research conducted and material availability. Rhodamine 6G and Fluorescein are both well-documented organic luminescent dyes. To explore more and expand knowledge, an additional dye normally used for medical research was also investigated due to its large Stokes shift property, which would reduce the self-absorption of an LSC.

Each luminescent material was dissolved in an appropriate solvent, usually chloroform or distilled water, along with a host material. The substrate samples were cut to approximately 2cm x 2cm x 1mm from larger sheets of quartz. Table 4.1 lists the luminescent, host, and solvent materials used, along with measured weights for the spin coating mixture. The mixture was then spin coated onto the small quartz sample. The spin coating speed settings were one minute at 1200 rpm followed by five seconds at 5500 rpm.

Table 4.1: Luminescent, host, and solvent materials used for spin coating onto quartz substrates.

Material	Amount of luminescent material (mg)	Host material	Amount of Host material (mg)	Solvent	Amount of Solvent (ml)
Rhodamine 6G (R6G) from Lambda Physik,Lambdachrome laser dye	14.9	Polymethyl methacrylate (PMMA) from Alrich Chemical	302.8	Chloroform	10
Fluorescein (F) from Eastman, Fluorescein Disodium Salt	100	Polyvinylpyrrolidine (PVP) from Alrich Chemical	440	Distilled water	10
Cyto 500LSS Large Stokes Shift Dye - carboxylic acid from Cytodiagnostics Large Stokes Shift (LSS) dye	1	Polyvinylpyrrolidine (PVP) from Alrich Chemical	20	Methenal	0.66

After the LSC plate was coated, it was cured for approximately 20 minutes on a hot plate set for 55 ^{o}C to speed evaporation of any residual material. See Figure 2.16 for examples of the samples.

4.2.2 LSS baseline

In order to compare how the absorption and emission of the new material changes with radiation exposure, a baseline characterization was measured. In liquid form, this LSS material is used as a medical dye for the labeling of proteins. Its large Stokes shift that prevents re-absorption may make it an advantageous LSC material. The manufacturer states that it is stable in liquid form, but it has not been used as a spin coating. They did not know the stability of spin coating it onto a substrate nor its radiation degradation.[73] Figure 4.1 shows the measured normalized absorption and emission spectrum overlaying the spectrum from the manufacturer data sheet. The

measurement instruments are listed in Section 4.2.3. Initially, the absorption measurement was too low to distinguish from the noise data. After some adjustments in manufacturing, discernable data was detectable.

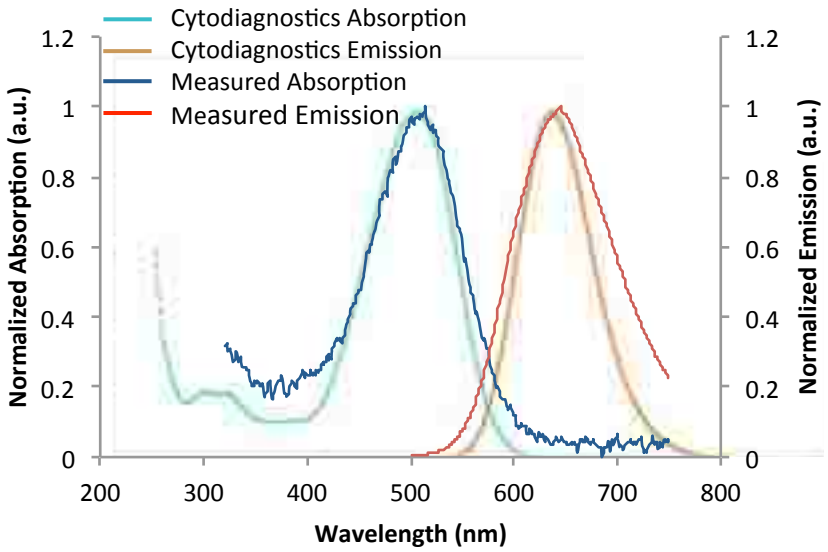

Figure 4.1: Comparison of measured and manufacturer's spectral data[74] of LSS absorption and emission showing near coinciding shape and peaks.

The peaks matched very well with the manufacturer data sheet, showing that the material can be spin coated onto a substrate. The manufacture reported 500 nm and 630 nm for absorption and emission peaks. The measured peaks were 501 nm and 645 nm respectively. The slight shift in the emission data from the manufacturer's data may be the result of the new form of the material or the method of measurement. As will be shown in Section 4.5.3, the stability in this form does not hold well.

4.2.3 Radiation exposure

A Cobalt-60 (^{60}Co) radiation pool was used as the radiation source. The pool uses pencil-sized ^{60}Co material in the center cylinder to generate a radiation exposure area. The pool was calibrated and has not been altered since the calibration. The

current dose amount was calculated using the half-life of 5.2714 years from the calibration date. Figure 4.2 shows the normalized dosimeter data versus height from the time of calibration.

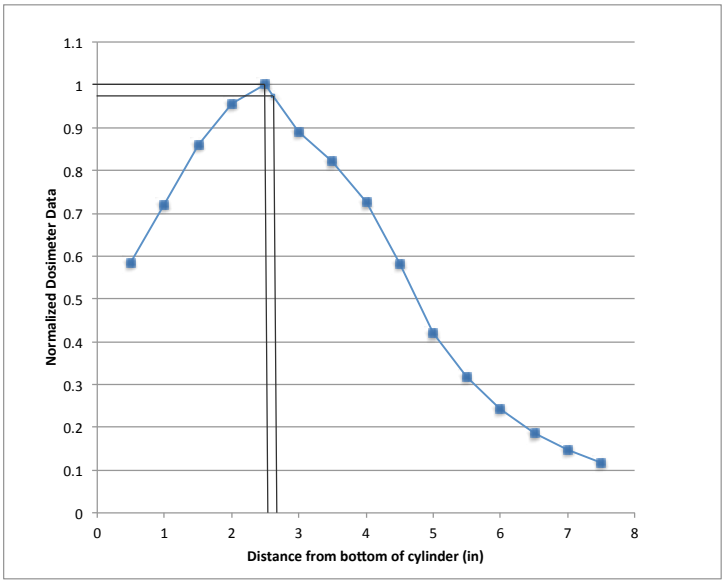

Figure 4.2: Normalized dosimeter data versus height in the radiation pool test cylinder with blacks lines indicating the bottom and top sample distances and corresponding exposure.

The difference of exposure from the bottom sample to the top sample is less than 2.5%. All samples were placed in the same height sequence to ensure uniform exposure. The wrapped test samples, along with a two and one half inch spacer, were put into a stainless steel cylinder. The cylinder was inserted into the center hole in the pool. See Figure 4.3 for a drawing of the cylinder and placement of samples. The spacer was inserted to ensure the samples were at the optimal height for the radiation exposure.

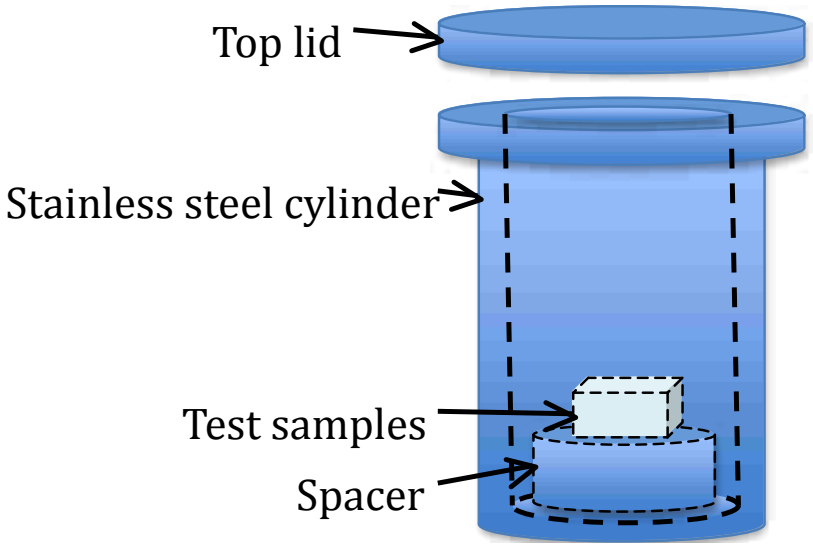

Figure 4.3: Stainless steel vessel for sample placement in ^{60}Co pool array (not to scale)

For brevity of testing, the center or the hole with the most exposure was used. Also, since the ^{60}Co rods are in the center, a more uniform exposure was possible. Once inserted, a timer was set and the amount of dose was based on the calculated rate of dose for a specified time. After exposure, the entire sample group was then taken for absorption and emission measurements.

4.2.4 Absorption and emission measurement method

For absorption measurements, the Perkin Elmer UV/Vis/NIR Spectrophotometer model Lambda 1050 was used. See Figure 4.4 for the 1050 model. The model had a built in test stand and the sample was inserted perpendicular to the light source. The machine was referenced with a clear sample

Figure 4.4: Perkin Elmer Spectrophotometer 1050[75]

at the start of each test sequence. After referencing, measurements were taken from 320 nm to 750 nm for each sample. The data were stored and post-processed.

The emission characteristics of the samples were measured through the HORIBA FluoroLog® Fluorometer, shown in Figure 4.5.

Figure 4.5: HORIBA FluoroLog® Fluorometer[76]

The test piece was held at ~45 degree angle from the excitation beam with a split beam, taking a sample of the light to autocorrect for the fluctuations in the light source. Figure 4.6 shows the simple block diagram of the Fluorometer configuration.

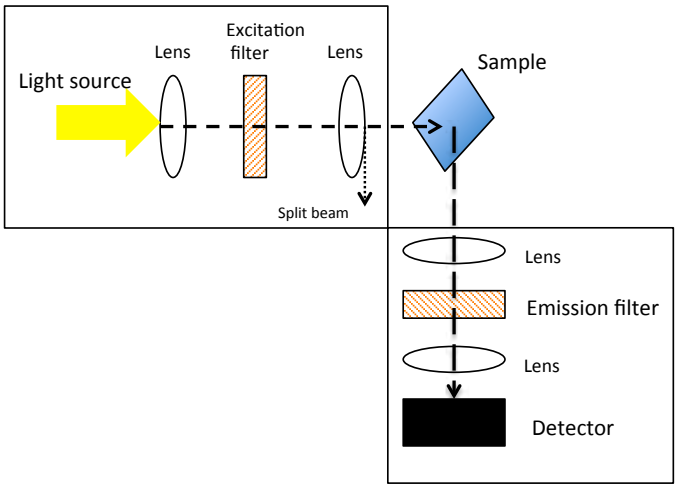

Figure 4.6: Fluorometer block diagram

Consistent measurements were measured from 500 nm to 750 nm with an excitation wavelength of 450 nm. This measurement method proved to be very sensitive to the angle and positioning of the test subject. The first test bench used an existing piece of hardware and black tape to visually align the test sample. See Figure 4.7 for this crude method of testing.

Figure 4.7: Crude tape aligned test bench

After many experiments, it was determined that the error was extremely high due to the placement of the individual test samples and the angle of the test sample. A better test method was needed to reduce the amount of error.

The first error reducing method was simply to average many test measurements to reduce the overall error of the measurement. In order to determine the upper and lower 95% confidence limits, a standard error of the mean was computed from the standard deviation (σ):

$$Error = 1.96 \times \frac{\sigma}{\sqrt{n}} \tag{4.1}$$

where n is the number of test measurements taken and 1.96 represents the 0.975 quantile of the normal distribution. An experiment was conducted out to 24 test measurements to determine the necessary number of measurements needed to reduce the error to an acceptable range. The blue diamonds in Figure 4.8 show how the percentage of error was reduced through the use of multiple measurements for a Rhodamine 6G sample. In order to show changes in the emission characteristics, an accuracy of ~ 10% was needed. Sixteen separate measurements for each test point achieved the consistency in accuracy needed.

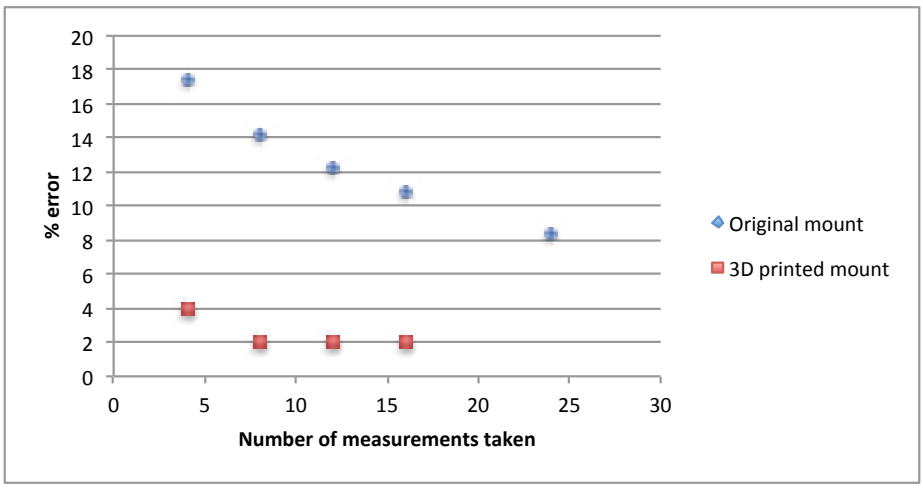

Figure 4.8: Percent error vs. number of measurements for both the original and new 3D printed sample mount.

After discussions with other lab partners, a more stable and reproducible test bench would further improve accuracy. With the assistance of a co-worker and his 3D printer, a holding stand was designed and printed. See Figure 4.9 for the new test stand.

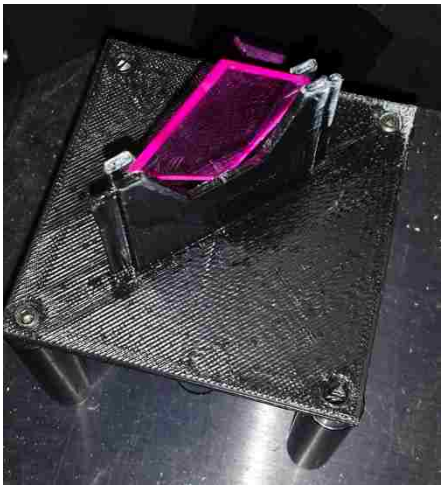

Figure 4.9: Printed test stand for Fluorometer measurements.

This new stand, while improving the reproducibility and speed of testing, was still not accurate enough to facilitate a single measurement per test point. In order to continue to maintain tolerable uncertainties, sixteen measurements were taken at each

test point using the new stand. See the red squares in Figure 4.8. This method resulted in consistently less than 5% error rates, with most test points within 2%. This method proved to be accurate enough for comparison of samples, as each was irradiated stepwise to the maximum radiation dose of 10 Mrad.

The absorption and emission spectra were measured at the initial test point to verify that the method produced typical results. See Figure 4.10. All three samples showed the characteristic shape and peaks representative of the materials.

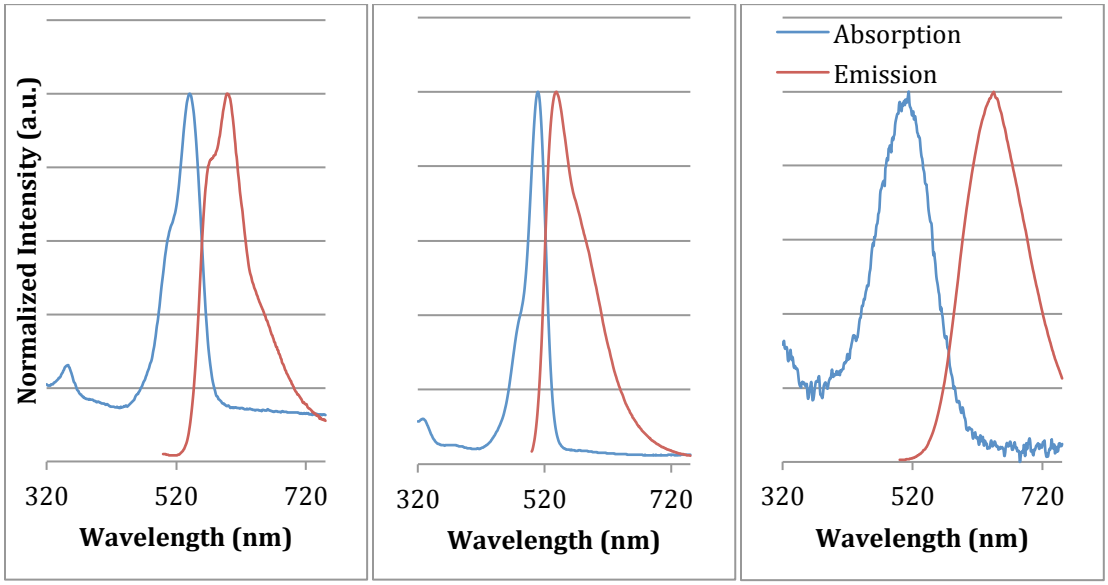

(a) (b) (c)

Figure 4.10: Measured absorption and emission spectral data using the test technique, (a) Rhodamine 6G, (b) Fluorescein, and (c) Cytodiagnostics Large Stokes Shift 500 dye.

Finally, a plain sample of host material and substrate was measured to ensure that the changes in these materials did not affect the results. The results showed less than 0.1% change in the absorption range of the test. Therefore, the contributions from the host and substrate are neglected.

4.3 Statistical analysis

Due to the limited population sizes, careful statistical analysis is required to ensure the significance of the results. To help mitigate unmodeled environmental effects that might change over time, a control sample was measured at each test condition for comparison with the test sample.

Once the data were corrected for environmental conditions by subtracting the control measurement from the test piece, a linear trend line was plotted in order to determine any positive or negative slope. The R-squared correlation was then used to see how closely the data followed that linear trend. The definition of the R-squared correlation is the probability of the response variation that is explained by a linear model, or more simply stated:

$$R^2 = \frac{Explained\ variation}{Total\ variation} \tag{4.2}$$

The value of R-squared ranges from 0 to 1, with a higher number indicating that the data fits the model better. Some of the calculated R-squared terms indicate a better correlation. Other data showed much lower correlation values.

In order to better assess the trending of the data, especially when it did not have a strong linear correlation, an Analysis of Variation (ANOVA) employing an F-test was conducted. The F-Test is from the R.A. Fischer F-distribution, where F is a ratio of variances. Specifically, the F-test compares the amount of variation between groups with the amount of variation within groups, and the assumptions are that there is a normal distribution of the data, variance is similar between groups, and data points are independent. The null hypothesis is then stated and either rejected or not,

depending on the results of the F-test. In the current analysis, the goal is to find a possible correlation between the amount of radiation exposure and the emission/absorption characteristics of the luminophore. The null hypothesis is then that there is no such correlation. The null hypothesis (H_0) is stated as:

H_0 = all population means are equal

The alternate hypothesis (H_A) is:

H_A = at least one of the population means is different from the others.

The F-ratio is calculated as:

$$F_{ratio} = \frac{explained\ variance}{unexplained\ variance} = \frac{\frac{variance\ between\ groups}{ndf}}{\frac{variance\ within\ groups}{ddf}} \quad (4.3)$$

where *ndf* is the numerator degrees of freedom = # of groups -1 and *ddf* is the denominator degrees of freedom = # of observations - # of groups. After the F-ratio is calculated, it is compared to the critical F-test value, which is derived from the numerator (*ndf*) and denominator (*ddf*) degrees of freedom at a prescribed significance level. The specific F-distribution is written as $F_{(ndf,\ ddf)}$.

A type 1 error of 0.05 was used, implying a significance of 5%. If the calculated value of F-ratio is greater than the critical value, then the null hypothesis is rejected with 95% confidence. In this experiment, if the calculated F-distribution is greater than the critical F value, then some effect that cannot be attributed to measurement error is indicated. The current assumption is that this effect is due to radiation exposure, which is the main variable that has been changed between groups. Figure 4.11 illustrates the differing regions for F-distribution.

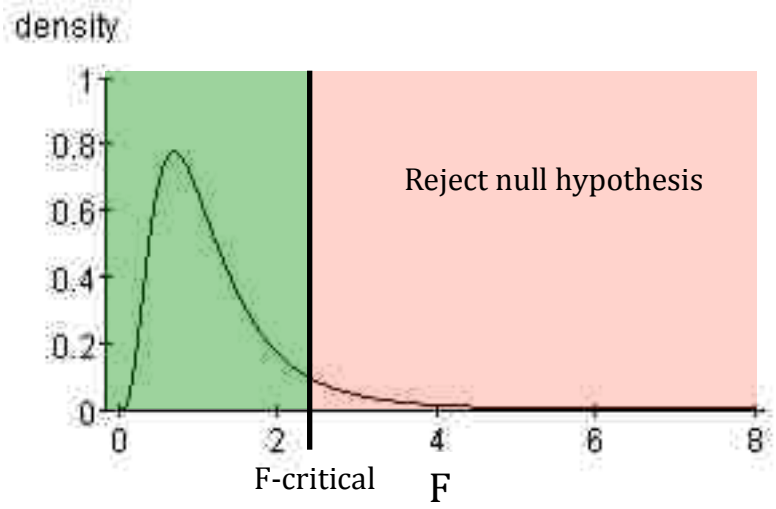

Figure 4.11: F-distribution curve illustrating F critical value and null hypothesis rejection region. Derived from [77]

While the F-test does not determine the trend of the data, it is able to show whether the data is changing with increasing doses. Just to reiterate the test method, each test point at each dose amount had six absorption and 16 emission measurements taken to improve accuracy for each test and control sample. The control samples were not exposed to radiation, but are documented with the associated radiation test point for ease of comparison. Once the data was compiled and the initial trend of the data observed, an F-test was performed on the original data to verify whether the radiation was having a statistically significant effect on the sample. In order to mitigate other environmental factors, the control measurements were subtracted from the test sample measurements. Sections 4.4 and 4.5 present the results.

4.4 Absorption characterization

All three materials' absorption degraded over the course of the testing. The F-test was used to see if the changes were due to the radiation dosage or if the changes

relative to the control sample were minimal enough such that it was within the natural variation of the samples over time. For ease of annotation, the first letter of the material designated the material used. The preceding numbers were the test point representing the dose in units of Megarads (Mrads). The following number or letter represented the test sample, whether control (C) or test sample 1. As an example, 10RC means the control sample of Rhodamine 6G at the 10 Mrad test point. No number in front indicates the initial test at 0 Mrad.

4.4.1 Rhodamine 6G absorption

The spectral data showed a small change in absorption following the increase in radiation dosage, as shown in Figure 4.12. The area of the intensity for both the control and test sample showed minimal changes on the absorption characteristics over the test period. See Figure 4.13.

The environment-corrected data (test sample – control sample) was computed and plotted on Figure 4.13. Figure 4.14 is plot of just the environment-corrected data, showing the trend line, R-squared term, and line indicating the worst-case scenario. The worst-case maps the initial value to include error to the end lowest value at the end of the test sequence. Thus, this blue line shows the worst-case assumed reduction for the material. An F-ratio was calculated to be 60.18. This calculated value is much higher than the F-critical value of 2.759. Therefore, there is an environmental effect that cannot be attributed to experimental error that is changing between samples. The planned environmental change is radiation, however there is no obvious correlation between the absorption and the radiation. Based on the worst-

case scenario, there is an indication of a positive trend in the data with longer exposure times. Therefore, the material's absorption characteristic is not degrading due to radiation exposure.

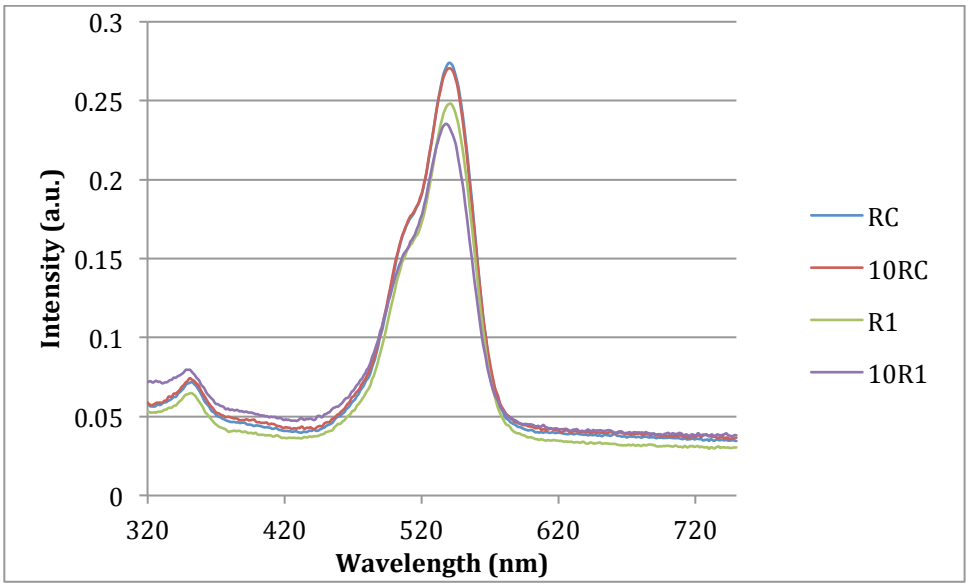

Figure 4.12: Absorption data from Rhodamine 6G at initial and 10 Mrad test point for control and test samples.

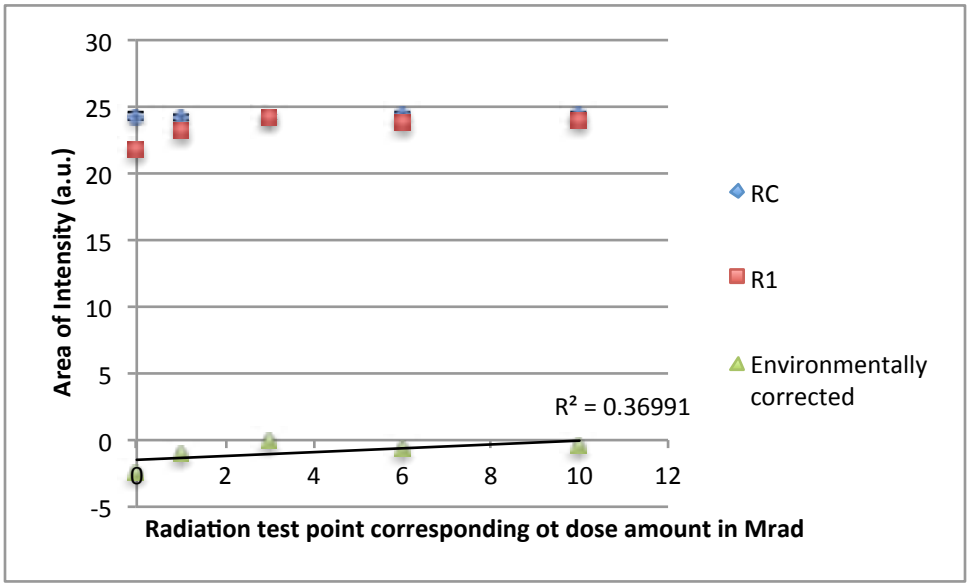

Figure 4.13: Area of intensity measured at each test point for Rhodamine 6G with standard error bars on the control sample, mapped trend line and R-squared term.

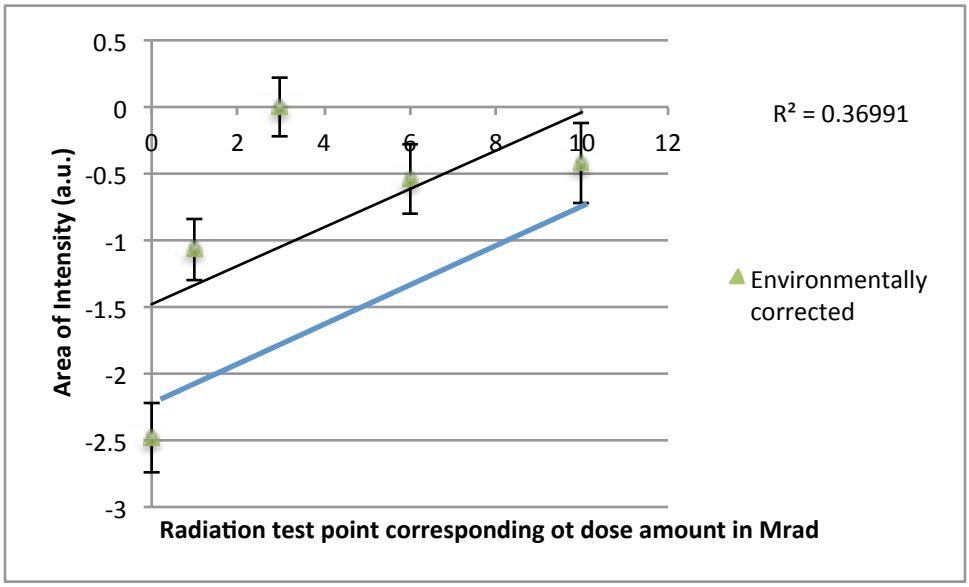

Figure 4.14: Plot of environment-corrected data for Rhodamine 6G absorption.

4.2.2 Fluorescein absorption

Dissimilar to Rhodamine 6G, the Fluorescein material degraded over the test period, though not necessarily from radiation. The control sample is not changing in a similar fashion. This decrease implies that Fluorescein is affected by radiation or other factors, most probably molecular oxygen, since it has been shown to degrade Fluorescein.[78] The issue of oxygen quenching is discussed in Section 4.5.2. The spectral data is shown in Figure 4.15 with the control and test sample almost perfectly matching at the initial test, but both degrade over the test period. As can be seen Figure 4.16 and a close up of the environment-corrected data in Figure 4.17, the absorption characteristics change as the test progresses.

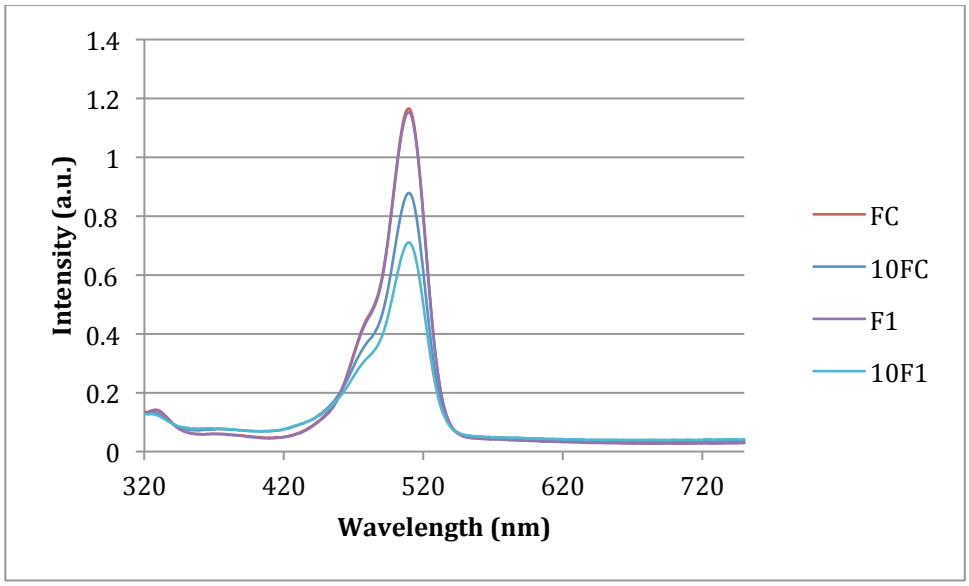

Figure 4.15: Absorption data from Fluorescein at initial and 10 Mrad test point for control and test samples.

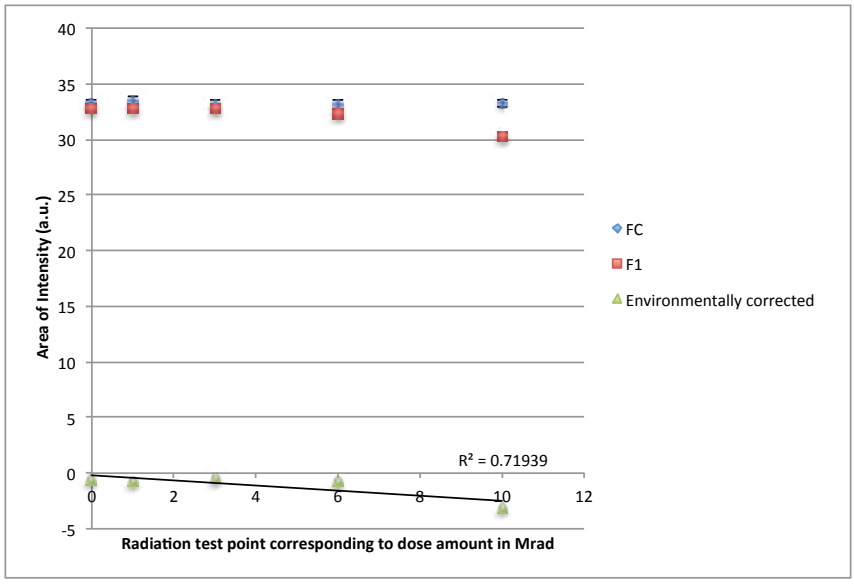

Figure 4.16: Area of intensity measured at each test point for Fluorescein with standard error bars on the control sample, mapped trend line and R-squared term.

As with Rhodamine 6G, an F-test was used to compare the significance of the divergence. The results are similar to the Rhodamine 6G; the F-ratio is calculated to be 30.13. This value is much higher than the critical F-value of 2.758. The

conclusion is that an external environmental effect is impacting the absorption characteristics, and while radiation is the assumed cause, it is possible that temporary degradation of the material due to atomic oxygen may be occurring. This is discussed further in Section 4.5.2.

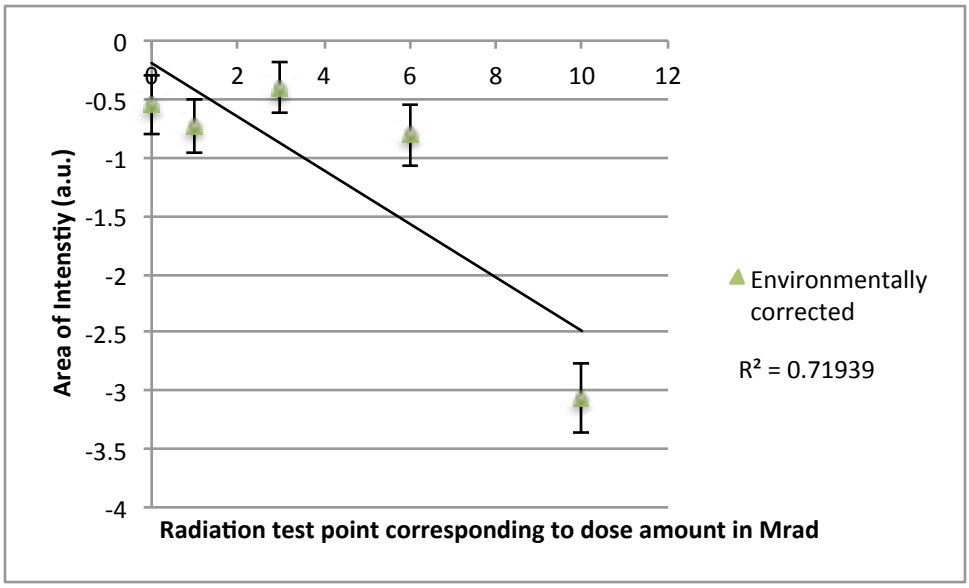

Figure 4.17: Plot of environment-corrected data for Fluorescein absorption.

4.4.3 Large Stokes Shift absorption

Due to the much lower molar absorption of the LSS material, absorption measurements were more difficult to obtain. A concentration of over 3 times the other materials was needed to get discernable absorption measurements. The absorption data is presented in Figure 4.18. Figure 4.19 is the area of intensity. The environment-corrected data is shown in Figure 4.20. As with the previous material tests, the calculated F-ratio of 22.58 is greater than the critical F-value. The high F-ratio does not provide sufficient results to determine the radiation effects on the

material. The lower R-squared term shows that the data does not fit the linear model well, but, similar to Rhodamine 6G, the worst-case scenario is plotted from the initial data point to include the associated error. The results show all subsequent test points after the baseline are greater than the initial value, as illustrated by the blue line. An external environmental effect, presumably radiation, seems to affect that absorption characteristic for all test samples. As with the Rhodamine 6G, the LSS material shows a positive indication from the initial baseline, outside of the associated error.

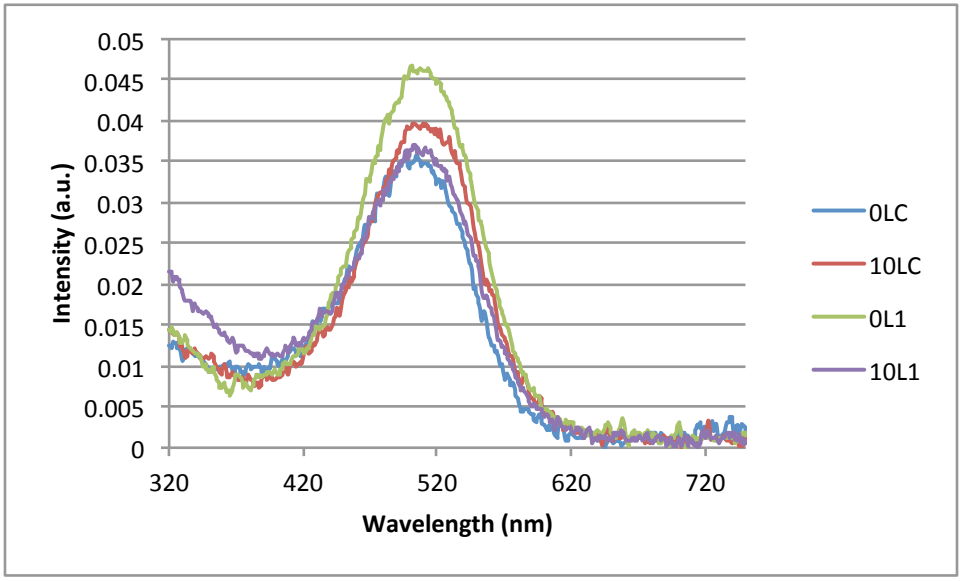

Figure 4.18: Absorption data from Large Stokes Shift material at initial and 10 Mrad test point for control and test samples.

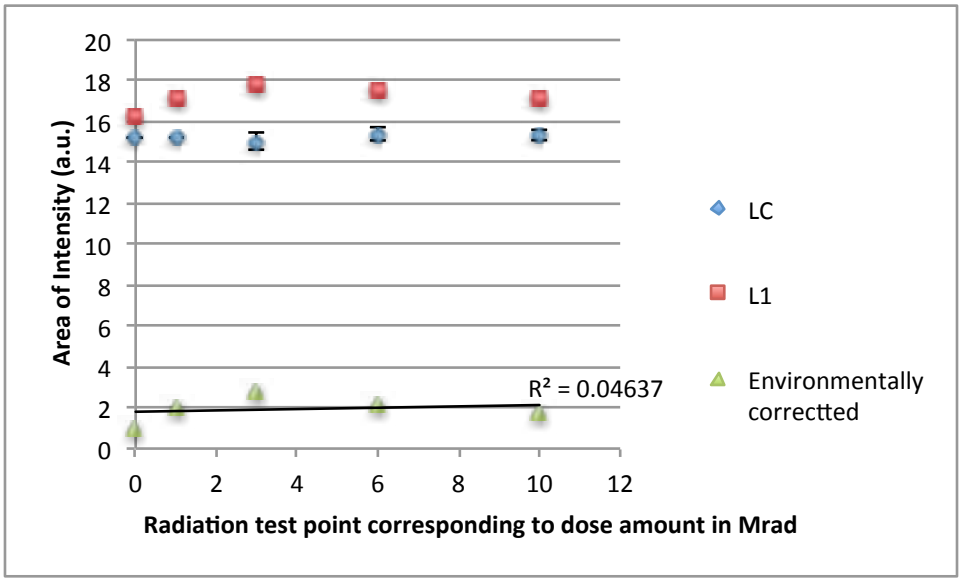

Figure 4.19: Area of intensity measured at each test point for Large Stokes Shift material with standard error bars on the control sample, mapped trend line and R-squared term.

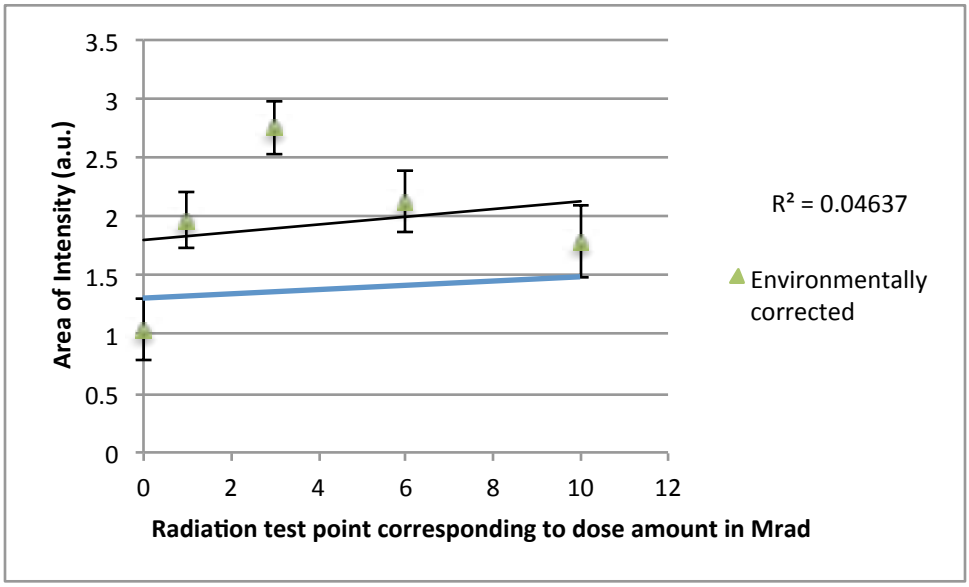

Figure 4.20: Plot of environment-corrected data for Large Stokes Shift absorption.

4.4.4 Summary Table of absorption results

In summary, all three materials indicated that their absorption changed with increasing radiation dose. Two of the materials showed a positive trend, taking into account the error of the baseline. The other material showed a negative trend,

which may be associated with another phenomenon visibly observed with the sample. Table 4.2 summarizes the analysis data, and presents the conclusions about the changes in absorption due to radiation exposure for the different materials tested.

Table 4.2: Summary of T-tests with conclusions for the absorption characteristics of tested materials.

Material	Critical F-value	Calculated F-test value	R-squared of environmentally corrected data and slope	Conclusion
Rhodamine 6G	2.758	60.18	0.370 positive	The calculated F-value exceeds the critical value so the null hypothesis is rejected. Based on the trend line and measurements outside of initial error, radiation exposure shows a positive trend for increasing radiation dose.
Fluorescein	2.758	30.13	0.719 negative	The calculated F-value exceeds the critical value so the null hypothesis is rejected. Based on trend line and measurements outside of initial error, the radiation shows a negative trend for increasing radiation exposure.
Cytodiagnostics Large Stokes Shift dye	2.758	22.58	0.046 positive	The calculated F-value exceeds the critical value so the null hypothesis is rejected. Based on the trend line and measurements outside of initial error, radiation exposure shows a positive trend for increasing radiation dose.

4.5 Emission characterization

Similar to the absorption analysis, the raw data is first compiled. Due to the number of measurements needed to improve accuracy, the sixteen measurements were then averaged and compared for any trending. In order to remove other environmental factors, the average of the control sample was subtracted from the test sample measurements. A trend analysis was performed on the environment-corrected data, followed by the F-test. The results show some very interesting effects.

4.5.1 Rhodamine 6G emission

The sixteen measurements of the Rhodamine 6G control sample are presented in Figure 4.21 for a more complete demonstration of the methods used to determine the averages, to observe trends, and to analyze using the F-test. Figure 4.21 uses clear boxes at each test point for each measurement, with a black diamond showing the average for that data set. When only the averages are plotted, a much cleaner graph represents the trending of the averages with standard error bars. See Figure 4.22 for this plot. The environment-corrected data is also plotted in Figure 4.22 to illustrate the relationship between the overall emission values and the changes that occur from radiation. The error bars on the corrected data account for the error from the control sample, and the error from the test sample.

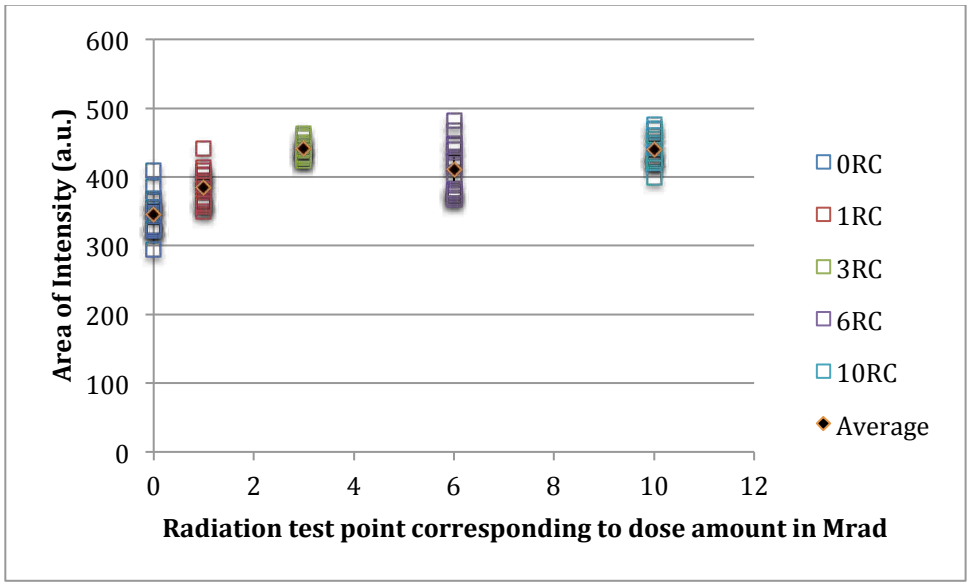

Figure 4.21: Sixteen emission measurements of Rhodamine 6G at each test point of the control sample with averages of each marked as a black diamond.

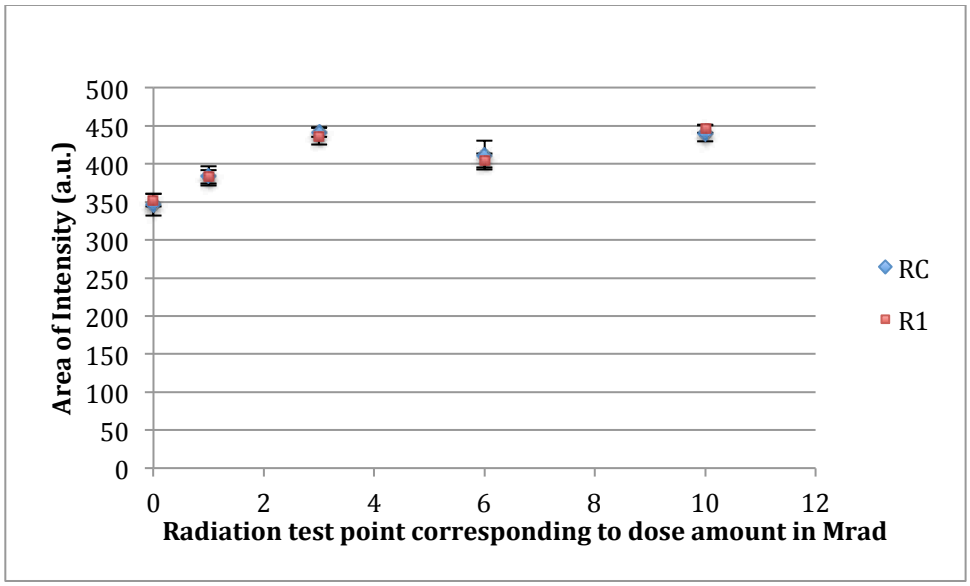

Figure 4.22: Averaged area of intensity of control and test samples of Rhodamine 6G based on Figure 4.21 data with standard error bars from the control sample. The environment-corrected data shown at the bottom of the scale is derived from subtracting the control sample data from the test sample data.

The near zero changes of the environment-corrected data illustrates that the radiation changes are on the order of a few percent of the overall emission. For clarity and further analysis, the environment-corrected data is plotted in Figure 4.23. As may be observed, the data shows an initial downward trend, and then increases for the last test point. While all the averages remain within the error of the initial value, there is some possibility that the variation of a test point may indicate a change in the emission performance of the material. For that reason an ANOVA with F-test was conducted to determine if null hypothesis is valid, and that the data is maintaining close enough to the mean for statistical purposes.

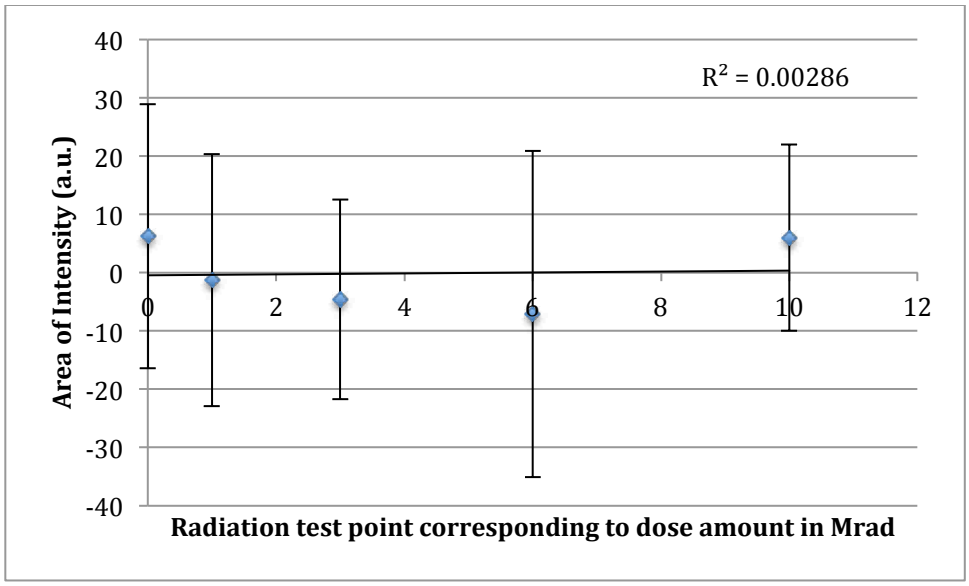

Figure 4.23: Environment-corrected data for Rhodamine 6G from each test point with trend line and standard error bars.

The critical F-value was 2.494 for all of these emission analyses, since the degrees of freedom do not change. The Rhodamine 6G F-test showed favorable results. The calculated $F_{(4, 75)} = 1.913$, and thus the calculated F-ratio was less than the critical F-value. This comparison means that the test points were nearly equal and not degrading as radiation increases.

4.5.2 Fluorescein emission

Even though sixteen measurements were taken, the analysis in Figure 4.24 displays the average of the sixteen measurements. Due to the small variation in the individual test points, the R-squared term shows that the data does not follow the linear model. It is still fairly flat but the larger error for the initial and 6 Mrad test point measurements reduce the linear trend line accuracy.

As with Rhodamine 6G, the environment-corrected data is plotted in Figure 4.25. And again, similar to the previous example, an ANOVA and F-test are needed

to determine if the variation is from the radiation or if the mean is maintained throughout the test sequence.

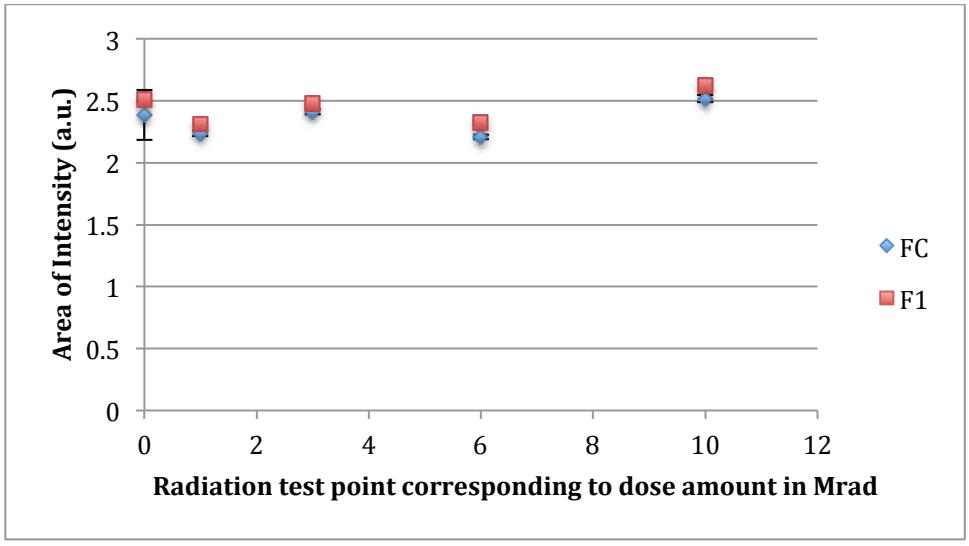

Figure 4.24: Averaged area of intensity of control and test samples of Fluorescein with standard error bars from the control sample. Calculated R-squared terms show trending. The environment-corrected data is derived from subtracting the control sample data from the test sample data.

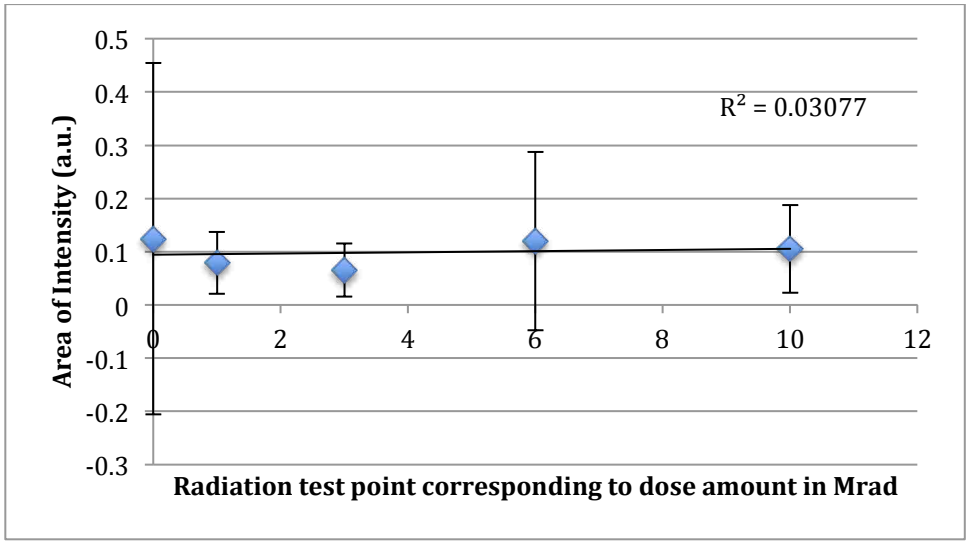

Figure 4.25: Environment-corrected data for Fluorescein from each test point with trend line and standard error bars.

The ANOVA and F-test showed promising results. The calculated value is $F_{(4, 75)} = 0.591$, which is less that the critical F-value of 2.494. Even though the R-squared term does not give much information, the lower calculated F-ratio shows that

the radiation did not alter the mean value of the corrected data over the 10 Mrad dose range.

As with all the tests, the samples were visually inspected at each test point. The Fluorescein exhibited an unusual behavior that was not seen in any other sample. The edges of the sample at higher radiation exposure (>3 Mrad) showed quenching of the luminescent material. See Figure 4.26 for the effect on the samples. The control piece does not exhibit any changes, while the test sample shows clearly where the edges were most exposed. This phenomenon can be explained by fluorescence quenching due to atomic oxygen.[79] As shown in Figure 4.27, the F1 test sample was in the center of the test stack. Since fluorescence quenching is a diffusion-controlled mechanism, the quenching started along the edges due to the protection of the other test samples and packaging. Thus, the edges are more exposed to these by-products in the test cylinder. The evidence of ozone was readily detected after the longest radiation test, illustrating the different oxygen environments between the test cylinder and the lab space. Only in the test sample did the difference in oxygen environments cause the quenching.

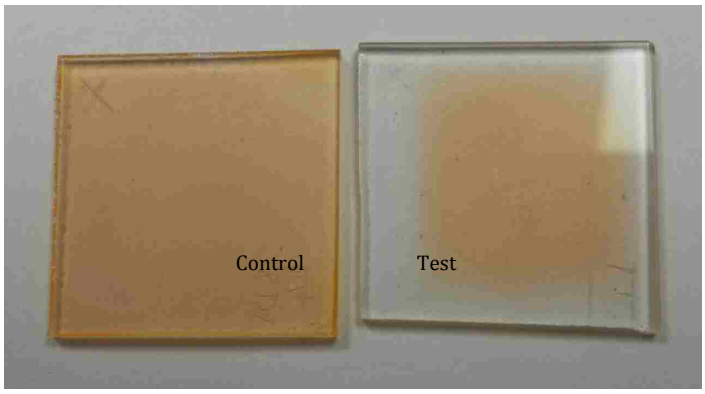

Figure 4.26: Visual inspection of the Fluorescein samples at the last test point after a 4 Mrad radiation step. Note the bleaching effect on the edges.

Figure 4.27: Stack of test samples used with Fluorescein sample in middle of the stack, being shielded from other effects.

This observation illustrates a flaw in the test technique. The test sample is placed in the Fluorometer stand. The excitation light is focused on the center of the sample, as shown in Figure 4.28. The area to be evaluated was the center of the sample. While visual inspection showed that the center material did not change after radiation exposure, other factors affected the sample. These factors would reduce the overall efficiency of the LSC plate. There are a couple of ways to prevent this issue. The test sample can be isolated from the environment while being irradiated, or

measurements could be taken utilizing an integrating sphere to capture the entire emission of the luminescent plate.

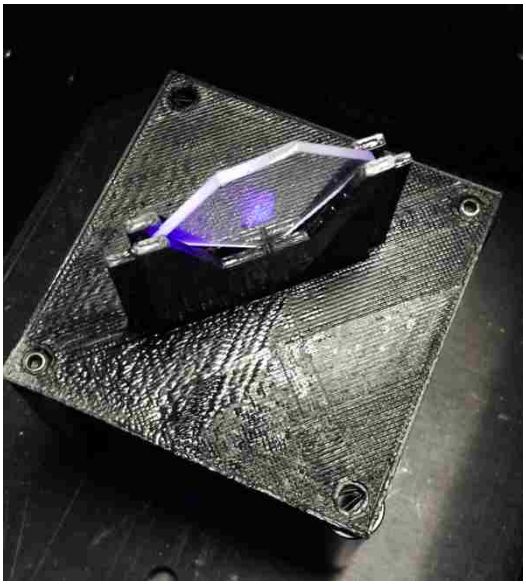

Figure 4.28: Emission measurements stand showing the position of the excitation beam in the Fluorometer.

4.5.3 Large Stokes Shift dye emission

The emission analysis process for the last sample material is very much the same as the previous two materials. The results come out to be very different than the Rhodamine 6G and the Fluorescein. The averaged control and test sample with environment-corrected data is shown in Figure 4.29. Figure 4.30 is a close up graph of the corrected data. The R-squared term is good, at >0.8 for both the control sample and test sample. Since both match the linear model, the slope of the trend line shows a decline in performance over the test period for both samples. The implication is that other degradation factors are decreasing the emission of the luminophores, not just the radiation.

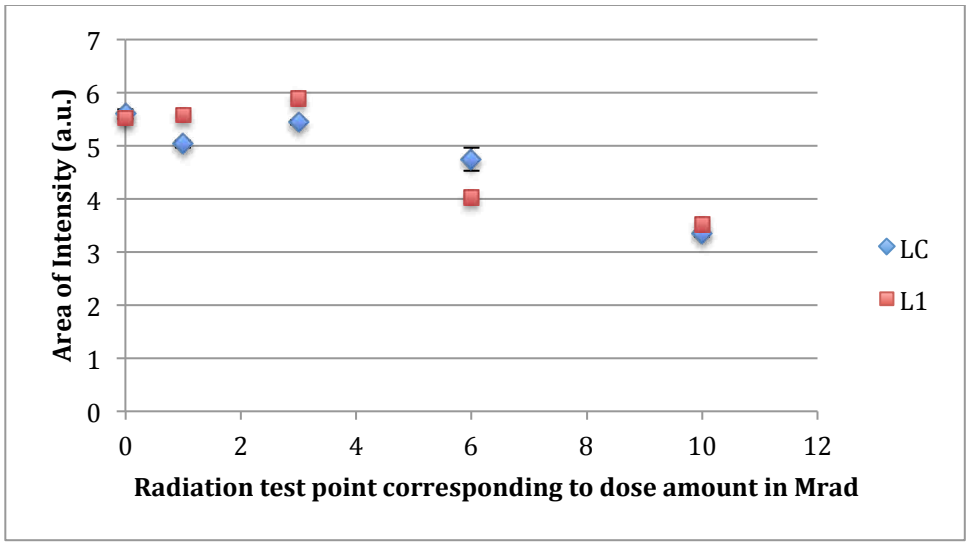

Figure 4.29: Averaged area of intensity of control and test samples of LSS with standard error bars from the control sample. Calculated R-squared terms show trending. The environment-corrected data is derived from subtracting the control sample data from the test sample data.

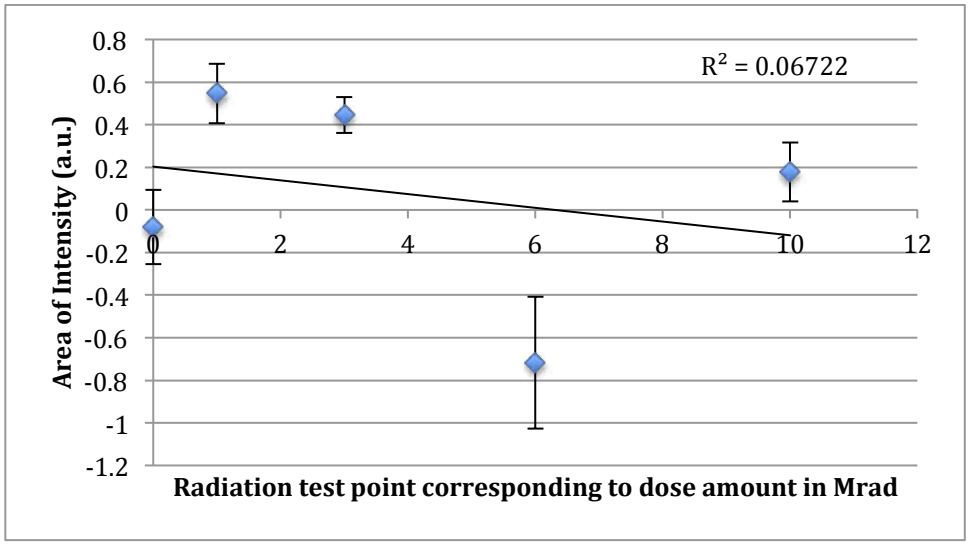

Figure 4.30: Environment-corrected data for LSS dye from each test point with trend line and standard error bars.

As with the previous materials, the ANOVA and F-test of the environmental corrected data gives the true results on the radiation effects. As the wide changes in mean show, the calculated $F_{(4, 75)} = 83.78$, which is much greater than the critical F-value of 2.494. This material is truly affected by radiation exposure.

4.5.4 Summary Table of emission results

Table 4.3 summarizes the analysis data and presents the conclusions about the changes in emission due to radiation exposure for the different materials tested.

Table 4.3: Summary of F-tests with conclusions for the emission characteristics of tested materials.

Material	Critical F-value for correected data (based on (4, 75) degrees of freedom))	Calculated F-test value for corrected data	Conclusion
Rhodamine 6G	2.494	1.91	Since calculated F-values are less than the critical F-value, these materials do not appreciably deviate from the mean. Therefore, radiation does not have an appreciable affect on the absorption characteristic of the material.
Fluorescein	2.494	0.59	
Cytodiagnostics Large Stokes Shift dye	2.494	83.78	The calculated F-value exceeds the critical value so the null hypothesis is rejected. The radiation shows a nagative trend for increasing radiation exposure.

4.6 Chapter conclusions

The end results were not as promising as desired. Only one material, Rhodamine 6G, emerged as being both radiation and environmentally tolerant. The other two materials had problems withstanding the radiation test environment. Table 4.4 summarizes these conclusions. Fluorescein showed great promise but the quenching effect would need to be investigated further. As a reminder, these test

samples were placed in the center of the ^{60}Co rods to accelerate the testing. This dosage rate is not typical of the space environment, so a lower dose rate may slow the changes due to the local environmental exposure.

Table 4.4: Summary of absorption and emission of tested materials, showing analytical test results, trending of data, and results of suitability for use in the space environment.

	Absorption		Emission	Determination of	
Material	Pass the F-test	R-squared of environment-corrected data and slope	Pass the F-test	Radiation tolerence	Suitability
Rhodamine 6G	No	0.651 positive	Yes	Yes	
Fluorescein	No	0.719 negative	Yes	Quenching issue	
Cytodiagnostics Large Stokes Shift dye	No	0.046 positive	No	No	No, stabilty and radiation degradation

The promise of the Large Stokes Shift dye was to improve efficiency by reducing re-absorption. Even though the dye was reported by the company to have good stability, the suspension of the luminescent material in a host material after spin coating did not maintain that stability. More testing into the stability of this material would be needed to ascertain if it is viable for an LSC system. This dissertation did not investigate the stability aspects of these materials.

The emission characteristics, while physically coupled to the absorption characteristics, did not vary in accordance with the changes in absorption. The LSS

absorption remained positive or flat. Yet, the LSS emission had a pronounced decrease over the test. The important part of this testing shows that this problem is not one sided. Both absorption and emission measurements are needed to explain the overall effect. There is much more to be tested but that will be left for postdoctoral work.

Chapter 5 A review and discussion on spectral conversion

5.1 Introduction

As was acknowledged in the beginning of this dissertation, one way to improve the radiation tolerance of the solar cell panels is to increase the thickness of the shielding covering the solar panels. Luminophores could be added to the shield to possibly improve solar cell efficiency as well. A review of the use of luminophores to augment solar cell performance is presented. Simulations from the ray-tracing program were used to determine if standard solar cells could benefit from the addition of a spectral-matching luminescence. To reduce the solar cell efficiency losses due to thermalization, surface recombination, and transmission, two major application methods were reviewed -- down-conversion and up-conversion.

As previously stated in Chapters 2 and 3, one of the major losses to solar cells is due to thermalization, which happens when the excess energy becomes heat after a high-energy photon creates an electron-hole pair. The use of luminescent materials that down-convert these high-energy photons can reduce the losses due to thermalization. There are two methods to down-convert: photon cascade emission (PCE) and photoluminescence. The illustrations in Figure 5.1 show the band energy diagrams for the two processes, along with an example application to a solar cell. As shown in Figure 5.1(a), photoluminescence takes place via relaxation of an excited electron, which results in the loss of excess energy while emitting a photon. In Figure 5.1(b), PCE is shown as a two-step emission process, which allows two photons to be

emitted for each incoming photon. The down-conversion process shifts the high-energy photon to better match the band gap energy. Thus, less excess energy is available to generate heat in the solar cell.

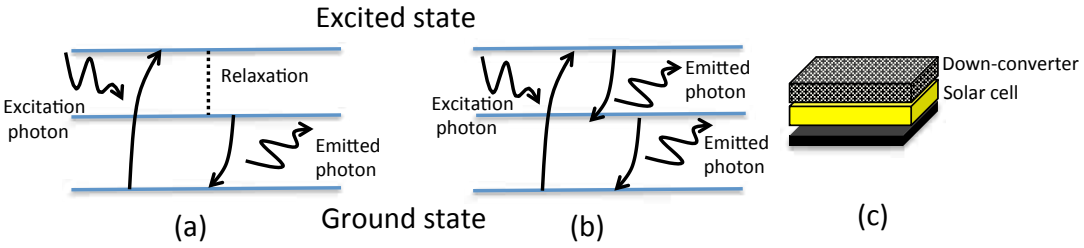

Figure 5.1: (a) Photoluminescence: after excitation non-radiative relaxation takes place followed by radiative relaxation, which leads to emission of lower energy photons. (b) PCE: after excitation, step-wise relaxation takes place, which leads to emission of two (or more) lower energy photons. (c) Down-converter is placed on front of the solar cell.[86]

At present, the promise of improved efficiency through photoluminescence has been elusive. Van Sark et al.'s work, they calculated an increase by nearly 10% in short-circuit current, but their simulations did not show any overall improvement.[80] Svrcek et al.'s work with silicon nanocrystals did show enhanced spectral response due to shorter wavelengths, gaining ~0.4% in efficiency.[81]

Another loss in solar cell efficiency is through transmission when a photon with less energy than the band gap energy just passes through the solar cell. Up-conversion uses two or more low energy photons to create a photon with sufficient energy, such that it can be utilized by the solar cell. See Figure 5.2 for an example application to a solar cell and the band gap energy diagram illustrating this process. These processes are explained more in the following sections.

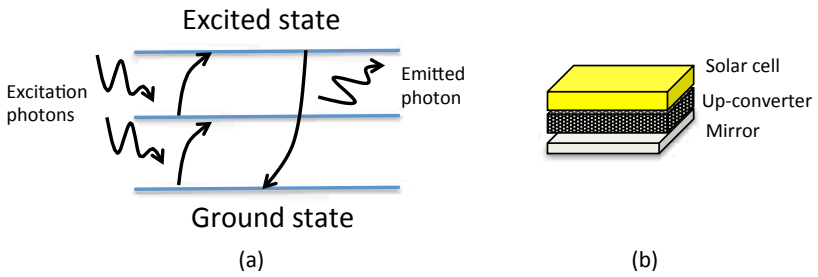

Figure 5.2: (a) Up-converter uses two incoming, low energy photons to excite an electron to the highest energy level. A single, high-energy photon is emitted when the electron relaxes to the ground state. (b) Application of an up-converter to the rear side of a bifacial solar cell. Electrical isolation between the cell and the up-converter is necessary to prevent recombination at the rear side.[86]

Up-conversion research has progressed for a number of years. The first response from up-converter on a GaAs solar cell was in 1995, by Gibart et al.[82] Gibart et al. demonstrated a 2.5% increase in measured efficiency with an input excitation of 1 *W* at 1.39 eV. The first application of an up-converter on a silicon solar cell was in 2003, by Shalav et al.[83] Shalav et al.'s later investigation showed an increase of 2.5% to EQE when excited by a 5.1 mW laser at 0.81 eV.[84] Though using different materials and not related to each other, each experiment showed positive responses under longer wavelength excitation.

As can be observed from the solar cell examples, both up- and down-conversion can be used on solar cells to modify the spectrum for improvements in efficiency. Another important aspect is that existing solar cells can be modified without changing their manufacturing processes or characteristics. Figure 5.3 shows how the wavelengths of the solar spectrum could be modified by spectral conversion to potentially improve a Si solar cell.

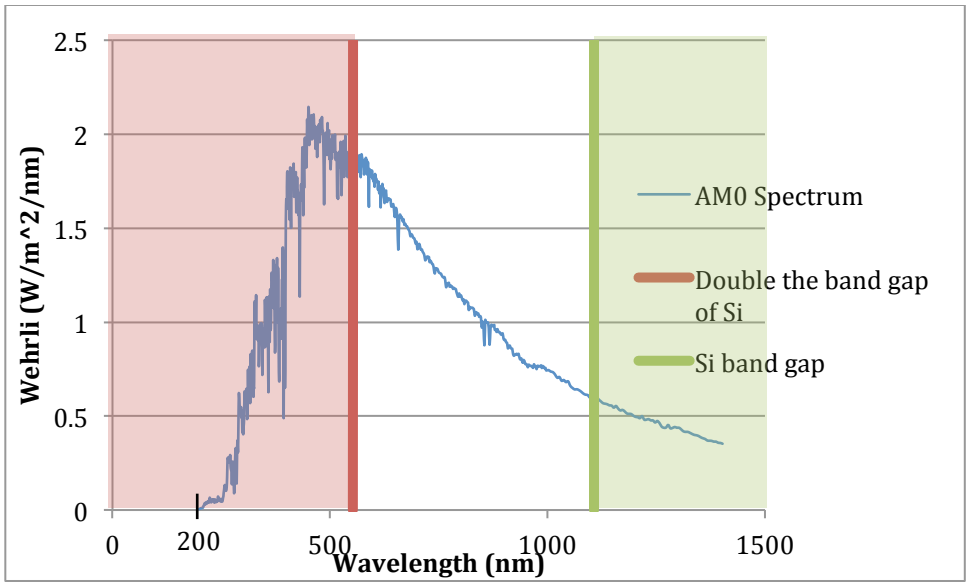

Figure 5.3: Wavelengths of spectrum conversion based on down-conversion (red) and up-conversion (green) for an Air Mass 0 (AM0) solar spectrum.[85]

5.2 Down-conversion

In order to reduce the thermalization of the solar cell due to excess energy of short wavelength photons, two spectral methods can be used: photoluminescence or photon cascade emission (sometimes called quantum cutting, quantum splitting, or multi-photon emission). The highest energy photons can use PCE to create a higher than unity quantum efficiency through absorption of high-energy photons with twice the band gap energy of the semiconductor material. Photoluminescence downshifts the photon from a higher than band gap energy to a better spectral-matching energy, thus reducing the thermalization of the solar cell.

The two phenomena are distinguished by their quantum efficiencies. For photoluminescence the QE is always less than or equal to one, whereas QE of PCE can exceed one assuming non-radiated losses are prevented.[86] Figure 5.1 shows the energy diagrams illustrating how these two processes work. For an example silicon

solar cell to benefit from down-conversion, the following conditions must be met by the luminophores:

- Excitation at wavelengths longer than 200 nm for AM0 spectrum
- Excitation at wavelengths shorter than 550 nm for use by a silicon solar cell with band gap energy of 1.12 eV
- Emission in a more favorable range of spectral response (500 nm – 1000 nm)
- Low excitation intensity
- High quantum efficiency
- Low absorption in the emitted region and the regions that will not be shifted.[86]

The shifting of the high-energy photons to lower energies reduces the probability of surface recombination and thermalization, leading to a higher short circuit current and a more efficient solar cell.[86]

The interaction of the luminescent material with incident light for a down-conversion system is shown in Figure 5.4. As with an LSC system, the escape cone is a major source of loss due to the isotropic emission from the luminophore. Simulations to be discussed in Section 5.5 were used to determine if the red-shifting of the light to a more favorable spectral response could mitigate these losses.

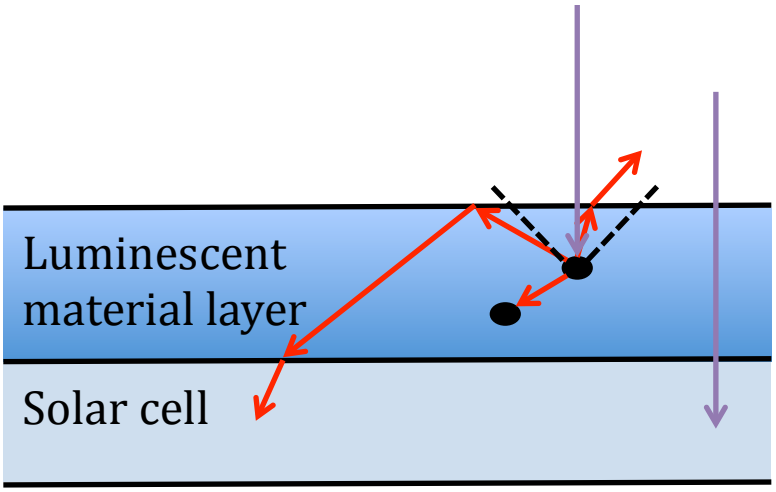

Figure 5.4: Diagram of solar cell augmented by a luminescent material on its surface with incident light as violet and emitted light as red, showing losses and photon transmission.[87]

5.2.1 Photon Cascade Emission

There are many materials that can be used for PCE, but the excitation wavelengths for a silicon solar cell are between 125 nm and 215 nm.[86] Based on Strumpel et al.'s analysis of ionic down converters for this range of wavelengths, a theoretical QE of 194% is possible, with one empirically measured at 140% with excitation wavelengths ~202 nm.[86] These examples show the potential of a PCE material in front of a solar cell. A major drawback is that most of these materials require higher energy photons than are typical in the solar spectrum. As shown in Figure 5.3, the 200 nm wavelength is at the initial increase in the AM0 spectrum. Solely due to escape cone losses, a material with a refractive index of 1.5 needs an EQE of 115% to break even.[88] While some materials have demonstrated the necessary EQE, the combination of QE and absorption range has not been developed.

Other experiments presented in the next section are trying to demonstrate that down-conversion can still benefit a solar cell through photoluminescence.

5.2.2 Photoluminescence

While the classical efficiency limit for a silicon solar cell was estimated at 29%, detailed-balance calculation showed that this could improve to approximately 37% using spectrum modification.[86] This efficiency increase is the promise of photoluminescence, however an idealized luminophore has not been realized. The simulations in Section 5.5 illustrate why such efficiencies have not been achieved, due mainly to optical efficiency losses from absorption and the escape cone.

5.3 Up-conversion

Up-conversion uses photons that are transmitted through the solar cell, so the luminescent material is placed on the back side of a bifacial cell. As with all luminescent material applications, good optical coupling is needed to ensure efficient transmission of the light to the up-converter and for the emission of the up-converter to reach the solar cell. As listed for the down-converter, the following conditions must be met for up-conversion to benefit a silicon cell:

- Absorption range higher than 1100 nm (>1.12 eV)
- Emission lower than 1100 nm
- Low excitation intensity
- High up-conversion efficiency
- High transmittance of the up-converted light.[86]

Results have shown a small increase in QE for the longer wavelengths. In the work of Shalav, et al.,[89] an up-converting device of Er^{3+} (Erbium) ions on a silicon wafer was illuminated with a 1500 nm, 5 mW laser. It generated an EQE of 3.4%. While this efficiency seems low, the conversion did not require any modification to the solar cell. Thus, any improvements can directly translate into real improvements to the solar cell efficiency. A major disadvantage is that up-conversion is a nonlinear process, thus requiring substantial increases in the incoming intensity to produce higher steps of up-conversion. The intensity of up-converted light is proportional to the square of the incident light for a two-step up-conversion. For a three-step process, it is proportional to the cube of the incident light.[90] As materials improve in the above listed conditions, further gains can be reached.

For the materials used in in current work, Rhodamine 6G has been previously shown to perform up-conversion. Qui et al.'s work showed that Rhodamine 6G was excitable at 1054 nm with an emission range of 617-620 nm. One of the necessary conditions was grossly violated for practical use: the material required an input power in the GW/cm^2 versus the practical W/cm^2 range.[91] Such a high input intensity makes this material impractical for up-conversion. The review of Strumpel et al.'s work showed that many materials have demonstrated the up-conversion process, but more research is needed to properly match the solar cell with the necessary up-conversion properties.

5.4 Radiation tolerance

Chapter 4 showed that certain luminophores are radiation tolerant. The radiation tolerance of luminophores can provide advantages to solar cells that are unrelated to direct improvements in efficiency. For example, Cerium luminophores have been added to the cover glass of GaAs space solar cells for the purpose of protecting the glass and encapsulation material from high-energy UV radiation. [92,93] While these luminophores do not offer the benefits of spectral conversion, there are others that exhibit both radiation tolerance as well as spectral conversion -- such as Rhodamine 6G. A radiation tolerant luminophore that met the spectral conversion requirements listed above could provide both benefits, even if the gains in efficiency were small. As long as the introduction of the luminophores does not greatly impact complexity or cost, even small gains would offer an advantage.

5.5 Efficiency changes based on ray-tracing simulations

5.5.1 Ray-tracing simulations

As with the sizing analysis, the ray-tracing simulation developed by Ferrell[58] was modified, and then run as another tool for determining the effectiveness of spectral conversion. Due to the lack of very short wavelengths in the solar spectrum, the process of PCE was not incorporated into the simulations. The primary concern in adding a luminescent material to the cover glass of a solar cell was a change to the overall optical efficiency of the shield. The trade-off is that the incoming photon

density is reduced by the absorption of the photons in the luminescent material. The homogeneous luminophore material absorption characteristics were modified to replicate a typical range of short wavelength material. The QE of the material was set at three levels to compare the effects of different materials.

5.5.2 Resulting efficiency changes based on simulations

The results of the simulations for photoluminescent down-conversion illustrate a possible cause for the lack of improvement to the solar cell efficiency with the addition of a luminescent material down-converter.

Table 5.1: Optical Efficiency in percent of photon emission for various luminophore Quantum Efficiencies for two plate thicknesses using ray-tracing simulator.

	For a 6cm x 4cm x 1mm cover glass plate			For a 6cm x 4cm x 0.1mm cover glass plate		
	95% QE luminescent material	50% QE luminescent material	26% QE luminescent material	95% QE luminescent material	50% QE luminescent material	26% QE luminescent material
Optical Efficiency from photons generated by emission (in %)						
Emission from bottom of cover glass to solar cell	4.43	2.18	1.03	0.555	0.162	0.101
Ideal emission from bottom and sides of cover glass to solar cell	20.85	10.67	5.38	1.398	0.689	0.3626
Optical Efficiency from incident photons (in %)						
Top of cover glass (due to reflection and scattering)	6.52	6.08	6.25	7.73	7.29	7.51
Bottom of cover glass to solar cell	64.06	60.66	59.86	89.95	89.23	88.16
Percent change to incident light to solar cell	-28.32	-31.72	-32.52	-2.43	-3.15	-4.22
Net percent change to Optical Efficiency as seen by solar cell under ideal emission	-7.47	-21.05	-27.14	-1.032	-2.461	-3.8574

As seen in the last row of Table 5.1, the overall optical efficiency from the front to the rear of the cover glass decreases in every case. The chart has two areas of optical efficiency based on emitted photons and incident photons. The emitted photons are generated from the luminescent material while the incident photons are the photons

from the light source. Above the double line and on the left side of the table are the various surfaces that have photons escaping. The solar cell is under the bottom plate, so the photons from this side can be utilized by the solar cell. The ideal emission assumes only escape cone losses by incorporating all emitted photons from the sides and bottom surfaces. A clear, undoped PMMA model was simulated as the baseline for comparison to the doped materials. For analysis presentation, the 95% QE 1mm thick material was selected. Using an AM0 spectrum, the spectral response of a silicon solar cell, and the emission from the bottom, the results of the downshifting showed that an absolute increase of 0.5% to the solar cell efficiency could be realized. If only escape cone losses were considered, then an absolute increase of almost 5% could be achieved. But, after incorporating the overall loss of 28% of the incident light, the calculated value results in a drop of over 2% absolute to the solar cell efficiency. A more realistic 0.1mm thick luminescent shield yields a similar loss to solar cell efficiency -- a net decrease of 0.7% absolute under the best circumstance. A thinner shield permitted more incident light to reach the solar cell, but less emitted light was generated. The results were an overall decrease in efficiency. As the simulations demonstrated and as stated in van Sark's research, the promise of improved efficiency due to photo luminescent down-conversion has yet to be realized.

5.6 Chapter Conclusions

Under ideal conditions, the promise of luminescent materials and spectral conversion could greatly improve solar cell efficiencies. The review of the topics has

indicated some successes in spectral modifications. Most of the promises have not been fulfilled, due to non-ideal materials and other loss mechanisms overtaking the benefits. As these materials and methods mature, improvements can be easily incorporated into a space system.

Chapter 6 Conclusions

6.1 Objectives of this research

The objective of this research was to investigate the feasibility of using luminescent materials in space. The main emphasis was on characterizing the degradation of luminescent materials due to radiation exposure. Thermal modeling was used to evaluate the temperature effects on LSC system efficiency. Based on these two results, a comparison between state-of-the-art solar cells and a potential LSC system was presented. Finally, the works on spectral conversion were reviewed for specific space application.

6.1.1 Investigation of non-traditional LSC luminescent material

A substantial body of literature on the various types, quantities, and applications of luminescent materials exists and is ever growing. To contribute to the growing data, a material from a different arena was selected for testing. One of the stated problems with LSC systems is reabsorption. This reabsorption can be overcome with an increase in the Stokes shift properties of the material. Therefore, a Large Stokes Shift material normally reserved for biomedical purposes was selected to characterize its use as a thin-film on a substrate and follow-on radiation testing.

The LSS material did not perform up to the expectations, due to its lack of stability. Therefore, the follow-on radiation tests were not conclusive either.

6.1.2 Thermal simulations on an LSC system

One of the stated problems with directly exposed solar cells is thermalization, creating a less efficient solar cell due to higher operating temperatures. The reduction in thermalization created a more conducive temperature operating range and improved the solar cell performance. As with the radiation problem, the end result could be that the overall efficiency of the system does not improve because of the trade in thermalization from the solar cell to the thermalization of the luminescent material.

The first part of the problem was to determine the temperature changes that occurred over the orbit. Simulations using COMSOL's Multiphysics software were used to determine the extreme temperatures that a satellite may experience in a middle altitude. These simulations set the analysis range for the LSC system.

The next part was to use previous works to determine how luminophores change with increased temperatures. As expected, the shift of thermalization from the solar cell to luminescent material created similar issues. Increased heat degraded the performance of the luminophores.

Finally, an analysis was done to compare the decreases in efficiency to see how the overall LSC system would be affected by these temperature changes. The results were nominal changes to the overall system. The decrease in efficiency to the luminescent material was offset by the improvements in efficiency due to the solar cell's operations in a more suitable temperature range. The combination of radiation tolerance and offsetting thermalization showed the promise of using LSC systems in space.

6.1.3 Radiation effects on Luminophores

The use of luminophores in space in power systems has been limited due to their lack of efficiency. As research progresses and new materials and systems are explored, the natural design of an LSC system creates a more radiation tolerant system. The concern was the survivability of the actual luminophores to radiation. The thrust of the radiation test was not to determine all degradation effects for all possible luminophores, but to demonstrate the capability of luminescent materials to tolerate radiation. The test results showed the ability of some luminophores to withstand radiation, thus surviving the space environment.

Rhodamine 6G, a common organic luminescent dye, showed very little changes to its characteristics. By staying close to its initial values, this material demonstrated that it would not degrade over the lifetime of a space system in some very harsh regions. The problem with using such a material is the narrow absorption range and small Stokes shift.

The Fluorescein sample was used to illustrate a second luminescent material and its changes due to radiation. The quenching of its edges due to oxygen showed that other environmental exposures might preclude its use in space. Whether it will recover from quenching in a vacuum was not answered. Obviously, in the middle altitudes of space, quenching may not be a factor since oxygen is not present. Even though the measurements showed a good tolerance to radiation exposure, a physical examination showed that this material is not well suited for the radiation environment.

The new material tested was the Large Stokes Shift dye. To overcome the reabsorption problem experienced by other luminescent materials, the LSS dye was a good fit for the experiment. It was demonstrated that it could be spin-coated onto substrates with strong emission. The LSS dye did not stand up well to radiation testing. It was the only material to see appreciable changes in its emission characteristics after exposure. These changes maybe linked to the instability of the dye in the tested format, but the overall changes from the environment noticeably degraded the luminescence of this material. Even though this material has good Stokes shift qualities, further investigation is needed to see if it would make for a good LSC system.

The materials tested demonstrated that some luminescent materials do well in the radiation environment of space. Thus, luminophores can work well in space applications for LSC systems and solar cell augmentation.

6.1.4 Spectral conversion luminophores for use in space applications

A final area of investigation was the altering of the incoming spectrum in order to improve the efficiency of solar cells. This idea was presented over thirty years ago and much research has been done.[94] The results have been promising. As materials mature and methods improve, spectral conversion will benefit solar cell efficiency.

The presentation in this dissertation was a review of the current materials and simulations using the ray-tracing program to validate optical efficiency. The

simulations did not show any improvement in the overall efficiency of the solar cell system. The red-shifting of the incoming spectrum facilitated better use of the shortest wavelengths, but the loss in incident spectrum due to absorption created an overall loss in incoming photons for electron-hole pair generation. The net result from the simulations is a loss in output power.

6.1.5 Overall results of luminophores in space applications

In spectral conversion, radiation tolerance, and thermal resilience, luminophores show the potential for application in space. By maintaining its power generating capability throughout its lifetime in a harsh radiation environment, an improved LSC system can be an effective technology. Luminophores can also augment existing solar panel systems, by shifting unusable light to a usable wavelength. The radiation tolerance of luminophores has been demonstrated, and the applications of these luminophores in space are just beginning to be explored.

6.2 Further research

6.2.1 Luminescent Concentrator improvements

One of the assumptions throughout this research is that an LSC system will become more efficient with technology and material advances. These necessary advances were not investigated, but more research could validate the use of a highly efficient LSC in space. As proposed by Ferrell and Yoshida[42], the next generation of LSC systems needs to markedly improve optical efficiency, in order to take advantage of the geometric gain. The reabsorption and escape cone losses that are

still plaguing the system's development prevents a large LSC with good optical efficiency. Large Stokes shift materials and selective waveguides can mitigate these losses. A large Stokes shift material will minimize the reabsorption losses. The selective waveguide material that permits the excitation light to enter but captures more of the emitted light. Research into a white bottom reflectors and photonic structures, used as a selective material, have shown a relative improvement in the LSC system of over 20%.[60] Another collection improvement uses silver nanoparticles, improving collection efficiencies by 12%. These changes could improve the current state-of-the-art LSC system to close to 10% efficiency.[95] With further waveguide improvements, a second generation LSC should be able to achieve 10-25% efficiency.[42]

To uncover the improvements necessary for the next generation LSC system, new luminescent materials need to be developed that will reduce reabsorption losses, selective mirrors or emission orientation should be developed to reduce escape cone losses, and emission-solar cell matching needs to improve.

6.2.2 Other space conditions not investigated

Only a few of the space environment effects were investigated. The effects of vacuum, micrometeoroids, atomic oxygen, and electrostatic discharge will still need to be addressed for an LSC system in space. Each presents its own problems, but some issues remain dependent of the operational characteristics of the satellite. Depending on the mission requirements, these other effects may or may not need to be considered.

6.2.2.1 Vacuum and out-gassing

While luminescent materials are being used throughout many terrestrial applications from power generation to light bulb enhancement to biomedical research, the use of these materials in a vacuum may create unknown issues. In the past, plastics and other materials have displayed issues, such as lenses clouding or cover glass degradation due to out-gassing onto sensitive lens or solar arrays. Luminescent materials could present similar problems. They may out-gas into space and degrade their own efficiency. The natural stability of luminescent materials could be altered in a vacuum environment. Vacuum stability and out-gassing would need further investigation, prior to using a luminophore system in space.

6.2.2.2 Micrometeoroids/orbital debris

Micrometeoroids and orbital debris represent a hazard to all spacecraft parts. For traditional solar arrays, larger particles can create holes in the solar arrays, thus, degrading their efficiency. Smaller particles may not directly damage the solar cells, but the pitting of the anti-reflective coatings and shielding degrades the cell efficiency. In an LSC system, the solar cells would be better shielded from the direct damage of micrometeoroids, but another problem is introduced. With an LSC's reliance on total internal reflection to transport the photons to the edges of the plate, surface damage would degrade its ability to transport the fluorescence. Therefore micrometeoroids could have a profound effect on an LSC system. Simulations and experimental tests would answer the question of overall efficiency changes to an LSC system due to micrometeoroid/orbital debris strikes.

6.2.2.3 Atomic Oxygen

As seen distinctly with the Fluorescein samples, some materials are sensitive to oxygen. As noted in many space missions, atomic oxygen (also called molecular oxygen) is very detrimental to materials. The single atom of oxygen easily attaches to materials and is very corrosive. The breakdown of materials due to atomic oxygen is well documented at lower Earth orbits. If a luminescent material were to be used at a low Earth orbit (<3000 km), then further research into this effect would be needed.

6.2.2.4 Charging and discharging

An ongoing problem with power generation systems and structures in space is the charging and unexpected discharging of spacecraft components due to charged particles encountered in space. With proper grounding, most of these problems can be reduced or mitigated. With the power generation components in an LSC systems well protected from the environment, charging of such components should not be an issue, but a prudent space systems engineer will investigate such a possibility. The basic structure of an LSC is an aluminum backing that would need to be properly grounded to the spacecraft with the proper cabling to transport the power to the spacecraft bus.

6.2.3 Luminophore Stability

Similar to a solar cell, a luminescent material naturally degrades over time due to environmental exposure. As with any design, the trade of radiation tolerance may be overshadowed by the natural degradation of the luminophores to light, especially UV light. There have been studies done that document the stability of certain

luminophores out to 20 years, while maintaining ~90% of their quantum efficiency.[96] Since it is material specific, one of the design characteristics of an LSC system for space will need to be the luminophore stability per the mission life of the satellite.

6.3 Final thoughts

6.3.1 Research methodology

As stated in the beginning, the luminescent solar concentrator still needs further enhancements before it will be able to replace traditional solar cells. The assumptions presented in this research would need to be reassessed with the structure and materials used. The ad hoc approach to the various methods of investigating luminescent materials has hampered their benefits in power generation. In trying to remove some of the comparison issues, the investigation characterized the emission data and used previously well-known solar cell data to draw conclusions. By measuring the emission spectrum via a Fluorometer, a re-creatable source was utilized, thus, removing the error associated with different light sources. Also, by measuring only the emission, the various types of PV cells were removed from the measurements. The purpose of this investigation was not to build the perfect space LSC system, but to determine whether a system is worthy of further consideration.

Some of the test materials were chosen due to availability and prior research. Rhodamine 6G is a well-documented organic dye that is easy to use with much research as a laser dye. Fluorescein was chosen due to its similar characteristics to Rhodamine. Cytodiagnostics Large Stokes Shift 500 dye was chosen to add depth to

the luminescent research and to address an on-going concern with the reabsorption problem in LSC design. Other materials were tried, such as lab-grown Quantum Dots and Rubrene dye, but the manufacturing and implementation results were very poor, so they were dropped from further investigation.

6.3.2 Future vision of luminescent materials both in space and terrestrial applications

Luminescent materials have advanced greatly, since their first suggested use in the 1970's. Modern luminophores have not shown much improvement over other renewable sources, whether as an LSC or an augmentation to solar cells. Industry has not yet determined the benefits of using luminescent materials in their manufacturing process. This lack of use is due, partly, to the confusing array of variables in the luminescent processes and methods, from up-conversion to down-conversion. The unfulfilled promise of cheaper materials and the advances in solar cell design have prevented the luminescent materials from reaching the mass production and experimentation needed to advance their implementation. Through their passive, optical approach, luminescent materials can address the need for increased power generation in space systems, as solar cells reach their theoretical maximum.

Appendix A: Rhodamine 6G Spectral Data

Control sample

Absorption

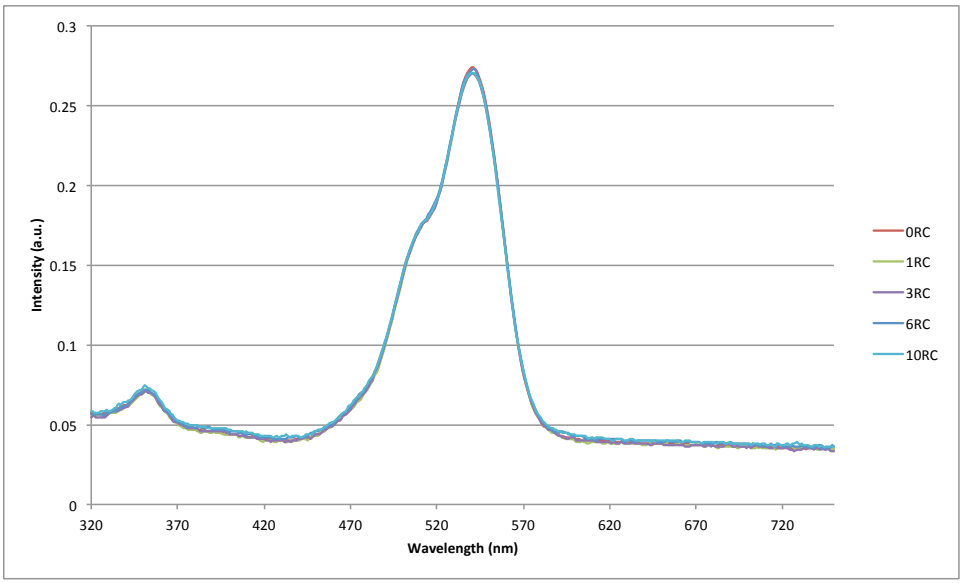

Emission

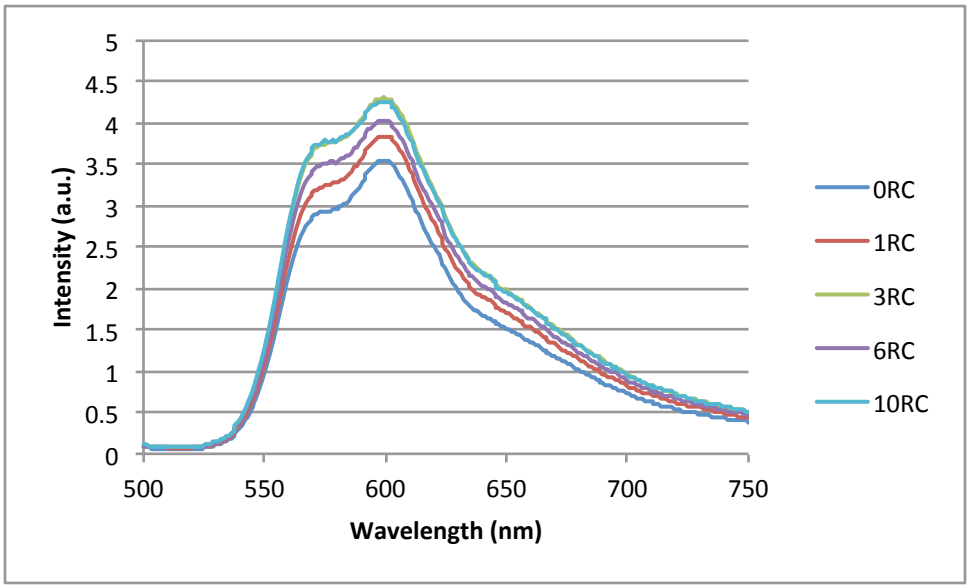

Test sample

Absorption

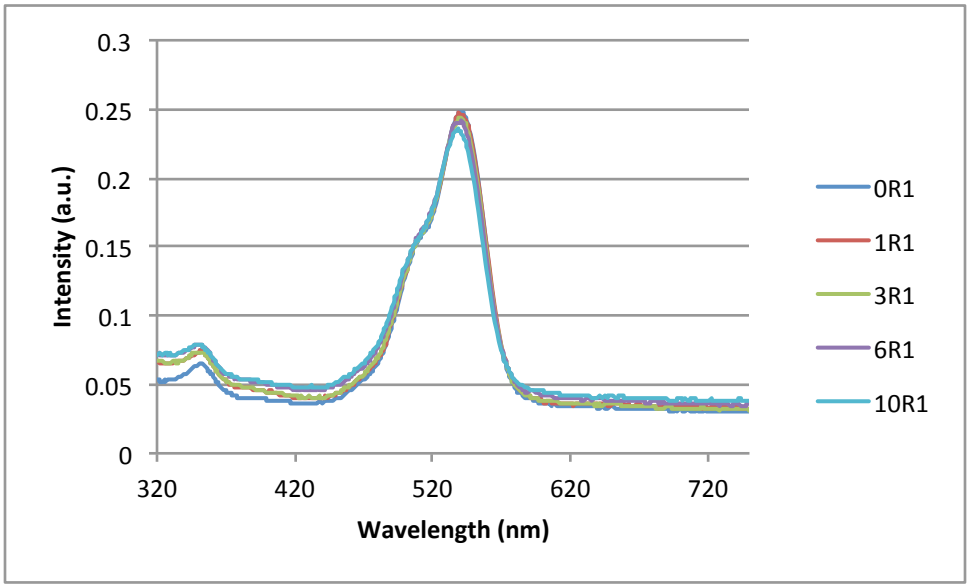

Emission

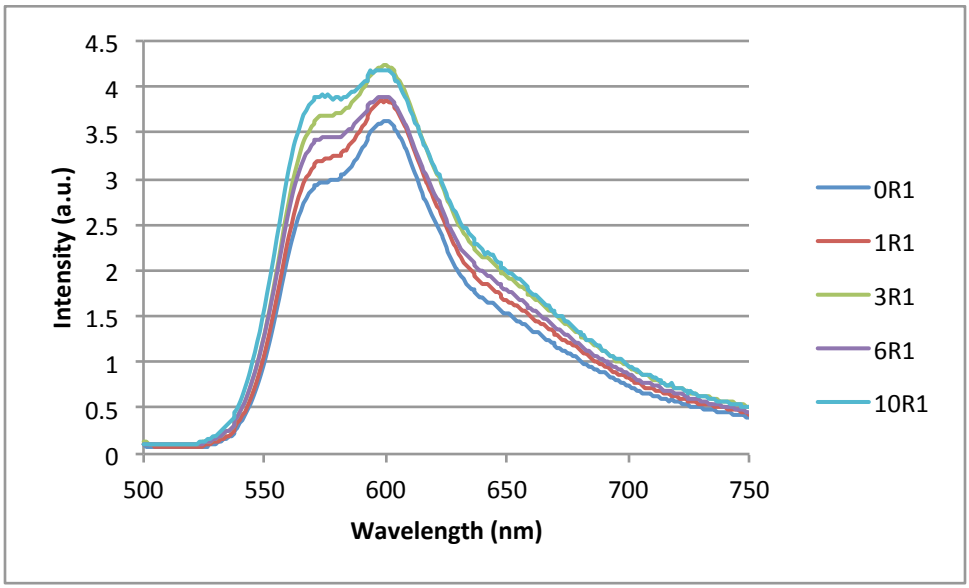

Appendix B: Fluorescein Spectral Data

Control sample

Absorption

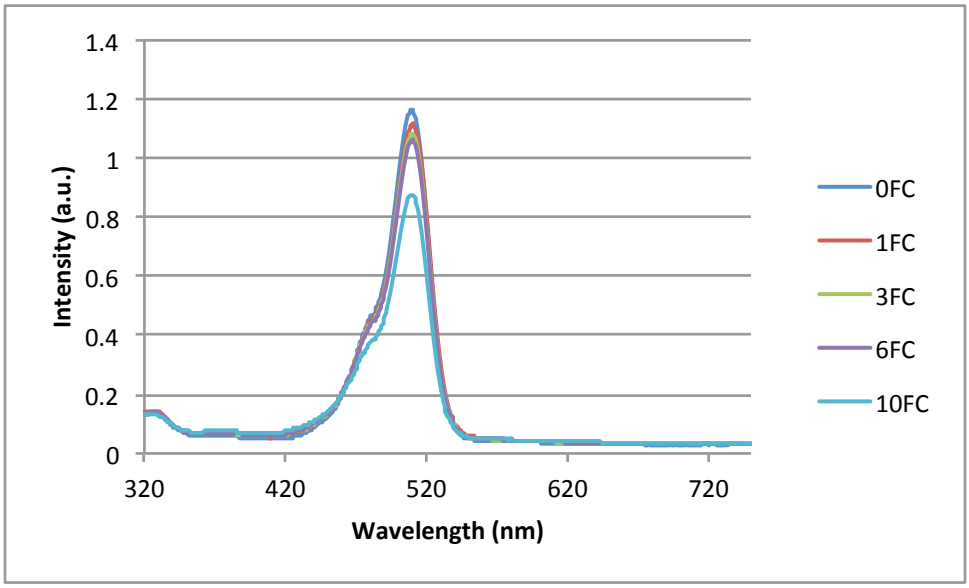

Emission

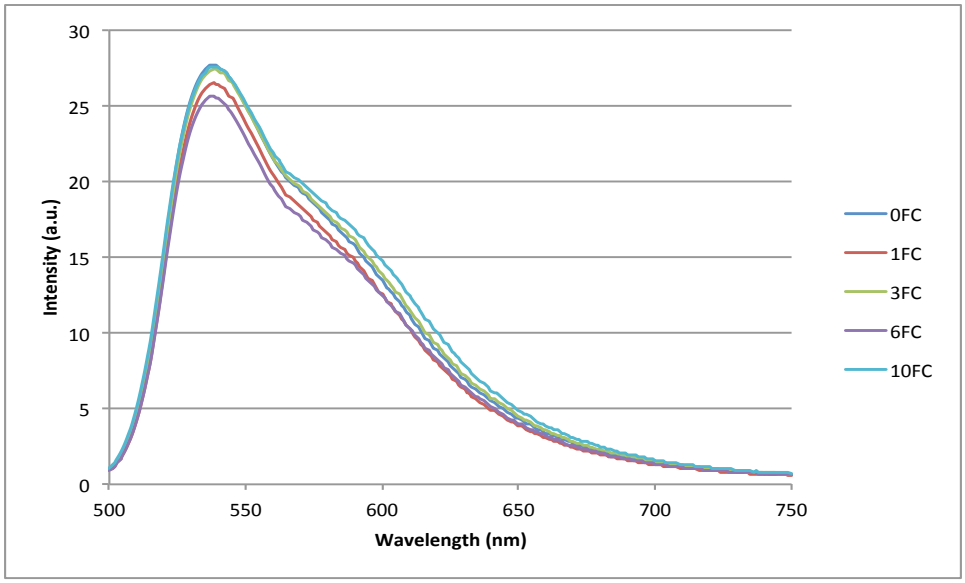

Test sample

Absorption

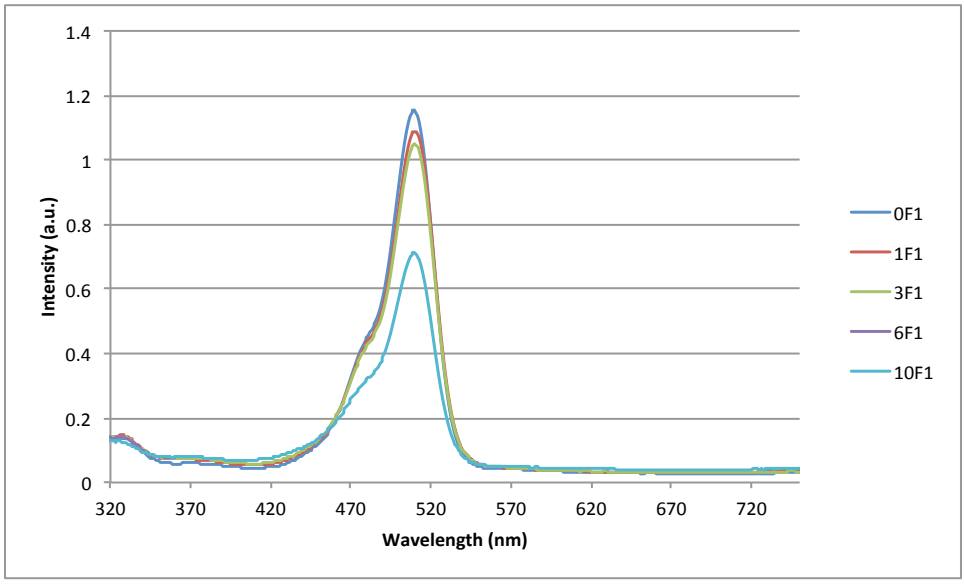

Emission

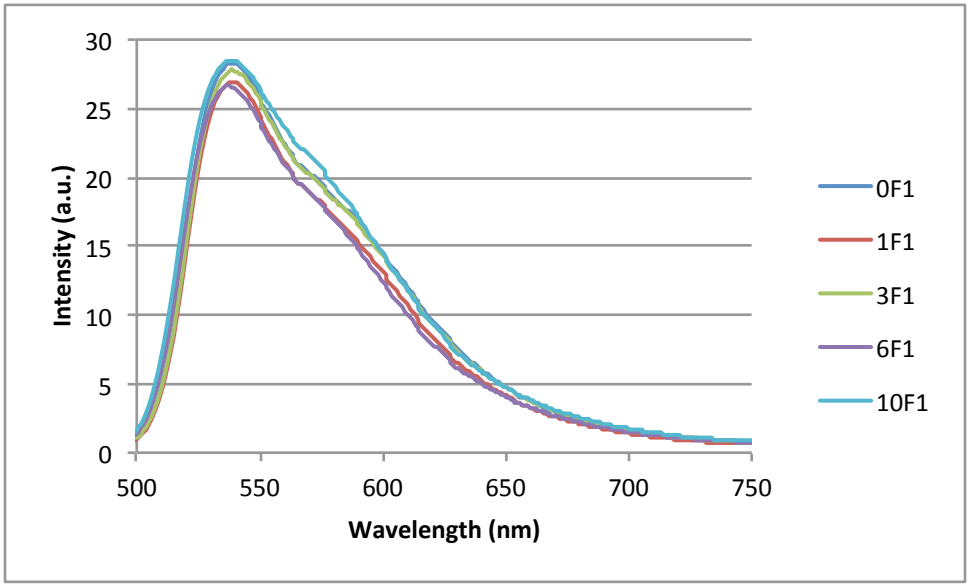

Appendix C: Large Stokes Shift Dye Spectral Data

Control sample

Absorption

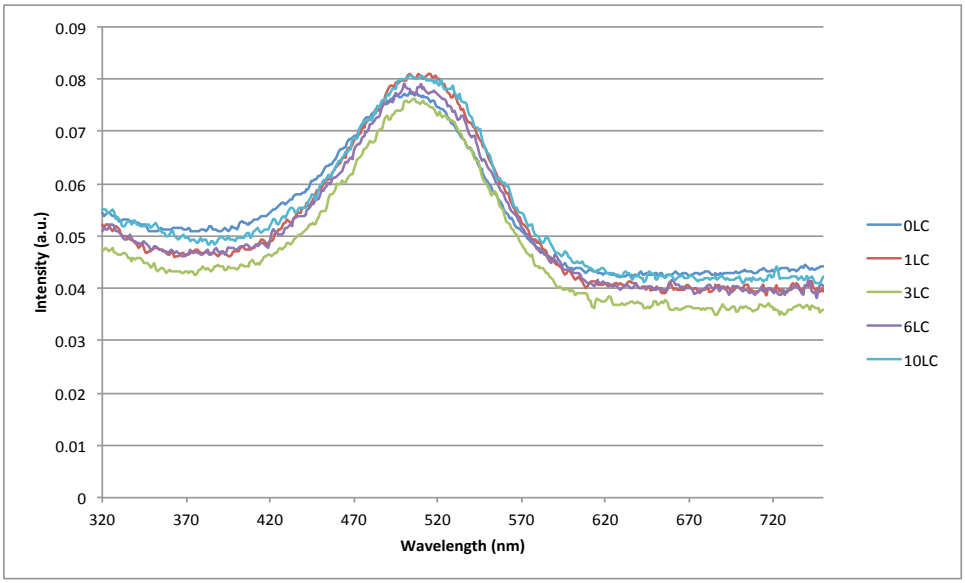

Emission

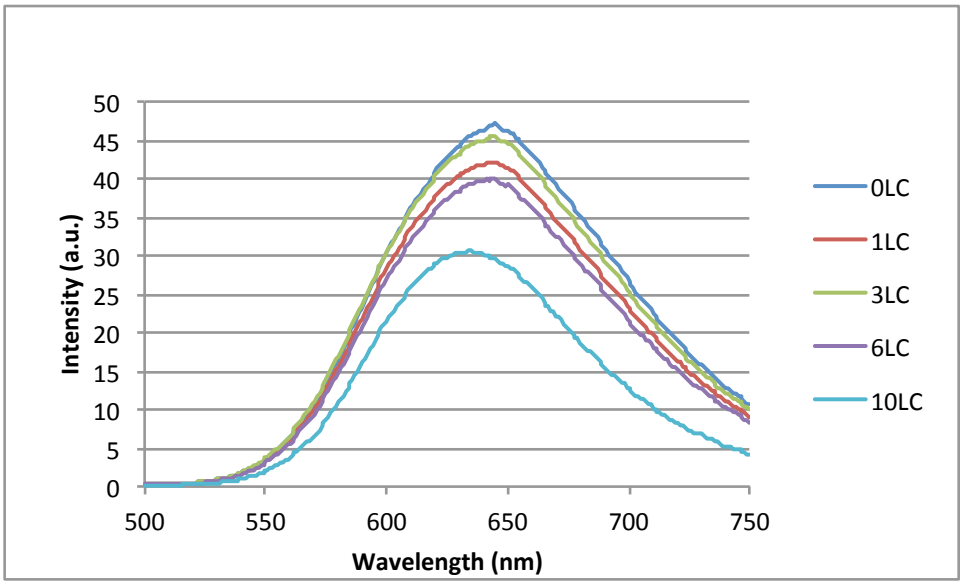

Test Sample

Absorption

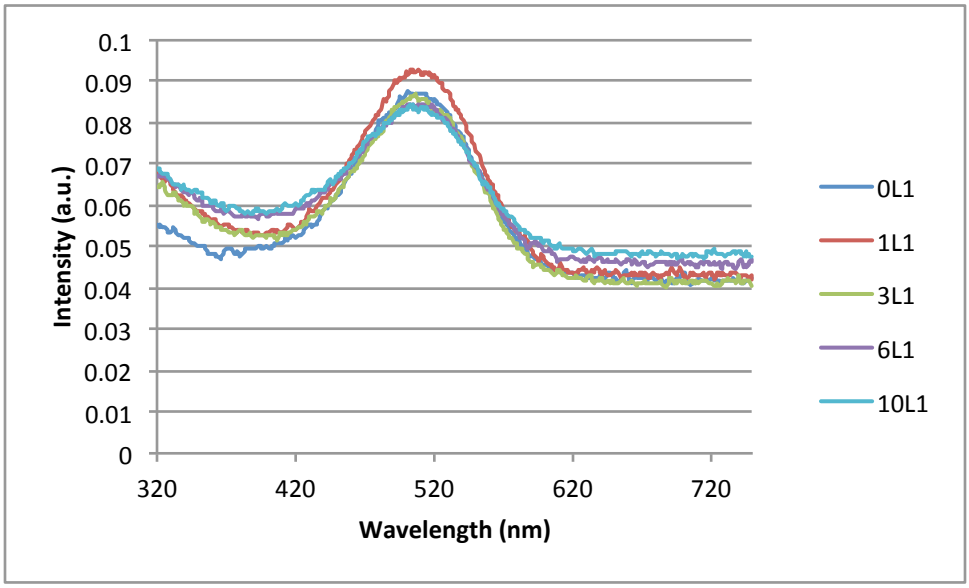

Emission

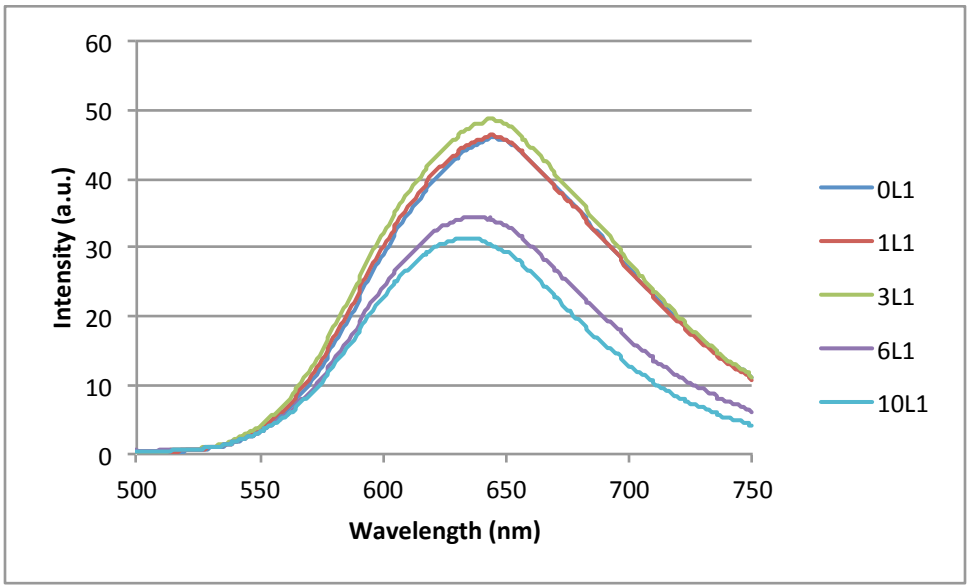

Bibliography

[1] Choi, Charles Q. "NASA Discovers New Radiation Belt Around Earth." *Space.com*. N.p., 28 Feb. 2013. Web. 16 Oct. 2014.
[2] Kramer , H. (n.d.). *Tacsat-4 (tactical satellite-4)*. Retrieved from https://directory.eoportal.org/web/eoportal/satellite-missions/t/tacsat-4
[3] Sten Odenwald. (n.d.). *IMAGE: Weekly Problem Archive*.
[4] *Vanguard, the world's oldest satellite still in orbit* . ((2004, June 06)2004, June 06). Retrieved from http://code8100.nrl.navy.mil/about/heritage/vanguard.htm
[5] Zadunaisky, Pedro E. (October 1960). "The Orbit of Satellite 456 Alpha (Explorer I) during the First 10500 Revolutions". *SAO Special Report #50 (1960)*
[6] Green, M. A., Emery, K., Hishikawa, Y., Warta, W., & Dunlop, E. D. (January 01, 2014). Solar cell efficiency tables (version 43). *Progress in Photovoltaics: Research and Applications, 22,* 1, 1-9.
[7] Conibeer, G. "Third-generation Photovoltaics." *Materials Today* 10.11 (2007): 42-50. Web.
[8] Yoon, Hojun; Joslin, D.E.; Law, D.C.; Krut, D.; King, Richard R.; Vijayakumar, P.; Peterson, D.; Hanley, J.; Karam, N.H., "Application of infrared reflecting (IRR) cover glass on multijunction III-V solar cells," *Photovoltaic Energy Conversion, Conference Record of the 2006 IEEE 4th World Conference on* , vol.2, no., pp.1861,1864, May 2006.
[9] Herro, A. (2013). *new solar cell "most efficient ever"*. Retrieved from http://www.worldwatch.org/node/4803
[10] Spectrolab, Inc. (2009). *Photovoltaics*. Retrieved from http://www.spectrolab.com/solarcells.htm
[11] World record solar cell with 44.7% efficiency developed. (October 29, 2013). *Chemical Weekly, 59,* 12, 181-184.
[12] Aleksandra Vasic, Predrag Osmokrovic, Nenad Marjanovic, and Momčilo Pejović, "Radiation Effects in Solar Cells and Optoelectronic Devices," International Journal of Photoenergy, vol. 2013, Article ID 171753, 3 pages, 2013.
[13] Emcore ATJ solar cell datasheet, http://www.emcore.com/wp-content/uploads/ATJ_datasheet1.pdf last accessed 6/27/2014
[14] Weiss, L., Coyle, P., Fowler, C., Frosch, R., Kaminow, I., Patel, K., Remo, J., & Roxborough, I. Federation of American Scientists, (2004). *Ensuring America's Space Security: Report of the FAS Panel on Weapons in Space*. Retrieved from website: http://www.fas.org/pubs/_pages/space_report.html
[15] Batchelder, J. S., A. H. Zewail, and T. Cole. "Luminescent Solar Concentrators 1: Theory of Operation and Techniques for Performance Evaluation." *Applied Optics* 18.18 (1979): 3090. Web.

[16] "SPENVIS - Space Environment, Effects, and Education System." *SPENVIS - Space Environment, Effects, and Education System*. N.p., n.d. Web. 28 July 2014.
[17] "How the Hubble Space Telescope Works (Infographic)." *Space.com*. N.p., n.d. Web. 9 May 2014. <http://www.space.com/20765-hubble-space-telescope-infographic.html>.
[18] Tribble, Alan C.. *The space environment: implications for spacecraft design*. Princeton, NJ: Princeton University Press, 1995.
[19] Modified from http://sec.gsfc.nasa.gov/popscise.jpg
[20] "NASA Probes Studying Earth's Radiation Belts to Celebrate Two Year Anniversary." *NASA*. Ed. Dwayne Brown and Geoff Brown. NASA, 29 Aug. 2014. Web. 28 Oct. 2014.
[21] Tech report: activation of color centers in glass, Michael Olsen
[22] R. D Evans, "The Atomic Nucleus", Chap 24, McGraw-Hill, New York, 1955.
[23] Haffner, James W.. *Radiation and shielding in space*. New York, London: Academic Press, 1967.
[24] O. Klein and y. Nishina, On the Scattering of Radiation by Free Electrons According to the Relativistic Quantum Mechanics of Dirac, Z. Physik 52, 853 (1928).
[25] R. D Evans, "The Atomic Nucleus", Chap 24, McGraw-Hill, New York, 1955.
[26] "The Compton Effect - an introduction to the Compton effect." *About.com Physics*. N.p., n.d. Web. 9 May 2014. <http://physics.about.com/od/quantumphysics/a/comptoneffect.htm>.
[27] Fox, Mark. *Optical properties of solids*. Oxford: Oxford University Press, 2001.
[28] Modified from "Transmittance." *Wikipedia*. Wikimedia Foundation, 24 Oct. 2014. Web. 28 Oct. 2014.
[29] Palmer, James W.. "CHAPTER 35 THE MEASUREMENT OF TRANSMISSION, ABSORPTION, EMISSION, AND REFLECTION." *Handbook of Optics*. : McGraw-Hill , 2009.
[30] Reisfeld ,Renata; Samuel Neuman. "Planar solar energy converter and concentrator based on uranyl-doped glass". *Nature* **274**: 144–145, 1978.
[31] Bose, R., Farrell, D. J., Pardo-Sanchez, C., Pravettoni, M., Mazzer, M., Chatten, A. J. and Barnham, K. W. J.. *Luminescent solar concentrators: cylindrical design*. In Proc. 24th Eur. Photovolt. Solar Energy Conf., Hamburg, Germany, 2009.
[32] Hecht, Eugene. *Optics*. Reading, Mass.: Addison-Wesley Pub. Co., 1987. Print.
[33] Goldschmidt, Jan Christoph, Marius Peters, Martin Hermle, and Stefan W. Glunz. "Characterizing the Light Guiding of Fluorescent Concentrators." *Journal of Applied Physics* 105.11 (2009): 114911. Web.
[34] Verbunt, Paul PC, and Michael G. Debije. "Progress in luminescent solar concentrator research: solar energy for the built environment." *World Renewable Energy Congress (Linköping University Electronic Press, 2011)*. 2011.

[35] Debije, Michael G., and Paul PC Verbunt. "Thirty years of luminescent solar concentrator research: solar energy for the built environment." *Advanced Energy Materials* 2.1 (2012): 12-35.
[36] Reisfeld, Renata, Dimitri Shamrakov, and Christian Jorgensen. "Photostable solar concentrators based on fluorescent glass films." *Solar energy materials and solar cells* 33.4 (1994): 417-427.
[37] Baumberg, I., et al. "Effect of polymer matrix on photo-stability of photo-luminescent dyes in multi-layer polymeric structures." *Polymer degradation and stability* 73.3 (2001): 403-410.
[38] Currie, Michael J., et al. "High-efficiency organic solar concentrators for photovoltaics." *Science* 321.5886 (2008): 226-228.
[39] Hyldahl, Meredith G., Sheldon T. Bailey, and Bruce P. Wittmershaus. "Photo-stability and performance of CdSe/ZnS quantum dots in luminescent solar concentrators." *Solar Energy* 83.4 (2009): 566-573.
[40] Barnham, Keith, et al. "Quantum-dot concentrator and thermodynamic model for the global redshift." *Applied Physics Letters* 76.9 (2000): 1197-1199.
[41] Purcell-Milton, Finn, and Yurii K. Gun'ko. "Quantum dots for luminescent solar concentrators." *Journal of Materials Chemistry* 22.33 (2012): 16687-16697.
[42] Farrell, Daniel J., and Megumi Yoshida. "Operating regimes for second generation luminescent solar concentrators." *Progress in Photovoltaics: Research and Applications* 20.1 (2012): 93-99.
[43] Gutmann, Johannes, et al. "Electromagnetic simulations of a photonic luminescent solar concentrator." *Optics express* 20.102 (2012): A157-A167.
[44] Rowan, Brenda C., Lindsay R. Wilson, and Bryce S. Richards. "Advanced material concepts for luminescent solar concentrators." *Selected Topics in Quantum Electronics, IEEE Journal of* 14.5 (2008): 1312-1322.
[45] Moudam, Omar, et al. "Europium complexes with high total photoluminescence quantum yields in solution and in PMMA." *Chemical Communications* 43 (2009): 6649-6651.
[46] Wilson, Lindsay R., et al. "Characterization and reduction of reabsorption losses in luminescent solar concentrators." *Applied optics* 49.9 (2010): 1651-1661.
[47] Debije, Michael G., et al. "Measured surface loss from luminescent solar concentrator waveguides." *Applied optics* 47.36 (2008): 6763-6768.
[48] van Sark, Wilfried GJHM, et al. "Luminescent Solar Concentrators-A review of recent results." *Optics Express* 16.26 (2008): 21773-21792.
[49] Huang, Xiaoyong, et al. "Enhancing solar cell efficiency: the search for luminescent materials as spectral converters." *Chemical Society Reviews* 42.1 (2013): 173-201.
[50] Mansour, A. F. "On enhancing the efficiency of solar cells and extending their performance life." *Polymer testing* 22.5 (2003): 491-495.

[51] Slooff, L. H., et al. "Efficiency enhancement of solar cells by application of a polymer coating containing a luminescent dye." *Journal of Solar Energy Engineering* 129.3 (2007): 272-276.
[52] Bower, Kenneth E., et al., eds. *Polymers, phosphors, and voltaics for radioisotope microbatteries*. CRC press, 2002.
[53] Reisfeld, Renata, et al. "Luminescent solar concentrators based on thin films of polymethylmethacrylate on a polymethylmethacrylate support." *Solar energy materials* 17.6 (1988): 439-455.
[54] Reisfeld, Renata. "Energy transfer between dyes on glass surfaces and ions in glasses." *Chemical Physics Letters* 95.2 (1983): 95-96.
[55] Reisfeld, R. "Increase of pumping efficiencies of glass lasers by radiated energy transfer." *Chemical physics letters* 114.3 (1985): 306-308.
[56] Bose, Rahul. *Raytrace Simulations and Experimental Studies of Luminescent Solar Concentrators.* Diss. Imperial College London, 2010.
[57] Goldschmidt, Jan Christoph, Marius Peters, Armin Bösch, Henning Helmers, Frank Dimroth, Stefan W. Glunz, and Gerhard Willeke. "Increasing the Efficiency of Fluorescent Concentrator Systems." *Solar Energy Materials and Solar Cells* 93.2 (2009): 176-82. Web.
[58] Farrell, Daniel James. *Characterising the performance of luminescent solar concentrators*. Diss. Imperial College London, 2008.
[59] Debije, Michael G., et al. "Effect on the output of a luminescent solar concentrator on application of organic wavelength-selective mirrors." *Applied optics* 49.4 (2010): 745-751.
[60] Goldschmidt, Jan Christoph, et al. "Theoretical and experimental analysis of photonic structures for fluorescent concentrators with increased efficiencies." *physica status solidi (a)* 205.12 (2008): 2811-2821.
[61] Goldschmidt JC. "Luminescent Solar Concentrator." *Comprehensive Renewable Energy*, Vol 1, pp. 587–601. (2012)
[62] Bailey, Sheila, and Ryne Raffaelle. "Space Solar Cells and Arrays." *Handbook of Photovoltaic Science and Engineering* (2003): 413-448.
[63] "Effect of Temperature." *PVEducation*. N.p., n.d. Web. 23 June 2014. <http://www.pveducation.org/pvcdrom/solar-cell-operation/effect-of-temperature>.
[64] Guenette, Mathew. *The efficiency of photovoltaic solar cells at low temperatures*. Diss. Thesis, August 4 th, 2006.
[65] Shockley, William, and Hans J. Queisser. "Detailed Balance Limit of Efficiency of P-n Junction Solar Cells." *Journal of Applied Physics* 32.3 (1961): 510. Web.
[66] Flood D, Proc. NHTC'00, 34 th National Heat Transfer Conf. (2000).
[67] Incropera, Frank P., and David P. DeWitt. "Chapter 13 Radiation Exchange Between Surfaces." *Fundamentals of Heat and Mass Transfer*. New York: Wiley, 1996. 718-55. Print.

[68] Meseguer, F. J., et al. "Temperature effects on the efficiency of Luminescent Solar Concentrator (LSC) for photovoltaic systems." *Journal of Luminescence* 24 (1981): 865-868.
[69] Summers, Geoffrey P., et al. "Damage correlations in semiconductors exposed to gamma, electron and proton radiations." *Nuclear Science, IEEE Transactions on* 40.6 (1993): 1372-1379.
[70] Tada, H. Y., et al. "Solar cell radiation handbook." *Unknown* 1 (1982).
[71] Anspaugh, B. E. "GaAs solar cell radiation handbook." (1996).
[72] Yamaguchi, Masafumi. "Radiation-resistant solar cells for space use." *Solar Energy Materials and Solar Cells* 68.1 (2001): 31-53.
[73] "Cytodiagnostic Telephone Interview." Telephone interview. 12 Feb. 2014.
[74] "Cyto 500LSS Large Stokes Shift Dye." *Cytodiagnostics*. N.p., n.d. Web. 12 Feb. 2014.
[75] LAMBDA 1050 UV/Vis/NIR Spectrophotometer. Digital image. Perkin/Elmer, n.d. Web. 9 Nov. 2014. <http://www.perkinelmer.com/catalog/product/id/l1050>.
[76] HORIBA FluoroLog Fluorometer. Digital image. HORIBA, n.d. Web. 9 Nov. 2014. <http://www.horiba.com/us/en/scientific/products/fluorescence-spectroscopy/steady-state/fluorolog/fluorolog-r-our-modular-spectrofluorometer-522/>.
[77] "F Test Explained." *F Test Explained*. StatsToDo Trading Pty Ltd, n.d. Web. 15 Oct. 2014, https://www.statstodo.com/FTest_Exp.php
[78] Çelebi, Neslihan, Mustafa Arık, and Yavuz Onganer. "Analysis of fluorescence quenching of pyronin B and pyronin Y by molecular oxygen in aqueous solution." *Journal of luminescence* 126.1 (2007): 103-108.
[79] Arık, Mustafa, Neslihan Çelebi, and Yavuz Onganer. "Fluorescence quenching of fluorescein with molecular oxygen in solution." *Journal of Photochemistry and Photobiology A: Chemistry* 170.2 (2005): 105-111.
[80] Van Sark, W. G. J. H. M., et al. "Improvement of spectral response of solar cells by deployment of spectral converters containing semiconductor nanocrystals." *Proceedings of the 19th European Photovoltaic Solar Energy Conference, Paris*. 2004.
[81] Švrček, V., A. Slaoui, and J-C. Muller. "Silicon nanocrystals as light converter for solar cells." *Thin Solid Films* 451 (2004): 384-388.
[82] Gibart, P., et al. "IR response of substrate-free GaAs solar cells using two-photon up-conversion." *13th EPVSEC, Nice, France* (1995): 85.
[83] Shalav, A., et al. "The application of up-converting phosphors for increased solar cell conversion efficiencies." *Photovoltaic Energy Conversion, 2003. Proceedings of 3rd World Conference on*. Vol. 1. IEEE, 2003.
[84] Shalav, A., et al. "Application of NaYF4: Er3+ up-converting phosphors for enhanced near-infrared silicon solar cell response." *Applied Physics Letters* 86.1 (2005): 013505.

[85] Derived from "Solar Spectra: Air Mass Zero." *Solar Spectra: Air Mass Zero*. NREL, 1 Jan. 2000. Web. 8 Oct. 2014.
[86] Strümpel, C., et al. "Modifying the solar spectrum to enhance silicon solar cell efficiency—An overview of available materials." *Solar Energy Materials and Solar Cells* 91.4 (2007): 238-249.
[87] Klampaftis, Efthymios, et al. "Enhancing the performance of solar cells via luminescent down-shifting of the incident spectrum: A review." *Solar Energy Materials and Solar Cells* 93.8 (2009): 1182-1194.
[88] Richard, B. S., and A. Shalav. "The role of polymers in the luminescence conversion of sunlight for enhanced solar cell performance." *Synthetic metals* 154.1 (2005): 61-64.
[89] A. Shalav, BS Richards, KW Krämer, HU Güdel, in: Proceedings of the 31st IEEE Photovoltaic Specialists Conference, 3–7 January 2005, Florida, USA, pp. 114–117.
[90] Richards, B. S. "Enhancing the performance of silicon solar cells via the application of passive luminescence conversion layers." *Solar energy materials and solar cells* 90.15 (2006): 2329-2337.
[91] Qiu, P., and Alfons Penzkofer. "Intense ultrashort pulse generation in a two-photon pumped generator-amplifier system." *Applied Physics B* 48.2 (1989): 115-124.
[92] Luque, Antonio, and Steven Hegedus, eds. *Handbook of photovoltaic science and engineering*. John Wiley & Sons, 2003.
[93] Crabb, R. L. "Evaluation of cerium stabilised microsheet coverslips for higher solar cell outputs." *Photovoltaic Specialists Conference, 9 th, Silver Spring, Md*. 1972.
[94] Batchelder, J. S., A. H. Zewail, and T. Cole. "Luminescent Solar Concentrators 1: Theory of Operation and Techniques for Performance Evaluation." *Applied Optics* 18.18 (1979): 3090. Web.
[95] Reisfeld, Renata. "New Developments in Luminescence for Solar Energy Utilization." *Optical Materials* 32.9 (2010): 850-56. Web.
[96] Kinderman, R., L. H. Slooff, A. R. Burgers, N. J. Bakker, A. Büchtemann, R. Danz, and J. A. M. Van Roosmalen. "I-V Performance and Stability Study of Dyes for Luminescent Plate Concentrators." *Journal of Solar Energy Engineering* 129.3 (2007): 277. Web.